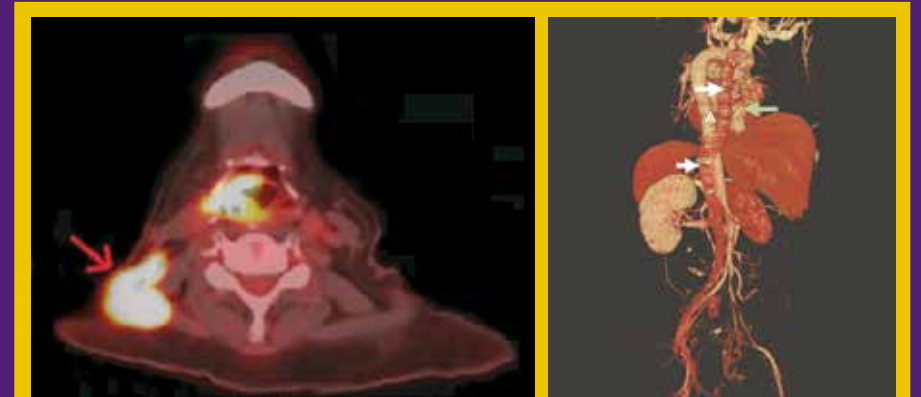


Highlights of this issue:

- Treatment Outcomes of Nasopharyngeal Carcinoma in Patients Aged 80 Years or Above
- Improving Breast Cancer Detection in Screening Mammography with Artificial Intelligence Assistance: A Multi-reader Retrospective Study
- Perilesional Sclerosis Associated with Dreaded Black Lines in Incomplete Atypical Femoral Fractures after Antiresorptive Therapy



In the article "Perineural and Muscular Involvement in Recurrent Diffuse Large B-Cell Lymphoma Detected by Fluorine-18 Fluorodeoxyglucose Positron Emission Tomography/Computed Tomography: A Case Report". Recurrence and suspected atypical lymphomatous involvement in neuromuscular regions. Fused positron emission tomography/computed tomography image shows a hypermetabolic right neck neuromuscular lesion over the right trapezius muscle and accessory nerve region (arrow).

In the article "Revisiting Preoperative Evaluation of the Inferior Vena Cava in Abdominal Malignancies: A Pictorial Essay". Posterior volume-rendered contrast enhanced computed tomography image shows a left inferior vena cava with hemiazygos continuation, crossing the midline posterior to the aorta (A) and draining into the azygos-superior vena cava pathway (white arrows). Hepatic veins are visible draining separately into the right atrium (green arrow).

EDITORIAL BOARD**Editor-in-Chief**

Prof. Winnie CW Chu 朱昭穎教授

Deputy Editors-in-Chief

Prof. Dora LW Kwong 鄭麗雲教授

Dr. MK Yuen 袁銘強醫生

Associate Editors

Dr. TK Au Yong 歐陽定勤醫生

Dr. YL Chan 陳宇亮醫生

Dr. Keith WH Chiu 趙允恒醫生

Dr. Frankie PT Choi 蔡柏達醫生

Dr. Kevin KF Fung 馮建勳醫生

Dr. MH Lai 賴銘曦醫生

Dr. Elaine YP Lee 李燕蘋醫生

Dr. Victor HF Lee 李浩勳醫生

Dr. WT Ng 吳偉棠醫生

Prof. Roger KC Ngan 顏繼昌教授

Dr. Frank CS Wong 黃志成醫生

Dr. T Wong 黃婷醫生

Assistant Editors

Dr. Mark KH Chan 陳加慶醫生

Dr. TH Chow 周子豪醫生

Dr. Lilianna C Chung 鍾晴醫生

Dr. KL Hui 許嘉暖醫生

Dr. KM Lam 林嘉銘醫生

Dr. BY Lee 李葆怡醫生

Dr. YT Lee 李懿婷醫生

Dr. WI Li 李焯燁醫生

Dr. Desmond TM Tse 謝德望醫生

Dr. Barry BW Wo 胡伯衡醫生

Dr. Henry CY Wong 黃進業醫生

Honorary Statistical Adviser

Dr. Eddy KF Lam 林國輝副教授

Honorary Chinese Translators

Dr. XB Qiu 丘熹彬醫生

Prof. YX Wang 王毅翔教授

Honorary Advisers**Clinical Oncology**

Dr. Zhijian Chen, PR CHINA

Prof. Edward LW Chow, CANADA

Dr. Melvin LK Chua, National Cancer Centre, SINGAPORE

Prof. Charlotte E Coles, UNITED KINGDOM

Prof. Peter J Hoskin, UNITED KINGDOM

Prof. Spring FM Kong, HONG KONG

Dr. Nancy Lee, UNITED STATES

Dr. Simon Lo, UNITED STATES

Diagnostic Radiology

Prof. Afshin Gangi, FRANCE

Prof. PL Khong, SINGAPORE

Prof. P Liang, PR CHINA

Prof. Suresh K Mukherji, UNITED STATES

Prof. Peter L Munk, CANADA

Prof. Wilfred CG Peh, SINGAPORE

Prof. Dr. med Heinz-Peter Schlemmer, GERMANY

Prof. Marilyn Siegel, UNITED STATES

Prof. H Xue, PR CHINA

Nuclear Medicine

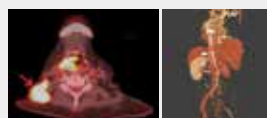
Prof. John Buscombe, UNITED KINGDOM

Prof. Richard Wahl, UNITED STATES

Prof. Oliver C Wong, UNITED STATES

Full details of the Editorial Board are

available online at

<http://hkjr.org/page/editorial-board>**COVER IMAGES**

..... SEE PAGES e32 & e46

Hong Kong Journal of Radiology is a continuation of the *Journal of the Hong Kong College of Radiologists*. This journal is dedicated to publish all aspects of clinical oncology, diagnostic radiology, and nuclear medicine.

VOLUME 29 • NUMBER 1 • MARCH 2026**Original Articles**

- e4 Treatment Outcomes of Nasopharyngeal Carcinoma in Patients Aged 80 Years or Above

CME

PW Kwok, I Yeung, WWY Tin, SY Tung

- e15 Improving Breast Cancer Detection in Screening Mammography with Artificial Intelligence Assistance: A Multi-reader Retrospective Study

CME

PL Lam, D Fenn, EH Chan, EWS Fok, PH Lee, KM Kwok, LKM Wong, WS Mak, WP Cheung, WI Sit, WK Ng, GCY Chan, LW Lo, EPY Fung

- e23 Perilesional Sclerosis Associated with Dreaded Black Lines in Incomplete Atypical Femoral Fractures after Antiresorptive Therapy

*KC Wong, GJW Cheok, SB Koh, P Chandra Mohan, MA Png, TS Howe, YH Ng***Case Reports**

- e30 Perineural and Muscular Involvement in Recurrent Diffuse Large B-Cell Lymphoma Detected by Fluorine-18 Fluorodeoxyglucose Positron Emission Tomography/Computed Tomography: A Case Report

JHY Lau, KK Ng, BT Kung

- e34 Urachal Adenocarcinoma in a Young Adult: A Rare Case Report

LLA Chan, IS Bandong

- e38 Salvaging Inadvertent Subintimal Stenting with Double-Barrel Subintimal Stenting: A Case Report

*ES Lo, SC Woo, SKH Wong, LF Cheng, KM Chan, WK Ng***Pictorial Essay**

- e44 Revisiting Preoperative Evaluation of the Inferior Vena Cava in Abdominal Malignancies: A Pictorial Essay

*A Mandava, V Koppula, M Kandati, AK Reddy, H Kacharagadla, SR Thammineedi*When citing this journal, abbreviate as **Hong Kong J Radiol.**



Submit through **HKAMedTrack**, a secure online manuscript submission and review system, which facilitates communication and access to manuscripts for authors, reviewers, and editors

www.hkamedtrack.org/hkjr

A screenshot of the HKJR website's HKAMedTrack interface. The page has a purple header with the text "HONG KONG JOURNAL OF RADIOLOGY" and "Official Publication of the Hong Kong College of Radiologists". Below the header is a navigation bar with links: Home, Journal Overview, Submit a Paper, Register, Guide for Author, Login, Help, and Contact Us (with an envelope icon). The main content area is divided into three columns. The left column features a thumbnail of the HKJR journal cover, the URL <http://www.hkjr.org>, the 2024 Journal Impact Factor (0.2), and a list of indexing services: Embase / Excerpta Medica, Index Copernicus, and SCOPUS. The middle column contains a welcome message, a "Guide for Author" link, a "LOGIN" section with input fields for "Login:" and "Password:" and a "SUBMIT" button, and links for "Register (for first-time user)" and "Forgot Your Password". The right column provides instructions for "FIRST-TIME USER" and "REGISTERED USER", including a note about not re-registering and instructions on how to change a username and password. The HKAMedTrack logo is positioned at the bottom right of the page.

Complete author instructions can be found on the HKJR website <www.hkjr.org> and the **HKAMedTrack** website <www.hkamedtrack.org/hkjr>.

All submissions have to be made through **HKAMedTrack**.



HONG KONG COLLEGE OF RADIOLOGISTS

Office Bearers

President

Dr. YC Wong 王耀忠醫生

Senior Vice-President

Dr. KK Yuen 袁國強醫生

Vice-President

Dr. Danny HY Cho 曹慶恩醫生

Warden

Dr. WL Poon 潘偉麟醫生

Honorary Treasurer

Dr. KO Lam 林嘉安醫生

Honorary Secretary

Dr. Kevin KF Fung 馮建勳醫生

Council Members

Dr. Keith WH Chiu 趙允恒醫生
Dr. James CH Chow 周重行醫生
Dr. WY Ho 何偉然醫生
Dr. KY Kwok 郭啟欣醫生
Dr. MH Lai 賴銘曦醫生
Dr. Hector TG Ma 馬天競醫生
Dr. Inda S Soong 宋崧醫生
Dr. SC Wong 黃思進醫生
Dr. SM Yu 余燊明醫生

Immediate Past President

Dr. CK Law 羅振基醫生

Founding President & Senior Advisor

Dr. Lilian LY Leong 梁馮令儀醫生

Honorary Legal Advisor

Mrs. Mabel M Lui 呂馮美儀女士

Honorary Auditor

Mr. Charles Chan 陳維端先生

Executive Officers

Ms. Karen Law 羅雅儀小姐
Ms. Phyllis Wong 黃詩汝小姐

Hong Kong Journal of Radiology

Aims and Editorial Policy

Hong Kong Journal of Radiology 香港放射科醫學雜誌 is the official peer-reviewed academic journal of Hong Kong College of Radiologists, a founder College of the Hong Kong Academy of Medicine. The Journal is published online quarterly and is indexed in EMBASE/*Excerpta Medica*, SCOPUS, Emerging Sources Citation Index, and Index Copernicus. Papers are published on all aspects of diagnostic imaging, clinical oncology, and nuclear medicine, including original research, editorials, review articles, and case reports. Papers on radiological protection, quality assurance, audit in radiology, and matters related to radiological training or education are included.

All papers submitted are subject to peer review, and the Editorial Board reserves the right to edit papers in preparation for publication in the Journal. Authors are asked to refer to the *Information for Authors* published in each issue of the Journal, regarding the style and presentation of their articles. Failure to do so may result in rejection of their papers by the Editorial Board.

Manuscripts should be submitted online via the HKAMedTrack <www.hkamedtrack.org/hkjr>. Correspondence should be sent to:

Managing Editor, HKJR Editorial Office
c/o Hong Kong Academy of Medicine Press
10/F, Hong Kong Academy of Medicine Jockey Club Building
99 Wong Chuk Hang Road, Aberdeen, Hong Kong
Tel: (852) 2871 8809; Fax: (852) 2515 9061
Email: hkjr@hkam.org.hk

Advertisements

Correspondence concerning advertisements should be addressed to:

Executive Assistant
Hong Kong College of Radiologists
Room 909, 9/F Hong Kong Academy of Medicine Jockey Club Building
99 Wong Chuk Hang Road, Aberdeen, Hong Kong.
Tel: (852) 2871 8788; Fax: (852) 2554 0739
Email: hkjr@hkcr.org

Reprints

Reprints of individual articles are available to authors only. Reprints in large quantities (non-authors), for commercial or academic use, may be purchased from the publisher. For information and prices, please send an email to: hkjr@hkam.org.hk.

Copyright

On acceptance of an article by the Journal, the corresponding author will be asked to transfer copyright of the article to the College. The Copyright Transfer Assignment Form will be sent to the author at the time of acceptance.

Disclaimer

Hong Kong Journal of Radiology and the publisher do not guarantee, directly or indirectly, the quality or efficacy of any product or service described in the advertisements or other material which is commercial in nature in this issue. All articles published, including editorials and letters, represent the opinions of the authors and do not reflect the official policy of the Journal, Hong Kong College of Radiologists, the publisher, or the institution with which the author is affiliated, unless this is clearly specified.

Copyright © 2026

Hong Kong Journal of Radiology is copyrighted by Hong Kong College of Radiologists. No part of this publication may be reproduced, stored in any retrieval system, or transmitted in any form or by any means, electronic, mechanical, photocopying, recording, or otherwise, without prior written permission from the copyright owner, except where noted.

Hong Kong Journal of Radiology
Online ISSN: 2307-4620

Treatment Outcomes of Nasopharyngeal Carcinoma in Patients Aged 80 Years or Above

PW Kwok, I Yeung, WWY Tin, SY Tung

Department of Clinical Oncology, Tuen Mun Hospital, Hong Kong SAR, China

ABSTRACT

Introduction: Optimal treatment for nasopharyngeal carcinoma (NPC) in patients aged 80 years or above remains controversial due to concerns about the tolerability of radical radiotherapy (RT). This study evaluated treatment outcomes and toxicities in octogenarians with NPC in Hong Kong.

Methods: This retrospective analysis included patients aged 80 years or above with NPC treated at a single institution in Hong Kong between January 2009 and December 2023. Patients with distant metastases at diagnosis were excluded. Patient characteristics, treatment outcomes, and toxicities were analysed.

Results: A total of 42 patients (median age, 83 years; range, 80-94) were included. The median follow-up duration was 20.3 months. In the entire cohort, the median overall survival (OS) was 22.8 months (95% confidence interval [95% CI] = 14.6-30.9) and the 5-year OS rate was 23.8%. Twenty-seven patients (64.3%) received radical RT using intensity-modulated radiotherapy (IMRT); none received chemotherapy. Among these patients (Cohort A), the median OS was 41.3 months (95% CI = 27.7-55.0), while the 5-year OS and cancer-specific survival rates were 38.1% and 74.2%, respectively. Grade ≥ 3 acute toxicities occurred in 22.2% of patients; one patient (3.7%) died due to treatment-related toxicity. Treatment failure occurred in five patients (18.5%), all due to distant metastases. Among patients who received non-radical RT (Cohort B), the median OS was 12.8 months (95% CI = 10.9-14.7), and none survived beyond 5 years. Most deaths in Cohort A (57.9%) were unrelated to NPC, whereas the majority in Cohort B (66.7%) were NPC-related.

Conclusion: In appropriately selected patients aged 80 years or above with NPC, radical RT using modern IMRT techniques is a viable treatment option, offering reasonable survival outcomes and an acceptable toxicity profile. Chronological age alone should not be regarded as a barrier to radical treatment in NPC.

Key Words: Nasopharyngeal carcinoma; Octogenarians; Radiotherapy

Correspondence: Dr PW Kwok, Department of Clinical Oncology, Tuen Mun Hospital, Hong Kong SAR, China
Email: kwokpw@ha.org.hk

Submitted: 1 July 2025; Accepted: 18 December 2025.

Contributors: All authors designed the study. PWK and IY acquired and analysed the data. PWK drafted the manuscript. PWK, WWYT and SYT critically revised the manuscript for important intellectual content. All authors had full access to the data, contributed to the study, approved the final version for publication, and take responsibility for its accuracy and integrity.

Conflicts of Interest: All authors have disclosed no conflicts of interest.

Funding/Support: This research received no specific grant from any funding agency in the public, commercial, or not-for-profit sectors.

Data Availability: All data generated or analysed during the present study are available from the corresponding author on reasonable request.

Ethics Approval: This study was approved by the Central Institutional Review Board of Hospital Authority, Hong Kong (Ref No.: CIRB-2024-421-1). The requirement for informed consent was waived by the Board due to the retrospective nature of the study.

Supplementary Material: The supplementary material was provided by the authors and some information may not have been peer reviewed. Any opinions or recommendations discussed are solely those of the author(s) and are not endorsed by the Hong Kong College of Radiologists. The Hong Kong College of Radiologists disclaims all liability and responsibility arising from any reliance placed on the content. To view the file, please visit the journal online (<https://doi.org/10.12809/hkjr2518007>).

中文摘要

80歲或以上鼻咽癌患者的治療結果

郭伯維、楊溢、佃穎恩、董煜

引言：對於年滿80歲或以上的鼻咽癌患者，其最佳治療方案仍具爭議，主要源於對根治性放射治療耐受性的顧慮。本研究旨在評估本港80歲或以上鼻咽癌患者的治療成效及相關毒性。

方法：本回顧性研究分析一所醫院於2009年1月至2023年12月期間治療的80歲或以上鼻咽癌患者資料。診斷時已出現遠處轉移者予以排除。研究分析內容包括患者特徵、治療成效及毒性情況。

結果：本研究共納入42名患者（年齡中位數83歲，介乎80至94歲），中位隨訪時間為20.3個月。整體患者的中位總生存期為22.8個月（95%置信區間：14.6-30.9），5年總生存率為23.8%。其中27名患者（64.3%）接受以調強放射治療進行的根治性放療，無人接受化療。在該組患者（A組）中，中位總生存期為41.3個月（95%置信區間：27.7-55.0），5年總生存率及癌症特異性生存率分別為38.1%及74.2%。3級或以上急性毒性發生率為22.2%；1名患者（3.7%）因治療相關毒性死亡。共有5名患者（18.5%）出現治療失敗，均為遠處轉移所致。接受非根治性放療的患者（B組）其中位總生存期為12.8個月（95%置信區間：10.9-14.7），且無人存活超過5年。A組多數死亡個案（57.9%）與鼻咽癌無關，而B組大多數死亡個案（66.7%）則與鼻咽癌相關。

結論：對於經審慎篩選的80歲或以上鼻咽癌患者，採用現代調強放射治療技術進行根治性放療屬可行治療選項，可帶來合理的生存成效及可接受的毒性水平。年齡本身不應被視為接受根治性治療的障礙。

INTRODUCTION

Nasopharyngeal carcinoma (NPC) is an epithelial carcinoma originating from the nasopharyngeal mucosa. This malignancy is most prevalent in Asia, accounting for over 80% of global incident cases in 2022.¹ In endemic regions, NPC incidence peaks in the 45-59 years age-group and declines thereafter.² Data from the Hong Kong Cancer Registry indicate that in 2023, approximately 4.9% of new NPC cases occurred in patients aged 80 years or above.³

Standard treatment for NPC involves high-dose radical radiotherapy (RT) of 66 to 70 Gy, often combined with concurrent, induction, and/or adjuvant chemotherapy for locally advanced disease.^{4,5} However, these treatment guidelines are largely based on clinical studies that have underrepresented or excluded older adult populations. For instance, in a meta-analysis of chemotherapy in NPC, only 13% of the cohort was aged 60 years or above.⁶

Older adults with NPC have worse survival outcomes compared to their younger counterparts.⁵ Previous studies have reported 5-year overall survival (OS)

rates ranging from 44% to 60% among patients aged 70 years or above with NPC,⁷⁻⁹ whereas those aged 80 years or above exhibit a considerably lower survival rate of approximately 30%.¹⁰ Treating older adults with NPC presents particular challenges due to increased comorbidities, nutritional issues, organ dysfunction, and greater susceptibility to treatment-related toxicities.¹¹ Despite these clinical challenges, studies specifically addressing treatment outcomes and strategies in older adults with NPC remain limited. Furthermore, inconsistencies exist regarding the definition of ‘older adults’ or ‘elderly’ across published studies, with age thresholds typically ranging from 65 to 70 years.^{7-10,12,13} Notably, outcomes for the oldest patients with NPC, specifically those aged 80 years or above, are rarely reported. These much older patients may represent a distinct subgroup, even within the broader geriatric population. Huang et al¹⁰ reported that patients aged 80 years or above with NPC had significantly worse survival than those aged 65 to 69 years. This study aimed to investigate treatment patterns and survival outcomes in older adults aged 80 years or above with NPC in Hong Kong.

METHODS

Patient Characteristics

We conducted a retrospective review of the medical records of patients with NPC who received care at Tuen Mun Hospital between 1 January 2009 and 31 December 2023. Patients aged 80 years or above at diagnosis with histologically confirmed NPC were included. Those with distant metastasis at initial diagnosis were excluded. Data on demographics, disease status, co-morbidities, and treatment outcomes were retrieved from electronic patient records and analysed. Patients were categorised into those who received radical RT to the nasopharynx (Cohort A) and those who did not (Cohort B).

Staging and Evaluation

Patients underwent clinical evaluation, including history taking and physical examination. Local and regional staging was performed using magnetic resonance imaging of the nasopharynx and neck and/or computed tomography. Between 2009 and 2017, positron emission tomography–computed tomography (PET-CT) was selectively performed in patients with symptoms, laboratory abnormalities, or chest radiograph findings suggestive of distant metastasis. From 2018 onwards, PET-CT has been routinely performed for all patients with tumour (T) stage T4, nodal (N) stage N3, or T3N2 disease, as well as those with clinical suspicion of metastatic disease, in accordance with Hospital Authority (HA) standard indications.

NPC staging was performed according to the 8th edition of the American Joint Committee on Cancer (AJCC) staging manual.¹⁴ Patients diagnosed prior to the introduction of the AJCC 8th edition were retrospectively re-staged. Patient performance status was assessed using the Karnofsky Performance Status (KPS) Scale.¹⁵ Co-morbidities and overall health status were retrospectively evaluated using the Adult Comorbidity Evaluation–27 (ACE-27),¹⁶ the Charlson Comorbidity Index (CCI),¹⁷ and the modified Frailty Index–11 (mFI-11).¹⁸

Radiotherapy

All patients who received radical RT underwent intensity-modulated radiotherapy (IMRT). Patients were immobilised in the supine position using a thermoplastic cast applied to the head and shoulders. A non-contrast simulation computed tomography scan was acquired and fused with the diagnostic magnetic resonance imaging scan. Target volumes were contoured according to international guidelines.^{19,20} The gross tumour volume encompassed the primary tumour and enlarged lymph

nodes. Clinical target volumes (CTVs) were defined as high-risk, intermediate-risk, and low-risk CTVs. The high-risk CTV included the gross tumour volume plus a 5-mm margin and the whole nasopharynx. The intermediate-risk CTV included the high-risk CTV plus a 5-mm margin and was expanded to cover sites at risk of microscopic extension, as well as the involved nodal levels. The low-risk CTV included uninvolved but potentially at-risk nodal levels. Prescribed doses to the high-, intermediate-, and low-risk CTVs were 70 Gy, 60 Gy, and 54 Gy, respectively, delivered in 33 daily fractions using the simultaneous integrated boost technique. A 3-mm margin from CTV to planning target volume was added to account for setup uncertainty. The planning target volume was subsequently cropped 3 mm from the external body contour, and midline avoidance structures were created to minimise skin and mucosal toxicities.

Treatment Evaluation and Follow-up

Patients undergoing radical RT were monitored weekly during treatment. RT-related toxicities were prospectively recorded and graded according to the National Cancer Institute Common Terminology Criteria for Adverse Events, version 5.0.²¹ Treatment response evaluations were conducted 8 to 12 weeks after completion of RT and included physical examination and nasopharyngoscopy. For patients treated after 2021, routine magnetic resonance imaging of the nasopharynx and neck was also performed in addition to physical examination and nasopharyngoscopy. Patients were subsequently followed up at regular 3- to 6-month intervals by oncologists and otolaryngologists. Each visit included a clinical examination and nasopharyngoscopy. Further investigations (e.g., imaging and blood tests) were performed when recurrence was suspected.

Cause-of-Death Analysis

Causes of death were determined from electronic medical records and classified into four categories: (1) NPC-related death, defined as death resulting from the primary NPC or its metastases; (2) treatment-related death, defined as death due to complications arising from NPC treatment; (3) non-NPC death, defined as death from causes unrelated to the cancer or its treatment; and (4) unknown, defined as death for which a definitive cause could not be established based on the available clinical information. Classification as NPC-related death required the terminal event to be attributable to metastatic disease or to a documented complication of symptomatic or progressive local disease. When

competing causes were present, the primary cause was determined based on clinical documentation, imaging findings, and its temporal relationship to treatment. For example, aspiration pneumonia occurring with documented dysphagia secondary to progressive local NPC was classified as an NPC-related death, whereas aspiration pneumonia in the absence of documented treatment-related dysphagia or residual tumour was classified as a non-NPC death.

Statistical Analyses

OS was defined as the interval from the date of histological diagnosis to the date of death. Progression-free survival was defined as the interval from histological diagnosis to the date of disease progression (including local, regional, or distant progression) or death. Cancer-specific survival (CSS) was defined as the interval from histological diagnosis to the date of NPC-related death. Survival rates were estimated using the Kaplan–Meier method. Univariable and multivariable Cox proportional hazards regression models were used to identify factors associated with survival. Variables with $p < 0.05$ in univariable analysis and those deemed clinically relevant were considered for multivariable modelling. To reduce multicollinearity, closely related clinical variables were not included simultaneously in the multivariable model, such as individual TNM (tumour-nodal-metastatic) components and overall stage or measures of performance status and frailty. Hazard ratios (HRs) with 95% confidence intervals (95% CIs) were reported. The Mann–Whitney U test was used to compare distributions of ordinal variables between patient cohorts. For categorical variables, the Chi squared test or Fisher's exact test was applied, as appropriate. All statistical tests were two-sided, with a significance threshold of $p < 0.05$. Statistical analyses were performed using SPSS (Windows version 26.0; IBM Corp, Armonk [NY], United States).

RESULTS

Patient Characteristics and Treatment

In total, 42 patients were included. Patient characteristics are summarised in Table 1. The median age was 83 years (range, 80–94) and 29 patients (69.0%) were men. Most patients presented with stage III disease (33.3%), followed by stage II (26.2%), stage IVa (19.0%), and stage I (11.9%). A higher proportion of patients in Cohort A underwent PET-CT for distant metastasis screening compared with Cohort B (29.6% vs. 6.7%). Staging information was unavailable for four patients (9.5%), all of whom were in Cohort B.

Overall, 27 patients (64.3%) received radical RT to the nasopharynx (Cohort A), while 15 patients (35.7%) did not (Cohort B) [Table 1]. Reasons for not undergoing radical RT included patient refusal ($n = 9$), concomitant malignancy ($n = 1$), and medical unfitness for radical treatment ($n = 5$). Of the 15 patients in Cohort B, two (13.3%) received palliative RT. Chemotherapy was not administered to any patients in either cohort.

Cohort A had significantly more patients with a KPS score $\geq 70\%$ compared with Cohort B. No significant differences were observed in ACE-27 scores or CCI scores. Although a higher proportion of patients in Cohort B had a mFI-11 score ≥ 0.27 (categorised as frail) compared with Cohort A, this difference was not statistically significant (Table 1).

Survival Outcome and Prognostic Factors

At the time of analysis, eight patients (19.0%) were alive. The median follow-up duration was 20.3 months (range, 1.5–138) for the entire cohort, and 28.2 months for those who were alive. The median OS was 22.8 months (95% CI = 14.6–30.9).

Among patients who received radical RT (Cohort A), the median OS was 41.3 months (95% CI = 27.7–55.0). The median CSS was not reached. The median progression-free survival was 39.6 months (95% CI = 22.4–56.7). The 5-year OS and CSS rates were 38.1% and 74.2%, respectively (Figure 1).

Among patients who did not receive radical RT (Cohort B), the median OS was 12.8 months (95% CI = 10.9–14.7) and the median CSS was 14.4 months (95% CI = 10.9–17.9). No patient in Cohort B survived to 5 years (Figure 2).

Univariable analysis identified several factors significantly associated with worse OS, including absence of radical RT (no vs. yes; HR = 5.03, $p < 0.001$), male sex (male vs. female; HR = 2.55, $p = 0.031$), advanced nodal stage (N2–3 vs. N0–N1; HR = 2.70, $p = 0.017$), advanced overall AJCC stage (stage III–IV vs. stage I–II; HR = 2.99, $p = 0.005$), poor KPS score ($< 70\%$ vs. $\geq 70\%$; HR = 3.29, $p = 0.003$), and frailty based on the mFI-11 (mFI-11 score ≥ 0.27 vs. < 0.27 ; HR = 4.22, $p = 0.010$). On multivariable analysis, no receipt of radical RT (HR = 13.33; $p = 0.006$) and male sex (HR = 3.22; $p = 0.033$) were independently associated with worse OS (Table 2).

Table 1. Baseline patient and disease characteristics.*

	Overall (n = 42)	Cohort A (Radical RT, n = 27)	Cohort B (No radical RT, n = 15)	p Value
Age, y	83 (80-94)	83 (80-92)	84 (80-94)	0.439
Sex				0.089
Male	29 (69.0%)	16 (59.3%)	13 (86.7%)	
Female	13 (31.0%)	11 (40.7%)	2 (13.3%)	
Tumour (T) stage				0.546
T1	11 (26.2%)	6 (22.2%)	5 (33.3%)	
T2	9 (21.4%)	8 (29.6%)	1 (6.7%)	
T3	15 (35.7%)	11 (40.7%)	4 (26.7%)	
T4	3 (7.1%)	2 (7.4%)	1 (6.7%)	
Missing	4 (9.5%)	0	4 (26.7%)	
Nodal (N) stage				0.485
N0	12 (28.6%)	8 (29.6%)	4 (26.7%)	
N1	16 (38.1%)	14 (51.9%)	2 (13.3%)	
N2	5 (11.9%)	3 (11.1%)	2 (13.3%)	
N3	5 (11.9%)	2 (7.4%)	3 (20.0%)	
Missing	4 (9.5%)	0	4 (26.7%)	
Overall stage				0.132
I	5 (11.9%)	3 (11.1%)	2 (13.3%)	
II	11 (26.2%)	11 (40.7%)	0	
III	14 (33.3%)	9 (33.3%)	5 (33.3%)	
IVa	8 (19.0%)	4 (14.8%)	4 (26.7%)	
Missing	4 (9.5%)	0	4 (26.7%)	
Distant metastasis screening†				
PET-CT	9 (21.4%)	8 (29.6%)	1 (6.7%)	
CT of the thorax and abdomen	2 (4.8%)	1 (3.7%)	1 (6.7%)	
Abdominal ultrasound	1 (2.4%)	0	1 (6.7%)	
Bone scan	1 (2.4%)	0	1 (6.7%)	
Chest radiograph only	25 (59.5%)	18 (66.7%)	7 (46.7%)	
None	4 (9.5%)	0	4 (26.7%)	
KPS score				< 0.001
≥70	32 (76.2%)	26 (96.3%)	6 (40.0%)	
<70	10 (23.8%)	1 (3.7%)	9 (60.0%)	
ACE-27 score				0.654
0	6 (14.3%)	4 (14.8%)	2 (13.3%)	
1	23 (54.8%)	15 (55.6%)	8 (53.3%)	
2	8 (19.0%)	6 (22.2%)	2 (13.3%)	
3	5 (11.9%)	2 (7.4%)	3 (20.0%)	
CCI score				0.796
0	22 (52.4%)	14 (51.9%)	8 (53.3%)	
1	12 (28.6%)	7 (25.9%)	5 (33.3%)	
2	5 (11.9%)	4 (14.8%)	1 (6.7%)	
≥3	3 (7.1%)	2 (7.4%)	1 (6.7%)	
mFI-11 score				0.233
<0.27 (non-frail)	38 (90.5%)	26 (96.3%)	12 (80.0%)	
≥0.27 (frail)	4 (9.5%)	1 (3.7%)	3 (20.0%)	

Abbreviations: ACE-27 = Adult Comorbidity Evaluation–27; CCI = Charlson Comorbidity Index; KPS = Karnofsky Performance Status; mFI-11 = modified Frailty Index–11; PET-CT = positron emission tomography–computed tomography; RT = radiotherapy.

* Data are shown as No. (%) or median (range).

† Statistical comparison of imaging modalities was not performed due to small cell counts.

Cause-of-Death Analysis

Among the 34 patients who died, the most common cause of death was NPC-related death (n = 15, 44.1%), followed by non-NPC death (n = 13, 38.2%). Treatment-related mortality occurred in one patient (2.9% of deaths), and the cause of death was unknown in five patients

(14.7%). The causes of death among patients who underwent radical RT (Cohort A) and those who did not (Cohort B) are summarised in Table 3. The two cohorts demonstrated distinct cause-of-death profiles. In Cohort A, the most common cause of death was non-NPC death (n = 11, 57.9%), followed by NPC-related death (n = 5,

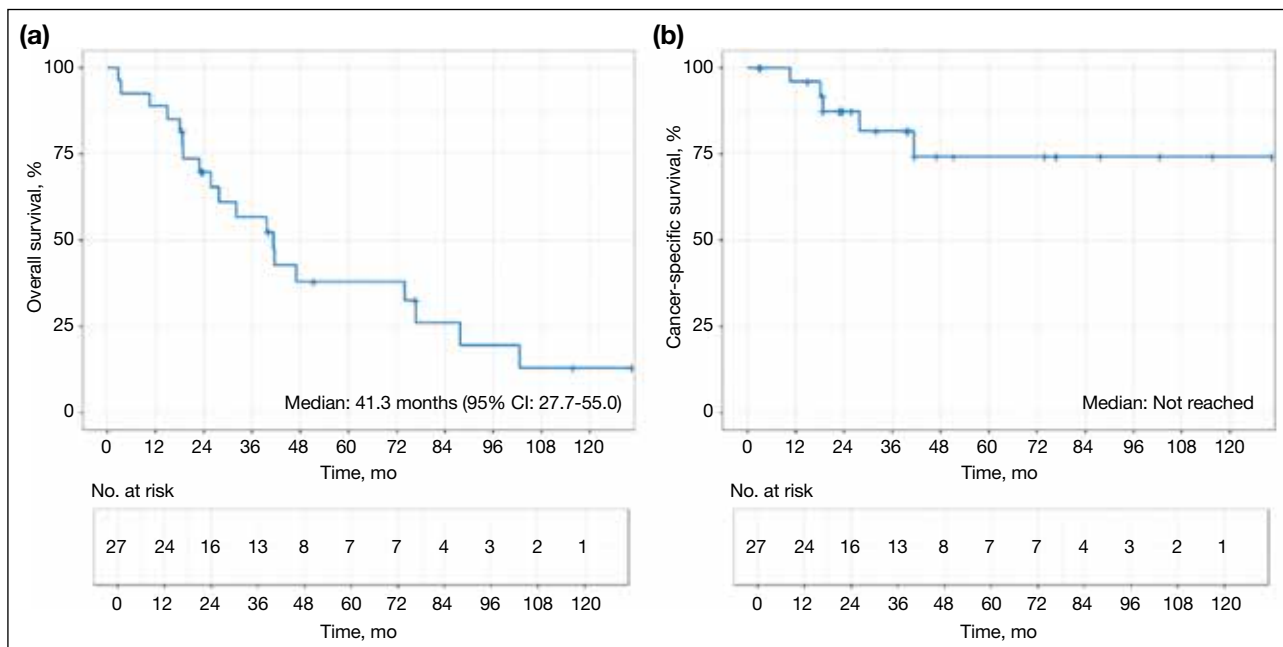


Figure 1. (a) Overall survival and (b) cancer-specific survival in Cohort A. Abbreviation: 95% CI = 95% confidence interval.

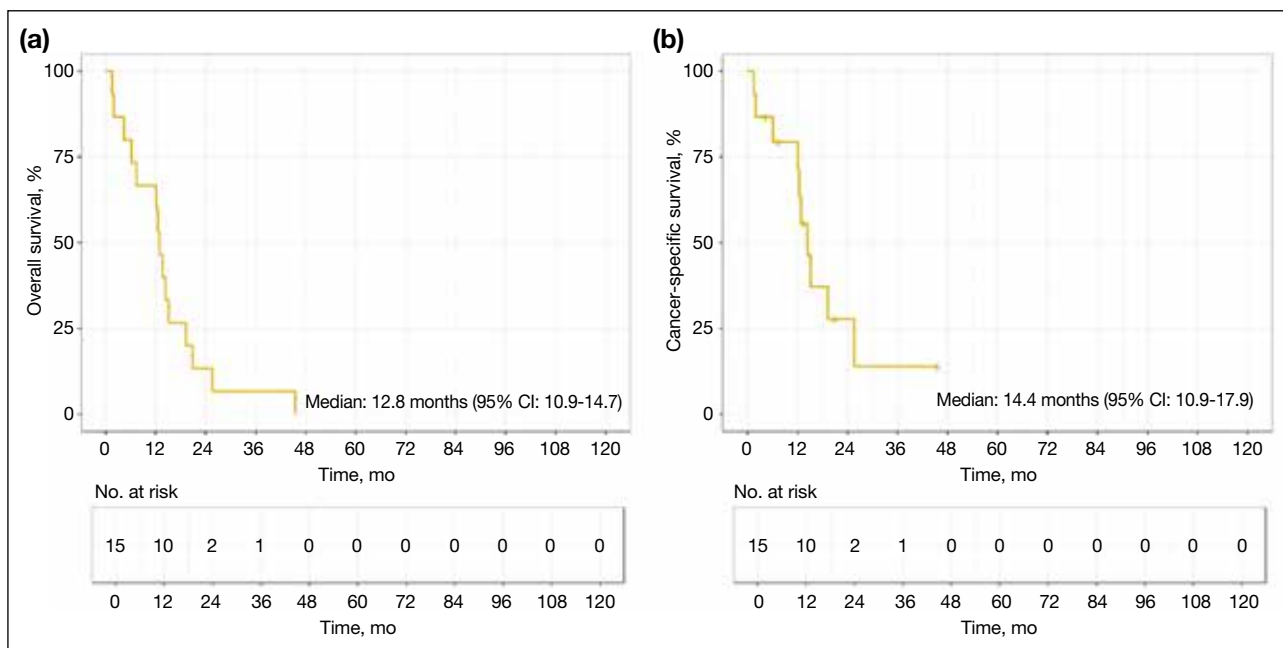


Figure 2. (a) Overall survival and (b) cancer-specific survival in Cohort B. Abbreviation: 95% CI = 95% confidence interval.

26.3%), unknown causes (n = 2, 10.5%), and treatment-related death (n = 1, 5.3%). Among patients in Cohort A who died of non-NPC causes, the median interval from the last day of RT to death was 36.9 months (interquartile range, 16.1-71.0). In Cohort B, the majority of patients

died of NPC-related causes (n = 10, 66.7%); two patients (13.3%) died of non-NPC causes and three patients (20%) died of unknown causes. Detailed descriptions of the circumstances of death for individual cases are provided in the online supplementary Table.

Table 2. Univariable and multivariable analyses of prognostic factors for overall survival.

	Univariable analysis		Multivariable analysis	
	HR (95% CI)	p Value	HR (95% CI)	p Value
Radical radiotherapy				
Yes	1.00 (reference)	N/A	1.00 (reference)	N/A
No	5.03 (2.33-10.87)	< 0.001	13.33 (2.08-83.33)	0.006
Sex				
Female	1.00 (reference)	N/A	1.00 (reference)	N/A
Male	2.55 (1.09-5.99)	0.031	3.22 (1.10-9.43)	0.033
Age, y				
80-84	1.00 (reference)	N/A	N/A	N/A
≥85	0.83 (0.41-1.69)	0.612	N/A	N/A
Tumour (T) stage				
T1-T2	1.00 (reference)	N/A	N/A	N/A
T3-T4	1.85 (0.90-3.83)	0.095	N/A	N/A
Nodal (N) stage				
N0-N1	1.00 (reference)	N/A	N/A	N/A
N2-N3	2.70 (1.19-6.10)	0.017	N/A	N/A
Overall stage				
I-II	1.00 (reference)	N/A	N/A	N/A
III-IV	2.99 (1.38-6.49)	0.005	N/A	N/A
Karnofsky Performance Status score				
≥70	1.00 (reference)	N/A	N/A	N/A
<70	3.29 (1.51-7.19)	0.003	N/A	N/A
ACE-27 comorbidity score				
<2	1.00 (reference)	N/A	N/A	N/A
≥2	1.67 (0.80-3.48)	0.173	N/A	N/A
Charlson Comorbidity Index score				
<2	1.00 (reference)	N/A	N/A	N/A
≥2	1.36 (0.54-3.40)	0.513	N/A	N/A
Modified Frailty Index-11 score				
<0.27	1.00 (reference)	N/A	N/A	N/A
≥0.27	4.22 (1.40-12.66)	0.010	N/A	N/A

Abbreviations: 95% CI = 95% confidence interval; ACE-27 = Adult Comorbidity Evaluation-27; HR = hazard ratio; N/A = not applicable.

Radical Radiotherapy

Treatment Outcomes

Among the 27 patients in Cohort A who underwent radical RT, the majority (96.3%) completed the planned course of treatment. Local treatment response to RT was documented in 22 patients; of these, 95.5% achieved a complete response. One patient had persistent disease in the nasopharynx and achieved successful salvage with brachytherapy. No local or regional relapse was observed. Five patients (18.5%) developed distant recurrence, with a median time to onset of distant metastasis of 17.6 months (range, 8.3-34.0). None of these patients received further systemic anticancer therapy for metastatic disease.

Acute and Late Treatment Toxicities

Table 4 summarises the acute toxicities observed in Cohort A. Grade ≥3 acute RT toxicities, defined as those occurring during RT or within 3 months after RT, were observed in six of 27 patients (22.2%). The

Table 3. Causes of death by treatment cohort.*

	Cohort A (Radical RT, 19 deaths)	Cohort B (No radical RT, 15 deaths)	Total (34 deaths)
NPC-related death	5 (26.3%)	10 (66.7%)	15 (44.1%)
Non-NPC death	11 (57.9%)	2 (13.3%)	13 (38.2%)
Myocardial infarction	1 (5.3%)	0	1 (2.9%)
Stroke	2 (10.5%)	0	2 (5.9%)
Chest infection	6 (31.6%)	2 (13.3%)	8 (23.5%)
Second cancer	2 (10.5%)	0	2 (5.9%)
Treatment-related death	1 (5.3%)	0	1 (2.9%)
Unknown	2 (10.5%)	3 (20.0%)	5 (14.7%)

Abbreviations: NPC = nasopharyngeal carcinoma; RT = radiotherapy.

* Data are shown as No. (%).

most frequently reported acute toxicities were mucositis (all grades, 96.3%; grade ≥3, 14.8%) and radiation dermatitis (all grades, 77.8%; grade ≥3, 3.7%). Seven patients (25.9%) required unplanned hospital admission

Table 4. Acute treatment-related toxicities in Cohort A (n = 27).*

	Any grade	Grade ≥ 3
Mucositis	26 (96.3%)	4 (14.8%)
Dermatitis	21 (77.8%)	1 (3.7%)
Dysphagia	13 (48.1%)	1 (3.7%)
Xerostomia	12 (44.4%)	0
Dysgeusia	11 (40.7%)	0
Infection [†]	1 (3.7%)	1 (3.7%)

* Data are shown as No. (%). One patient experienced both grade 3 mucositis and grade 3 dysphagia.

[†] Grade 5 chest infection occurred in one patient during week 2 of radiotherapy (after the sixth fraction).

during treatment: four for grade 3 mucositis, one for grade 3 dermatitis, one for feeding tube insertion to support nutrition in the absence of clinically significant mucositis, and one for a chest infection during the sixth RT fraction (this patient subsequently died). The fatal chest infection resulted in a treatment-related mortality rate of 3.7%. Two patients (7.4%) died within 90 days of completing RT.

Grade ≥ 3 late RT toxicities (defined as those occurring more than 3 months after RT) were observed in 14.8% of patients, the majority of which involved severe hearing loss. One patient (3.7%) required long-term feeding tube support due to dysphagia.

DISCUSSION

In this retrospective study of patients aged 80 years or above with NPC, radical RT using IMRT resulted in a median OS of 41.3 months and a 5-year OS rate of 38.1%, with manageable toxicity. To our knowledge, this is the first study to specifically evaluate treatment outcomes and toxicities in this group of patients, thereby addressing a critical knowledge gap.

The treatment of NPC in older adults is challenging and frequently overlooked, as this population is often excluded from or underrepresented in clinical trials. Older adults represent a heterogeneous group characterised by a wide range of co-morbidities and varying degrees of frailty. Management of NPC in this group is often complex, and survival outcomes are generally worse compared with those of their younger counterparts.

Yang et al⁸ reported outcomes in patients aged 70 years or above with NPC, most of whom received RT combined with chemotherapy, achieving a 5-year OS

rate of 59.5%. Notably, only 65.3% of patients in that cohort received IMRT, and most were younger than 75 years.⁸ Jin et al⁷ examined a similar cohort of patients aged 70 years or above with NPC who were treated exclusively with IMRT and reported a 5-year OS rate of 54%; however, chemotherapy was administered to 42.8% of patients, and the maximum age in that cohort was 73 years. Patients aged 80 years or above represent an especially challenging subgroup, even within the broader geriatric population. In a National Cancer Database analysis by Huang et al,¹⁰ patients aged 80 years or above with NPC who received radical RT had a 5-year OS rate of 31.3%. Toxicity outcomes were not reported in that study.

Due to prevalent co-morbidities and reduced bone marrow reserve, older patients with NPC often have limited tolerance for chemotherapy, whether administered as induction therapy or concurrently with RT. The benefit of chemotherapy in this population remains a subject of debate. While some retrospective studies have reported improved outcomes with the addition of chemotherapy to RT in older adults,^{12,22,23} others have shown no clear survival advantage.^{7,24,25} In clinical practice, chemotherapy is seldom administered to patients aged 80 years or above.⁸ Indeed, in our cohort, no patient in this age-group received chemotherapy.

High-dose RT to the head and neck region can be potentially morbid, and treatment tolerance is a significant concern, particularly among older adults. A study by Sze et al⁹ reported significantly higher rates of acute grade 3 toxicities, RT incompleteness, and 90-day mortality in patients aged 70 years or above with NPC compared with younger patients. As a result, clinicians may be hesitant to offer radical RT to patients aged 80 years or above.

Our findings demonstrated that radical RT is associated with meaningful survival outcomes in patients aged 80 years or above. Among those who received radical RT, a median OS exceeding 3 years and a 5-year OS rate of 38.1% are encouraging, suggesting that radical RT can provide reasonable survival even for octogenarians.

Our study also showed that patients who did not receive radical RT had poorer outcomes, with a median OS of only 12.8 months. However, direct survival comparisons between these two cohorts should be interpreted with caution due to important baseline differences. Patients in Cohort B had significantly worse performance status,

with a greater proportion exhibiting a KPS score below 70 compared with Cohort A. Although no significant differences were observed between cohorts in terms of co-morbidity indices, inherent disparities undoubtedly existed. These differences may introduce confounding bias, whereby the observed survival advantage of radical RT may be partially attributable to baseline patient characteristics. Despite these limitations, the considerable difference in outcomes suggests a potential benefit of radical RT in appropriately selected older adults.

Perhaps more importantly, the cause-of-death analysis offers additional insight into the potential benefit of radical RT. Among patients who received radical RT, most deaths were due to medical conditions unrelated to NPC or its treatment, whereas in the non-radical RT group, the majority of deaths were attributable to NPC progression.

These findings may assist clinicians in discussions with patients and caregivers, facilitating personalised management strategies. It is important for clinicians to recognise the potential benefits of radical RT in appropriately selected patients, ensuring that advanced age alone does not preclude access to potentially curative treatment.

IMRT has become the standard of care for NPC, providing optimal tumour coverage while sparing critical organs at risk.²⁶ It is associated with improved tumour control and a reduction in both acute and late toxicities.^{27,28} In our study, however, grade ≥ 3 acute toxicities remained common (22.2%) among patients undergoing radical RT with IMRT. It is important to recognise that older adults are at increased risk of developing severe treatment-related toxicities; all toxicities should be identified promptly and managed proactively. In particular, RT-induced mucositis and dysphagia can lead to life-threatening infectious complications, as demonstrated by the single grade 5 toxicity observed in our cohort. Intensive clinical monitoring throughout treatment—combined with appropriate supportive medications and multidisciplinary collaboration involving nurses, dietitians, and speech therapists—is essential. Vigilance in nutritional management is particularly important, as older adults may already be at high risk of sarcopenia and have limited physiological reserves.²⁹ Clinicians should maintain a low threshold for feeding tube insertion during RT, and a prophylactic approach to nutritional support may be considered.

Although the incidence of grade ≥ 3 acute toxicities was relatively high, it was not prohibitive. In our study, the rates of grade ≥ 3 dermatitis and mucositis were 3.7% and 14.8%, respectively, both of which appear lower than previously reported figures of 21.6% to 22.3% for grade ≥ 3 dermatitis and 18.9% to 68% for grade ≥ 3 mucositis.^{9,25} This difference is likely attributable to our institutional protocol, which routinely includes a 3-mm skin clip and the creation of midline structure avoidance volumes. In the present study, the treatment-related mortality rate was 3.7% and the 90-day mortality rate was 7.4%, a figure comparable to the 7.8% reported by Sze et al⁹ in patients aged above 70 years.

Late grade ≥ 3 RT toxicities were also infrequent in our study; only one patient remained dependent on a feeding tube. This observation may be partly explained by the relatively short follow-up period and limited survival duration, which may have precluded the full manifestation of late toxicities. Another contributing factor is that all patients received IMRT, which delivers a more conformal dose distribution to the target volume while better sparing adjacent normal tissues.³⁰

Although this study focuses on patients aged 80 years or above, it is essential for clinicians to recognise that chronological age alone should not serve as the sole criterion for risk stratification. Co-morbidity and frailty assessments provide critical information to guide the management of older patients with NPC. Comprehensive geriatric assessment, considered the gold standard for evaluating older adults, is recommended by both the International Society of Geriatric Oncology³¹ and the American Society of Clinical Oncology³² to support treatment decision making. However, comprehensive geriatric assessment is not widely implemented due to its time-consuming nature. Several tools are available for co-morbidity assessment, including the CCI,¹⁷ the ACE-27,¹⁶ and the mFI-11.¹⁸ Notably, both ACE-27 and CCI have been associated with survival outcomes. For example, Huang et al¹⁰ identified CCI score ≥ 2 as an independent prognostic factor for mortality, while higher ACE-27 scores have been associated with poorer survival outcomes.^{7,9,33} In our study, there was a trend towards worse survival outcomes in patients with higher CCI, ACE-27, and mFI-11 scores; however, none of these associations reached statistical significance in multivariable analysis, likely due to the small sample size.

Several questions remain unanswered. Although radical

RT of 70 Gy remains the current standard of care,⁴ it is unclear whether this ‘one-size-fits-all’ approach is appropriate for older adults with NPC. A logical consideration is RT dose de-escalation, aiming to balance optimal tumour control with minimised toxicity. Wang et al³⁴ demonstrated comparable outcomes between standard-dose RT (70 Gy) and reduced-dose RT (53–67 Gy) in patients with T1 to T3 NPC. However, there is currently no robust evidence supporting RT dose de-escalation specifically in older adults with NPC. Future studies are warranted to explore the optimal dose and fractionation schedules for this population.

Strengths and Limitations

This study has several strengths. To our knowledge, it is the first to specifically report treatment outcomes and toxicities in patients aged 80 years or above with NPC. All treatments were delivered using modern IMRT techniques, and acute and late treatment-related adverse events were prospectively documented.

This study has several important limitations. First, inherent selection bias exists in this retrospective cohort comparison, as patients who received radical RT were likely to have been healthier overall, despite similar comorbidity scores, and treatment decisions were influenced by unmeasured factors, including clinician judgement and patient preference. Second, comprehensive screening for distant metastases was not performed in some patients, particularly those who did not receive radical RT. It is therefore possible that a higher proportion of patients in Cohort B had undiagnosed stage IVb disease at presentation, which may have contributed to poorer outcomes. Third, the relatively small sample size limits the statistical power of the analysis and precludes the application of more sophisticated statistical methods, such as causal inference approaches (e.g., propensity score matching). Fourth, the follow-up duration was relatively short and some late toxicities may not yet have emerged. Fifth, formal geriatric assessments (such as comprehensive geriatric assessment) and quality-of-life evaluations were not conducted. Prospective multicentre studies with larger sample sizes, standardised geriatric assessments, and quality-of-life measurements are warranted to validate these findings and better inform clinical practice.

CONCLUSION

In appropriately selected patients aged 80 years or above with NPC, radical RT using modern IMRT techniques represents a viable treatment option, offering reasonable

survival outcomes with an acceptable toxicity profile. Chronological age alone should not be regarded as a barrier to radical treatment in NPC.

REFERENCES

1. Ferlay J, Ervik M, Lam F, Laversanne M, Colombet M, Mery L, et al. Nasopharyngeal cancer statistics. Global Cancer Observatory: Cancer Today. 2024. Available from: <https://gco.iarc.who.int/media/globocan/factsheets/cancers/4-nasopharynx-fact-sheet.pdf>. Accessed 9 Feb 2026.
2. Chang ET, Ye W, Zeng YX, Adami HO. The evolving epidemiology of nasopharyngeal carcinoma. *Cancer Epidemiol Biomarkers Prev*. 2021;30:1035-47.
3. Hospital Authority. Hong Kong Cancer Registry. Cancer statistics query system (All ages). Available from: <https://www3.ha.org.hk/cancereg/allages.asp>. Accessed 9 Feb 2025.
4. Lee VH, Lam KO, Lee AW. Chapter 10—Standard of Care for Nasopharyngeal Carcinoma (2018–2020). In: Lee AW, Lung ML, Ng WT, editors. *Nasopharyngeal Carcinoma: From Etiology to Clinical Practice*. London: Academic Press; 2019: 205-38.
5. Bossi P, Chan AT, Licitra L, Trama A, Orlandi E, Hui EP, et al. Nasopharyngeal carcinoma: ESMO-EURACAN Clinical Practice Guidelines for diagnosis, treatment and follow-up. *Ann Oncol*. 2021;32:452-65.
6. Blanchard P, Lee A, Marguet S, Leclercq J, Ng WT, Ma J, et al. Chemotherapy and radiotherapy in nasopharyngeal carcinoma: an update of the MAC-NPC meta-analysis. *Lancet Oncol*. 2015;16:645-55.
7. Jin YN, Zhang WJ, Cai XY, Li MS, Lawrence WR, Wang SY, et al. The characteristics and survival outcomes in patients aged 70 years and older with nasopharyngeal carcinoma in the intensity-modulated radiotherapy era. *Cancer Res Treat*. 2019;51:34-42.
8. Yang G, Huang J, Sun J, Wang L. Elderly nasopharyngeal carcinoma patients (aged ≥ 70 years): survival and treatment strategies. *Cancer Med*. 2023;12:19523-9.
9. Sze HC, Ng WT, Chan OS, Shum TC, Chan LL, Lee AW. Radical radiotherapy for nasopharyngeal carcinoma in elderly patients: the importance of co-morbidity assessment. *Oral Oncol*. 2012;48:162-7.
10. Huang Y, Chen W, Haque W, Verma V, Xing Y, Teh BS, et al. The impact of comorbidity on overall survival in elderly nasopharyngeal carcinoma patients: a National Cancer Data Base analysis. *Cancer Med*. 2018;7:1093-101.
11. Mascarella MA, Vendra V, Sultanem K, Tsien C, Shenouda G, Sridharan S, et al. Predicting short-term treatment toxicity in head and neck cancer through a systematic review and meta-analysis. *J Geriatr Oncol*. 2024;15:102064.
12. Liu H, Chen QY, Guo L, Tang LQ, Mo HY, Zhong ZL, et al. Feasibility and efficacy of chemoradiotherapy for elderly patients with locoregionally advanced nasopharyngeal carcinoma: results from a matched cohort analysis. *Radiat Oncol*. 2013;8:70.
13. Wen YF, Sun XS, Yuan L, Zeng LS, Guo SS, Liu LT, et al. The impact of Adult Comorbidity Evaluation–27 on the clinical outcome of elderly nasopharyngeal carcinoma patients treated with chemoradiotherapy or radiotherapy: a matched cohort analysis. *J Cancer*. 2019;10:5614-21.
14. Amin MB, Edge S, Greene F, Byrd DR, Brookland RK, Washington MK, et al (eds). *AJCC Cancer Staging Manual*. 8th ed. New York: Springer; 2017.
15. MDCalc. Karnofsky Performance Status Scale. Available from: <https://www.mdcalc.com/calc/3168/karnofsky-performance-status-scale>. Accessed 6 Feb 2026.

16. British Geriatrics Society. Adult Comorbidity Evaluation–27. Available from: https://www.bgs.org.uk/sites/default/files/content/attachment/2018-07-05/adult_comorbidity_evaluation.pdf. Accessed 6 Feb 2026.
17. MDCalc. Charlson Comorbidity Index (CCI). Available from: <https://www.mdcalc.com/calc/3917/charlson-comorbidity-index-cci>. Accessed 6 Feb 2026.
18. Evidencio. Modified Frailty Index. Available from: <https://www.evidencio.com/models/show/1777>. Accessed 6 Feb 2026.
19. Lee AW, Ng WT, Pan JJ, Poh SS, Ahn YC, AlHussain H, et al. International guideline for the delineation of the clinical target volumes (CTV) for nasopharyngeal carcinoma. *Radiother Oncol*. 2018;126:25-36.
20. Grégoire V, Ang K, Budach W, Grau C, Hamoir M, Langendijk JA, et al. Delineation of the neck node levels for head and neck tumors: a 2013 update. DAHANCA, EORTC, HKNPCSG, NCIC CTG, NCRI, RTOG, TROG consensus guidelines. *Radiother Oncol*. 2014;110:172-81.
21. United States Department of Health and Human Services. Common Terminology Criteria for Adverse Events (CTCAE) Version 5.0. 2017 Nov 27. Available from: <https://dctd.cancer.gov/research/ctep-trials/for-sites/adverse-events/ctcae-v5-5x7.pdf>. Accessed 6 Feb 2026.
22. Zeng Q, Xiang YQ, Wu PH, Lv X, Qian CN, Guo X. A matched cohort study of standard chemo-radiotherapy versus radiotherapy alone in elderly nasopharyngeal carcinoma patients. *PLoS One*. 2015;10:e0119593.
23. Lu Y, Hua J, Yan F, Jiang C, Piao Y, Ye Z, et al. Combined radiotherapy and chemotherapy versus radiotherapy alone in elderly patients with nasopharyngeal carcinoma: a SEER population-based study. *Medicine (Baltimore)*. 2021;100:e26629.
24. Lyu Y, Ni M, Zhai R, Kong F, Du C, Hu C, et al. Clinical characteristics and prognosis of elderly nasopharyngeal carcinoma patients receiving intensity-modulated radiotherapy. *Eur Arch Otorhinolaryngol*. 2021;278:2549-57.
25. Sommat K, Yit NL, Wang F, Lim JH. Impact of comorbidity on tolerability and survival following curative intent intensity modulated radiotherapy in older patients with nasopharyngeal cancer. *J Geriatr Oncol*. 2018;9:352-8.
26. Lee AW, Ng WT, Chan LL, Hung WM, Chan CC, Sze HC, et al. Evolution of treatment for nasopharyngeal cancer—success and setback in the intensity-modulated radiotherapy era. *Radiother Oncol*. 2014;110:377-84.
27. Fatima K, Andleeb A, Sofi MA, Rasool MT, Fir A, Nasreen S, et al. Clinical outcome of intensity-modulated radiotherapy versus two-dimensional conventional radiotherapy in locally advanced nasopharyngeal carcinoma: comparative study at SKIMS Tertiary Care Institute. *J Cancer Res Ther*. 2022;18:133-9.
28. Peng G, Wang T, Yang KY, Zhang S, Zhang T, Li Q, et al. A prospective, randomized study comparing outcomes and toxicities of intensity-modulated radiotherapy vs. conventional two-dimensional radiotherapy for the treatment of nasopharyngeal carcinoma. *Radiother Oncol*. 2012;104:286-93.
29. Morse RT, Ganju RG, Gan GN, Cao Y, Neupane P, Kakarala K, et al. Sarcopenia and treatment toxicity in older adults undergoing chemoradiation for head and neck cancer: identifying factors to predict frailty. *Cancers (Basel)*. 2022;14:2094.
30. Lai SZ, Li WF, Chen L, Luo W, Chen YY, Liu LZ, et al. How does intensity-modulated radiotherapy versus conventional two-dimensional radiotherapy influence the treatment results in nasopharyngeal carcinoma patients? *Int J Radiat Oncol Biol Phys*. 2011;80:661-8.
31. Wildiers H, Heeren P, Puts M, Topinkova E, Janssen-Heijnen ML, Extermann M, et al. International Society of Geriatric Oncology consensus on geriatric assessment in older patients with cancer. *J Clin Oncol*. 2014;32:2595-603.
32. Mohile SG, Dale W, Somerfield MR, Hurria A. Practical assessment and management of vulnerabilities in older patients receiving chemotherapy: ASCO Guideline for Geriatric Oncology Summary. *J Oncol Pract*. 2018;14:442-6.
33. Guo R, Chen XZ, Chen L, Jiang F, Tang LL, Mao YP, et al. Comorbidity predicts poor prognosis in nasopharyngeal carcinoma: development and validation of a predictive score model. *Radiother Oncol*. 2015;114:249-56.
34. Wang X, Wang Y, Jiang S, Zhao J, Wang P, Zhang X, et al. Safety and effectiveness of de-escalated radiation dose in T1-3 nasopharyngeal carcinoma: a propensity matched analysis. *J Cancer*. 2019;10:5057-64.

Improving Breast Cancer Detection in Screening Mammography with Artificial Intelligence Assistance: A Multi-reader Retrospective Study

PL Lam¹, D Fenn¹, EH Chan², EWS Fok³, PH Lee¹, KM Kwok², LKM Wong¹, WS Mak¹,
WP Cheung¹, WI Sit¹, WK Ng¹, GCY Chan¹, LW Lo¹, EPY Fung¹

¹Department of Diagnostic and Interventional Radiology, Kwong Wah Hospital, Hong Kong SAR, China

²Department of Diagnostic and Interventional Radiology, Princess Margaret Hospital, Hong Kong SAR, China

³Department of Radiology and Organ Imaging, United Christian Hospital, Hong Kong SAR, China

ABSTRACT

Introduction: This study aimed to compare the performance of radiologists in screening mammography for breast cancer detection, with and without artificial intelligence (AI) assistance, including subgroup comparison between breast radiologists and general radiologists in Hong Kong.

Methods: This was a single-centre multi-reader retrospective study. A screening mammography test set was used (the Hong Kong Personal Performance in Mammographic Screening Scheme), comprising 80 mammograms with negative or benign findings and 36 mammograms with pathologically proven breast cancer acquired from December 2009 to December 2023. Radiologists' performance with and without AI assistance from a commercially available tool (Lunit INSIGHT MMG) was evaluated from December 2023 to April 2024. The two reading sessions were separated by a 4-week washout period. Study endpoints included sensitivity and specificity in the mammographic detection of breast cancer. The Obuchowski–Rockette model was used to estimate and compare diagnostic accuracy.

Results: A total of 16 radiologists completed the test set, including nine (56.3%) breast radiologists and seven (43.8%) general radiologists. Without AI assistance, the overall sensitivity and specificity in breast cancer detection were 73.3% and 89.9%, respectively. With AI assistance, both metrics improved significantly to 80.7% ($p = 0.007$) and 94.3% ($p < 0.001$), respectively. Subgroup analysis showed that breast radiologists demonstrated improved specificity from 87.6% to 92.6% ($p < 0.001$), while general radiologists acquired more sensitivity from 54.0% to 66.7% ($p < 0.001$) with the use of AI.

Conclusion: AI assistance significantly improved the diagnostic accuracy of breast radiologists and general radiologists in screening mammography for breast cancer detection.

Key Words: Artificial intelligence; Breast neoplasms; Mammography; Mass screening

Correspondence: Dr PL Lam, Department of Diagnostic and Interventional Radiology, Kwong Wah Hospital, Hong Kong SAR, China
Email: lpl404@ha.org.hk

Submitted: 29 August 2024; Accepted: 9 December 2024.

Contributors: DF, EWSF and EPYF designed the study. DF, EWSF, PHL, KMK, LKMW, WSM, WPC, WIS, WKN, GCYC, LWL and EPYF acquired the data. PLL, DF, EHC, EWSF and EPYF analysed the data. PLL drafted the manuscript. All authors critically revised the manuscript for important intellectual content. All authors had full access to the data, contributed to the study, approved the final version for publication, and take responsibility for its accuracy and integrity.

Conflicts of Interest: All authors have disclosed no conflicts of interest.

Funding/Support: This research received no specific grant from any funding agency in the public, commercial, or not-for-profit sectors.

Data Availability: All data generated or analysed during the present study are available from the corresponding author on reasonable request.

Ethics Approval: This research was approved by the Central Institutional Review Board of Hospital Authority, Hong Kong (Ref No.: CIRB-2024-074-5). The requirement for informed consent from patients was waived by the Board due to the retrospective nature of the research.

Acknowledgement: The authors thank the Well Women Clinic of Tung Wah Group of Hospitals and radiologists from the Department of Diagnostic and Interventional Radiology of Kwong Wah Hospital for their support of this study.

Supplementary Material: The supplementary material was provided by the authors and some information may not have been peer reviewed. Any opinions or recommendations discussed are solely those of the author(s) and are not endorsed by the Hong Kong College of Radiologists. The Hong Kong College of Radiologists disclaims all liability and responsibility arising from any reliance placed on the content. To view the file, please visit the journal online (<https://doi.org/10.12809/hkjr2417896>).

中文摘要

利用人工智能輔助乳房X光檢查提高乳癌篩檢檢出率：一項多位閱片者回顧性研究

林栢麟、范德信、陳恩灝、霍泳珊、李璧希、郭勁明、黃嘉敏、麥詠詩、張偉彬、薛詠妍、吳詠淇、陳頌恩、羅麗雲、馮寶恩

引言：本研究旨在比較香港放射科醫生在乳房X光檢查篩檢乳癌時應用和不應用人工智能輔助兩種情況下的表現，並對乳腺放射科醫生和一般放射科醫生進行亞組比較。

方法：本研究為單中心多位閱片者回顧性研究。研究採用篩檢乳房X光攝影測試集（HKPERFORMS），此測試集包含於2009年12月至2023年12月期間採集的80例陰性或良性乳房X光攝影影像及36例經病理證實為乳癌的乳房X光攝影影像。研究於2023年12月至2024年4月期間評估了放射科醫生在應用和不應用商用人工智能輔助工具（Lunit INSIGHT MMG）兩種情況下的表現。兩次閱片之間相隔4週洗脫期。研究終點包括乳房X光攝影檢測乳癌的敏感性和特異性。我們採用Obuchowski-Rockette模型評估及比較診斷準確性。

結果：共有16位放射科醫生完成了測試集，其中9名（56.3%）為乳腺放射科醫生，7名（43.8%）為一般放射科醫生。在未使用人工智能輔助的情況下，乳癌檢測的整體敏感性和特異性分別為73.3%和89.9%。使用人工智能輔助後，這兩項指標均顯著提高，分別達到80.7%（ $p = 0.007$ ）和94.3%（ $p < 0.001$ ）。亞組分析顯示，使用人工智能後，乳腺放射科醫生的特異性從87.6%提高到92.6%（ $p < 0.001$ ），而一般放射科醫生的敏感性則從54.0%提高到66.7%（ $p < 0.001$ ）。

結論：人工能輔助顯著提高了乳腺放射科醫生和一般放射科醫生在乳癌篩檢中應用乳房X光攝影的診斷準確率。

INTRODUCTION

In Hong Kong, breast cancer has been the most common malignancy among the female population since the early 1990s, with increasing incidence every year. It accounted for over a quarter (28.9%) of new cancer cases in 2023.¹ It was also the third leading cause of cancer deaths in women.¹ Fortunately, breast cancer can be curable in its early stages, with over 95% 5-year survival for patients with stage I disease.² Previous randomised controlled trials and meta-analyses have demonstrated the efficacy of screening mammography in detecting early-stage tumours and reducing breast cancer-related deaths.³⁻⁶

Breast screening programmes have been established in multiple developed economies worldwide. In Western countries, the American Cancer Society recommends that women consider annual mammography screening starting at the age of 40 years,⁷ whereas in the United Kingdom, the National Health Service offers breast screening every 3 years for women aged between 50 and 71 years.⁸ In Asian countries, such as Japan,⁹ South

Korea¹⁰ and Singapore,¹¹ breast screening programmes have been in place for over a decade. In Hong Kong, the Centre for Health Protection recommends that women in the general population aged 44 to 69 years with an average risk of breast cancer consider mammography screening every 2 years.¹² Together with increased advocacy from non-profit organisations, which have heightened disease awareness among the public, screening mammography has become more popular.¹³

Like most tests, the diagnostic accuracy of screening mammography is not absolute. Sensitivity and specificity in breast cancer detection range between approximately 50% to 80% and about 80% to 90%, respectively, in the literature.¹⁴⁻¹⁷ False-positive results lead to additional workup and the associated anxiety in patients, while false-negative results can delay treatment and worsen prognosis.¹⁴

Recent advancements in machine learning have led to the increased use of artificial intelligence (AI) in clinical

radiology. Some studies, mainly conducted in Western countries, have shown promising results in employing AI-based tools to improve the diagnostic accuracy of screening mammography.¹⁸⁻²¹

AI-supported software has become more accessible and commercially available. To the best of our knowledge, there are no published studies evaluating the diagnostic performance of screening mammography with AI assistance in Hong Kong. The lack of established evidence in our local population could be a hurdle for radiologists to consider AI-assisted screening mammography. The external validity of previous research poses a major concern. Screening mammography tests employed in studies performed in Western countries were mainly selected from Caucasian patients.²² Asian women, on the other hand, generally have different breast composition, with a higher prevalence of dense breasts. This can obscure abnormalities on mammograms, limiting the detection of breast cancer and reducing diagnostic accuracy.²³⁻²⁵ Investigations on how AI-based tools could facilitate screening mammography using test sets derived from a local Asian population could bridge this data gap.

This study aimed to compare the performance of radiologists in screening mammography to detect breast cancer with and without AI assistance in the local population. Subgroup comparisons between breast radiologists and general radiologists were also performed.

METHODS

We developed a test set, the Hong Kong Personal Performance in Mammographic Screening Scheme (HKPERFORMS), to evaluate the diagnostic accuracy of radiologists in detecting breast cancer in the local Asian population with and without AI assistance. The test set comprised mammograms retrospectively selected from Asian adult female patients aged 40 years or above who underwent breast screening in a single well-woman clinic from December 2009 to December 2023. Exclusion criteria included symptomatic patients (e.g., those with a palpable breast mass), pregnant patients, and those with a history of breast implant augmentation surgery.

All studies in HKPERFORMS were two-dimensional (2D) screening full-field digital mammograms with standard craniocaudal and mediolateral oblique views. There were 80 mammograms showing negative or benign findings, confirmed as stable on subsequent

mammographic follow-up for at least 3 years as assessed by breast radiologists recognised by the Hong Kong College of Radiologists (HKCR). There were 36 mammograms with pathologically proven breast cancer, including invasive ductal carcinoma, invasive lobular carcinoma, and ductal carcinoma in situ. Their mammographic appearances included mass (n = 21, 58.3%), calcifications (n = 6, 16.7%), architectural distortion (n = 5, 13.9%), and asymmetry (n = 4, 11.1%). The mammograms in the test set (n = 116) included breasts of varying densities: extremely dense (13.8%), heterogeneously dense (72.4%), scattered areas of fibroglandular density (12.1%), and almost entirely fatty (1.7%) [Figure 1]. Patient information and identifiers, such as name and age, were anonymised before compiled into the HKPERFORMS test set (Figure 2).

Reader Assessment

This was a single-centre study. Radiologists were recruited from an acute general hospital with subspecialty training in breast radiology accredited by the HKCR. They included breast radiologists and general radiologists. Breast radiologists were defined as radiologists with at least 3 months of subspecialty training recognised by the HKCR, or post-fellowship breast radiology training, and at least 500 screening mammograms read in the past year. General radiologists were defined as HKCR members or fellows actively practising in clinical radiology, but without dedicated subspecialty training in breast radiology.

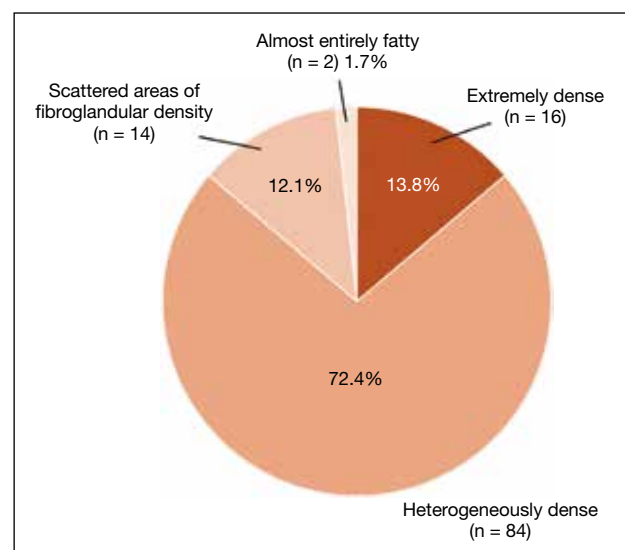


Figure 1. Proportion of breast densities in mammograms of the test set (n = 116).

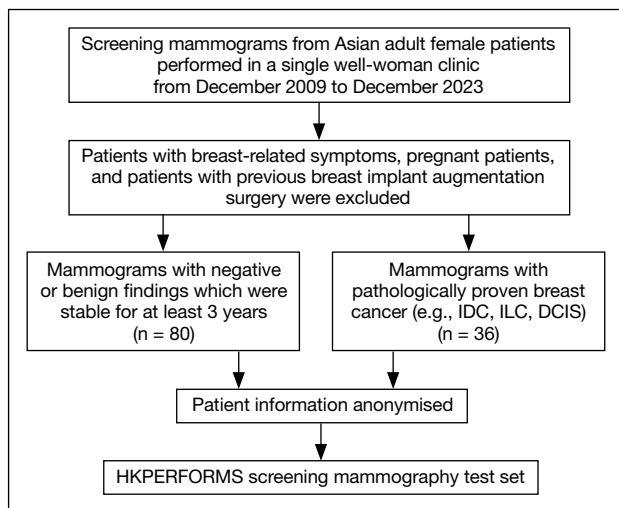


Figure 2. Development of the test set (n = 116).

Abbreviations: DCIS = ductal carcinoma in situ; HKPERFORMS = Hong Kong Personal Performance in Mammographic Screening Scheme; IDC = invasive ductal carcinoma; ILC = invasive lobular carcinoma.

The recruited radiologists were blinded to all patient information and identifiers in the HKPERFORMS screening mammography test set. They assessed the mammograms under standardised conditions using dedicated software (Selenia Dimensions version 1.11; Hologic, Bedford [MA], US) with diagnostic-quality monitors (Coronis Uniti MDMC 12133; Barco, Kortrijk, Belgium) in accordance with department standards. Readers documented their screening results digitally (SurveyMonkey; SurveyMonkey, San Mateo [CA], US). Data to be entered included breast density, laterality, quadrant, depth, and presence or absence of architectural distortion if an abnormality was identified. Respondents were required to classify each study as benign or suspicious for malignancy.

All radiologists assessed the HKPERFORMS test set twice. In the first reading, they read the screening mammograms without AI assistance. In the second reading, additional data were provided by a commercially available AI-based tool (INSIGHT MMG version 1.1.7.3; Lunit, Seoul, South Korea),²⁶ which automatically highlighted regions perceived as abnormal with a colour-coded heatmap indicating the degree of suspicion. A predicted probability of malignancy was also presented numerically (Figure 3). Both pre- and post-AI-processed mammograms were available during the second reading. Respondents were instructed to record their screening results after reviewing all images.

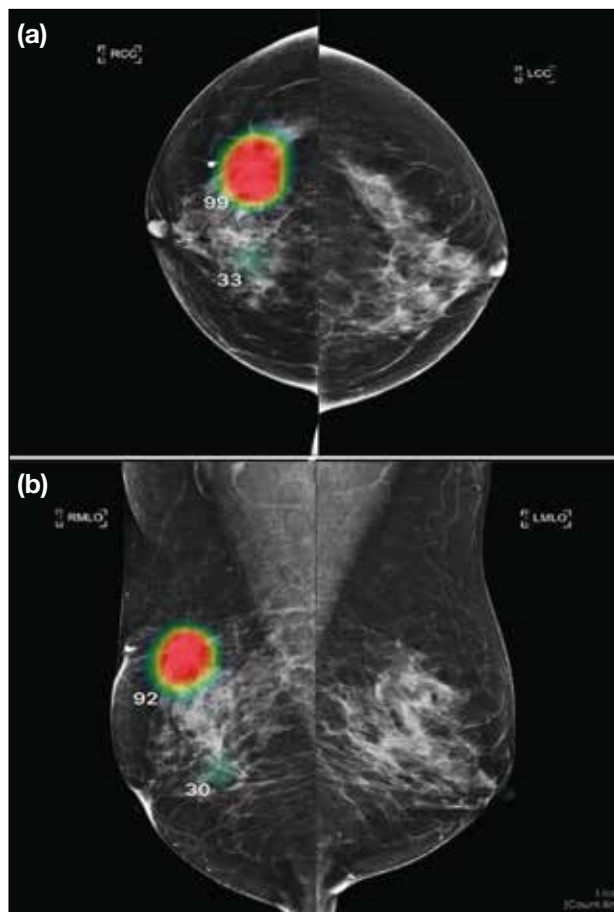


Figure 3. Screening mammogram of an adult female patient in (a) craniocaudal and (b) mediolateral oblique views with application of the artificial intelligence (AI)-based tool. A right breast upper outer quadrant mass has been colour-coded red, while central inner architectural distortion has been colour-coded green, indicating AI-perceived abnormal regions with different degrees of suspicion. Predicted probabilities of malignancy are also provided numerically. Subsequent biopsies of both lesions confirmed invasive ductal carcinoma of the right breast. The numbers on the images represent predicted probabilities of malignancy.

Abbreviations: LCC = left breast craniocaudal; LMLO = left breast mediolateral oblique; RCC = right breast craniocaudal; RMLO = right breast mediolateral oblique.

They were at liberty to follow or disregard the AI-based assessment entirely. A washout period of at least 4 weeks was observed between the two readings. The orders of the screening mammograms in the test set were different and randomised across the two sittings. Respondents who did not complete either reading were excluded from the study (Figure 4).

Background information of the recruited radiologists, including prior subspecialty training in breast radiology and experience in reporting breast imaging, was collected. All responses submitted electronically were

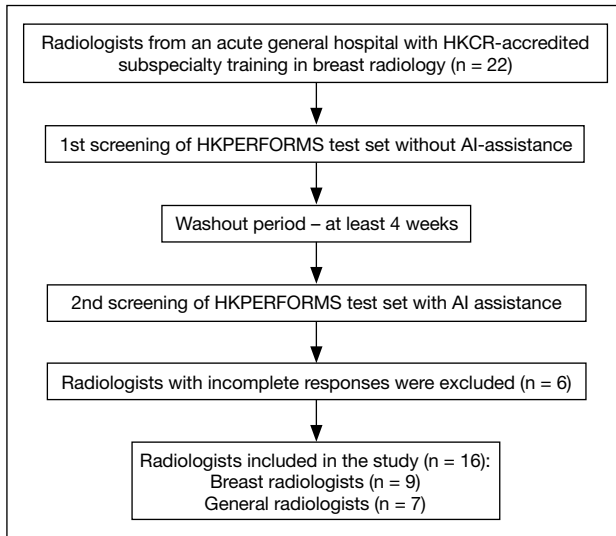


Figure 4. Assessment of screening mammograms in the test set (n = 22).

Abbreviations: AI = artificial intelligence; HKCR = Hong Kong College of Radiologists; HKPERFORMS = Hong Kong Personal Performance in Mammographic Screening Scheme.

anonymised and a random computer-generated number was assigned to each radiologist. Researchers were blinded to the identity of the respondents.

Statistical Analysis

Statistical analysis was performed using R (macOS version 4.4.1; R Core Team, Vienna, Austria).²⁷ Study endpoints of diagnostic accuracy included sensitivity and specificity in the mammographic detection of breast cancer. The Obuchowski–Rockette model was used to estimate and compare diagnostic accuracy.²⁸ A p value of < 0.05 was considered statistically significant.

This manuscript was prepared in accordance with the STROBE (Strengthening the Reporting of Observational Studies in Epidemiology) guidelines.

RESULTS

Overall Performance

A total of 22 radiologists were invited to participate in this study; six respondents who did not complete the HKPERFORMS screening mammography test set were excluded, resulting in 16 radiologists completing the test set (Figure 4). Without AI assistance, the mean sensitivity and specificity for detecting breast cancer were 73.3% and 89.9%, respectively. With AI assistance, there was significant improvement in diagnostic accuracy, with the mean sensitivity and specificity increasing to 80.7% (p = 0.007) and

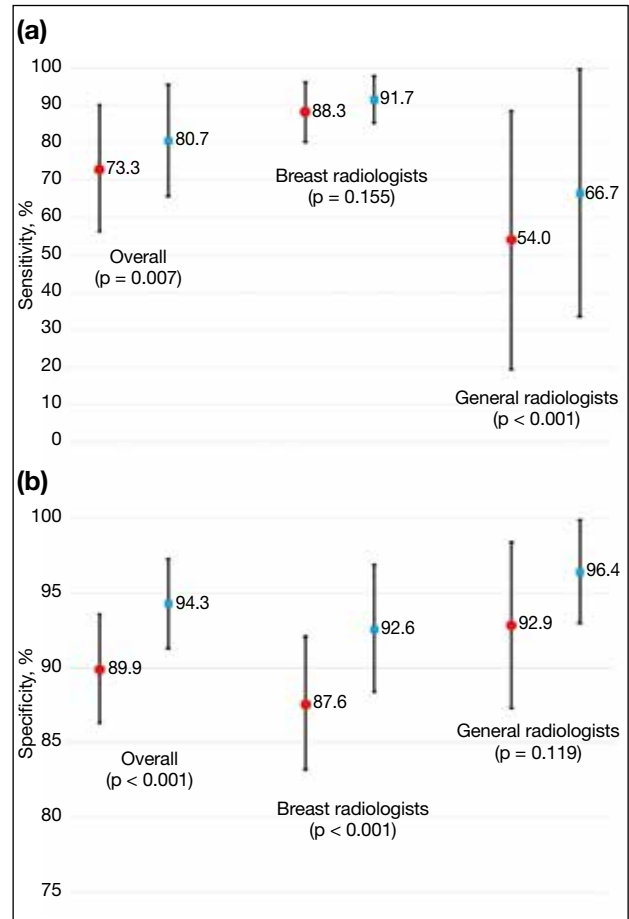


Figure 5. Dot plots and 95% confidence intervals showing (a) sensitivity and (b) specificity of all radiologists, breast radiologists, and general radiologists in screening mammography for breast cancer detection without (red circles) and with (blue squares) artificial intelligence assistance.

94.3% (p < 0.001), respectively (Figure 5 and online supplementary Table).

Subgroup Analysis

Among the respondents, nine (56.3%) were breast radiologists and seven (43.8%) were general radiologists. The experience of the breast radiologists is shown in Figure 6. Without AI assistance, the mean sensitivity of the breast radiologists (88.3%) was significantly higher than that of the general radiologists (54.0%) in identifying breast cancer (p = 0.017). There was no significant difference in the mean specificity between the two groups (breast radiologists: 87.6% vs. general radiologists: 92.9%; p = 0.051). Using the AI-based tool, there was significant improvement in the specificity of the breast radiologists (from 87.6% to 92.6%; p < 0.001) and the sensitivity of the general radiologists (from 54.0% to 66.7%; p < 0.001). No significant changes in

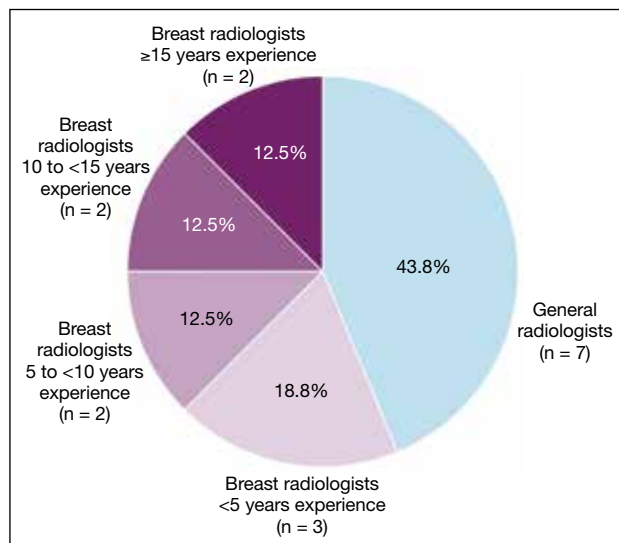


Figure 6. Proportion of breast radiologists and general radiologists included in the study (n = 16).

the sensitivity of breast radiologists and the specificity of general radiologists were observed after using the AI-based tool (Figure 5 and online supplementary Table).

DISCUSSION

Diagnostic Accuracy Without Artificial Intelligence Assistance

Without assistance from the AI-based tool, the diagnostic accuracy of the breast radiologists included in this study was comparable to figures reported in the literature, with both sensitivity and specificity exceeding 85%.¹⁵⁻¹⁷ In contrast, general radiologists were less likely to detect breast malignancy, with a sensitivity of about 54%. Screening tests with low sensitivity lead to a higher proportion of false-negative results, potentially leading to false reassurance and missed opportunities for early diagnosis and treatment.¹⁴ These findings highlight the importance of dedicated training in breast radiology.^{29,30} The HKCR Mammography Statement outlines the standards for radiologists involved in screening. These include a minimum of 3 months of subspecialty training in breast radiology, interpretation of at least 500 screening mammograms annually, and ongoing participation in continuing medical education and multidisciplinary meetings.³¹

Improved Performance with Artificial Intelligence Assistance

There were significant improvements in overall sensitivity and specificity in breast cancer detection when radiologists in this study performed AI-assisted

screening mammography. This echoed previous studies which demonstrated improved diagnostic accuracy in AI-assisted mammography readings.¹⁸⁻²¹ Subgroup analysis further showed that the benefits of AI assistance differed between general radiologists and breast radiologists.

For general radiologists, there was significant improvement in sensitivity, from approximately 50% when screening unaided to over 65% with the use of AI-based tool. A previous study also demonstrated reduced variability in screening results and increased inter-reader reliability with AI assistance.³² This indicates that utilising AI could yield more expertise-independent results. AI could act as an extra pair of eyes. Radiologists could refer to colour-coded heatmaps generated by AI-based software after initial mammography assessment to reduce the probability of missing breast cancer.²⁶

Among the breast radiologists, there was improvement in specificity, while sensitivity in detecting breast cancer remained similar with and without AI assistance. The crux of screening lies in striking a balance between sensitivity and specificity. Tests with high sensitivity but low specificity may lead to over-investigation, resulting in unnecessary stress and interventions for patients.¹⁴ While the specificity of the breast radiologists in breast cancer detection was satisfactory without AI assistance, it improved from over 85% to over 90% with the use of the AI-based tool without compromising sensitivity. Increased specificity in screening mammography would reduce call-back rates, avoid unwarranted workups for patients, and decrease the workload for radiologists.^{20,33} A study by Raya-Povedano et al³⁴ revealed a reduction of over 70% in radiologists' workload following the implementation of AI-based strategies. Additionally, AI tools could be helpful to prioritise screening mammograms with suspected malignancy. Such abnormal studies could be flagged for earlier reporting by radiologists, expediting subsequent workup and treatment. Furthermore, placing flagged studies at the beginning of a screening session could minimise the risk of missed breast cancers due to reader fatigue. With the burgeoning demand for screening mammography in Hong Kong, AI-based tools could potentially alleviate the stress faced by radiologists.

Limitations

The HKPERFORMS test set was enriched with abnormal mammograms, and the proportion of cases with biopsy-proven breast cancer was not representative of routine screening practice or the general population.^{1,2}

Although respondents were instructed to interpret each individual mammogram as an independent screening case, their diagnostic accuracy might have been negatively influenced by the study design. Second, test sets used in the sittings with and without AI assistance were identical. Despite a washout period of at least 4 weeks with randomisation of the image order, radiologists might have recalled the proportion of normal to abnormal cases, potentially introducing bias in the second sitting. Third, all mammograms in the test set were 2D full-field digital mammograms. In recent years, three-dimensional mammography or digital breast tomosynthesis (DBT) has become more popular, with evidence showing improved diagnostic accuracy compared with traditional 2D mammography. Studies on AI-assisted DBT have shown non-inferior or improved sensitivity and specificity in detecting breast cancer.^{35,36} Our study did not investigate DBT performance, which remains a potential direction for further research. Finally, this was a single-centre study with limited sample size. The performance and influence of AI may vary among radiologists with differing levels of experience across diverse clinical settings. Further large-scale multi-centre investigations would provide a more comprehensive assessment.

CONCLUSION

This multi-reader study evaluated the potential of AI to aid breast cancer detection using HKPERFORMS, an original screening mammography test set developed from a local Asian female population with a high incidence of dense breasts. The results demonstrated that diagnostic accuracy in screening mammography was improved across radiologists with varying levels of experience in breast radiology when supported by AI-based tools.

REFERENCES

1. Centre for Health Protection, Department of Health, Hong Kong SAR Government. Breast Cancer. 23 Jan 2026. Available from: <https://www.chp.gov.hk/en/healthtopics/content/25/53.html>. Accessed 2 Feb 2026.
2. Kwong A, Mang OW, Wong CH, Chau WW, Law SC; Hong Kong Breast Cancer Research Group. Breast cancer in Hong Kong, Southern China: the first population-based analysis of epidemiological characteristics, stage-specific, cancer-specific, and disease-free survival in breast cancer patients: 1997-2001. *Ann Surg Oncol*. 2011;18:3072-8.
3. Moss SM, Cuckle H, Evans A, Johns L, Waller M, Bobrow L, et al. Effect of mammographic screening from age 40 years on breast cancer mortality at 10 years' follow-up: a randomised controlled trial. *Lancet*. 2006;368:2053-60.
4. Duffy SW, Tabár L, Chen HH, Holmqvist M, Yen MF, Abdsalah S, et al. The impact of organized mammography service screening on breast carcinoma mortality in seven Swedish counties. *Cancer*. 2002;95:458-69.
5. Tabár L, Vitak B, Chen HH, Yen MF, Duffy SW, Smith RA. Beyond randomized controlled trials: organized mammographic screening substantially reduces breast carcinoma mortality. *Cancer*. 2001;91:1724-31.
6. Kerlikowske K, Grady D, Rubin SM, Sandrock C, Ernster VL. Efficacy of screening mammography. A meta-analysis. *JAMA*. 1995;273:149-54.
7. American Cancer Society. American Cancer Society recommendations for the early detection of breast cancer. Available from: <https://www.cancer.org/cancer/types/breast-cancer/screening-tests-and-early-detection/american-cancer-society-recommendations-for-the-early-detection-of-breast-cancer.html>. Accessed 20 Aug 2024.
8. National Health Service, Department of Health and Social Care, United Kingdom Government. Breast screening (mammogram). Available from: <https://www.nhs.uk/conditions/breast-screening-mammogram/>. Accessed 20 Aug 2024.
9. Hamashima CC, Hattori M, Honjo S, Kasahara Y, Katayama T, Nakai M, et al. The Japanese guidelines for breast cancer screening. *Jpn J Clin Oncol*. 2016;46:482-92.
10. Shin DW, Yu J, Cho J, Lee SK, Jung JH, Han K, et al. Breast cancer screening disparities between women with and without disabilities: a national database study in South Korea. *Cancer*. 2020;126:1522-9.
11. Loy EY, Molinar D, Chow KY, Fock C. National Breast Cancer Screening Programme, Singapore: evaluation of participation and performance indicators. *J Med Screen*. 2015;22:194-200.
12. Cancer Expert Working Group on Cancer Prevention and Screening, Centre for Health Protection, Department of Health, Hong Kong SAR Government. Recommendations on Prevention and Screening for Breast Cancer for Health Professionals. June 2020. Available from: https://www.chp.gov.hk/files/pdf/breast_cancer_professional_hp.pdf. Accessed 20 Aug 2024.
13. Hong Kong Breast Cancer Foundation. What is breast cancer. Available from: https://www.hkbcf.org/en/breast_cancer/main/422/. Accessed 20 Aug 2024.
14. Marmot MG, Altman DG, Cameron DA, Dewar JA, Thompson SG, Wilcox M. The benefits and harms of breast cancer screening: an independent review. *Br J Cancer*. 2013;108:2205-40.
15. Hollingsworth AB. Redefining the sensitivity of screening mammography: a review. *Am J Surg*. 2019;218:411-8.
16. Kerlikowske K, Grady D, Barclay J, Sickles EA, Ernster V. Likelihood ratios for modern screening mammography. Risk of breast cancer based on age and mammographic interpretation. *JAMA*. 1996;276:39-43.
17. Lehman CD, Wellman RD, Buist DS, Kerlikowske K, Tosteson AN, Miglioretti DL, et al. Diagnostic accuracy of digital screening mammography with and without computer-aided detection. *JAMA Intern Med*. 2015;175:1828-37.
18. Dombrower K, Crippa A, Colón E, Eklund M, Strand F; ScreenTrustCAD Trial Consortium. Artificial intelligence for breast cancer detection in screening mammography in Sweden: a prospective, population-based, paired-reader, non-inferiority study. *Lancet Digit Health*. 2023;5:e703-11.
19. Lång K, Josefsson V, Larsson AM, Larsson S, Högberg C, Sartor H, et al. Artificial intelligence-supported screen reading versus standard double reading in the Mammography Screening with Artificial Intelligence trial (MASAI): a clinical safety analysis of a randomised, controlled, non-inferiority, single-blinded, screening accuracy study. *Lancet Oncol*. 2023;24:936-44.
20. Lauritzen AD, Lillholm M, Lynge E, Nielsen M, Karssemeijer N, Vejborg I. Early indicators of the impact of using AI in mammography screening for breast cancer. *Radiology*. 2024;311:e232479.

21. Ng AY, Oberije CJ, Ambrózay É, Szabó E, Serfózó O, Karpati E, et al. Prospective implementation of AI-assisted screen reading to improve early detection of breast cancer. *Nat Med.* 2023;29:3044-9.
22. Chen Y, Gale A. Performance assessment using standardized data sets: the PERFORMS scheme in breast screening and other domains. In: Samei E, Krupinski EA, editors. *The Handbook of Medical Image Perception and Techniques*. 2nd ed. Cambridge, England: Cambridge University Press; 2018: 328-42.
23. Bao C, Shen J, Zhang Y, Zhang Y, Wei W, Wang Z, et al. Evaluation of an artificial intelligence support system for breast cancer screening in Chinese people based on mammogram. *Cancer Med.* 2023;12:3718-26.
24. Yan H, Ren W, Jia M, Xue P, Li Z, Zhang S, et al. Breast cancer risk factors and mammographic density among 12518 average-risk women in rural China. *BMC Cancer.* 2023;23:952.
25. Jackson VP, Hendrick RE, Feig SA, Kopans DB. Imaging of the radiographically dense breast. *Radiology.* 1993;188:297-301.
26. Kim HE, Kim HH, Han BK, Kim KH, Han K, Nam H, et al. Changes in cancer detection and false-positive recall in mammography using artificial intelligence: a retrospective, multireader study. *Lancet Digit Health.* 2020;2:e138-48.
27. R Core Team. *R: a language and environment for statistical computing*. Vienna: R Foundation for Statistical Computing; 2020.
28. Hillis SL, Obuchowski NA, Berbaum KS. Power estimation for multireader ROC methods: an updated and unified approach. *Acad Radiol.* 2011;18:129-42.
29. Trieu PD, Lewis SJ, Li T, Ho K, Wong DJ, Tran OT, et al. Improving radiologist's ability in identifying particular abnormal lesions on mammograms through training test set with immediate feedback. *Sci Rep.* 2021;11:9899.
30. Miglioretti DL, Gard CC, Carney PA, Onega TL, Buist DS, Sickles EA, et al. When radiologists perform best: the learning curve in screening mammogram interpretation. *Radiology.* 2009;253:632-40.
31. Hong Kong College of Radiologists. *Hong Kong College of Radiologists Mammography Statement*. Revised 25 August 2015. Available from: https://www.hkcr.org/templates/OS03C00336/case/lop/HKCR%20Mammography%20Statement_rev20150825.pdf. Accessed 20 Aug 2024.
32. Pacilè S, Lopez J, Chone P, Bertinotti T, Grouin JM, Fillard P. Improving breast cancer detection accuracy of mammography with the concurrent use of an artificial intelligence tool. *Radiol Artif Intell.* 2020;2:e190208.
33. Kim YS, Jang MJ, Lee SH, Kim SY, Ha SM, Kwon BR, et al. Use of artificial intelligence for reducing unnecessary recalls at screening mammography: a simulation study. *Korean J Radiol.* 2022;23:1241-50.
34. Raya-Povedano JL, Romero-Martín S, Elías-Cabot E, Gubern-Mérida A, Rodríguez-Ruiz A, Álvarez-Benito M. AI-based strategies to reduce workload in breast cancer screening with mammography and tomosynthesis: a retrospective evaluation. *Radiology.* 2021;300:57-65.
35. Goldberg JE, Reig B, Lewin AA, Gao Y, Heacock L, Heller SL, et al. New horizons: artificial intelligence for digital breast tomosynthesis. *Radiographics.* 2022;43:e220060.
36. Park EK, Kwak S, Lee W, Choi JS, Kooi T, Kim EK. Impact of AI for digital breast tomosynthesis on breast cancer detection and interpretation time. *Radiol Artif Intell.* 2024;6:e230318.

ORIGINAL ARTICLE

Perilesional Sclerosis Associated with Dreaded Black Lines in Incomplete Atypical Femoral Fractures after Antiresorptive Therapy

KC Wong¹, GJW Cheok¹, SB Koh¹, P Chandra Mohan², MA Png², TS Howe¹, YH Ng¹

¹Department of Orthopaedic Surgery, Singapore General Hospital, Singapore

²Department of Diagnostic Radiology, Singapore General Hospital, Singapore

ABSTRACT

Introduction: This study aimed to describe the demographic, clinical, and radiological features of sclerosis adjacent to 'dreaded black lines' or radiolucent fracture lines (RFLs) in atypical femoral fractures (AFFs) associated with antiresorptive therapy.

Methods: We reviewed radiographs acquired in our institution in Singapore between 2004 and 2020 from 100 femurs with AFFs, assessing the appearance and location of lesions, and the presence of endosteal or periosteal thickening. Demographic data, type and duration of antiresorptive therapy, and progression to complete fracture or need for prophylactic stabilisation were analysed. The cohort was subdivided into three groups: Group 1A included AFFs with an RFL and perilesional sclerosis; Group 1B included AFFs with an RFL but without perilesional sclerosis; and Group 2 included AFFs without an RFL.

Results: A total of 17 sclerotic RFLs were identified. The majority were non-linear in appearance. Most were located in the subtrochanteric (41.2%) and proximal diaphyseal regions (35.3%), and all were associated with endosteal or periosteal thickening. All sclerotic RFLs occurred in patients with a mean age of 69 years. Sixteen cases (94.1%) had a history of bisphosphonate use, while one case had received denosumab. The mean duration of antiresorptive therapy was 66 months. Three cases (17.6%) progressed to complete fractures and six (35.3%) required prophylactic fixation. No significant differences were observed among the three groups in terms of demographics, antiresorptive therapy, or surgical intervention.

Conclusion: We describe perilesional sclerosis as a previously unrecognised radiological feature adjacent to RFLs in AFFs, with distinctive characteristics. It occurs in approximately one-third of RFLs. Further research is needed to elucidate its pathophysiological and prognostic implications.

Key Words: Bisphosphonates; Femoral fractures; Sclerosis

Correspondence: Dr KC Wong, Department of Orthopaedic Surgery, Singapore General Hospital, Singapore
Email: khaicheong.wong@mohh.com.sg

Submitted: 12 June 2024; Accepted: 8 September 2025.

Contributors: SBK and TSH designed the study. KCW and GJWC acquired and analysed the data. All authors drafted the manuscript and critically revised the manuscript for important intellectual content. All authors had full access to the data, contributed to the study, approved the final version for publication, and take responsibility for its accuracy and integrity.

Conflicts of Interest: All authors have disclosed no conflicts of interest.

Funding/Support: This research received no specific grant from any funding agency in the public, commercial, or not-for-profit sectors.

Data Availability: All data generated or analysed during the present study are available from the corresponding author on reasonable request.

Ethics Approval: This research was approved by the SingHealth Centralised Institutional Review Board, Singapore (Ref No.: 2019/2668). The requirement for informed patient consent was waived by the Board as non-identifiable data were used and due to the retrospective nature of the research.

中文摘要

抗骨質吸收治療後不完全性非典型股骨骨折伴隨怪樣黑線周圍硬化

黃啟翔、石佳偉、許鑽美、P Chandra Mohan、方明愛、侯德生、黃勇輝

引言：本研究旨在描述接受抗骨質吸收治療的非典型股骨骨折（atypical femoral fractures, AFF）中，鄰近「怪樣黑線」或透光骨折線（radiolucent fracture lines, RFL）的骨質硬化之人口統計學、臨床及放射學特徵。

方法：我們對2004至2020年間在新加坡我院就診的100例AFF患者之X光片進行回顧性分析，評估病變的形態與位置，以及是否存在骨內膜或骨外膜增厚，同時分析患者的人口統計學資料、抗骨質吸收治療的類型與持續時間，以及是否進展為完全性骨折或需要預防性固定。我們根據影像表現將患者分為三組：1A組為伴有RFL及病灶周圍硬化的AFF；1B組為伴有RFL但無病灶周圍硬化的AFF；2組為無RFL的AFF。

結果：共發現17例硬化性RFL，多呈非線性形態。大多位於股骨大轉子下區（41.2%）及近端骨幹區（35.3%），所有病例均伴隨骨內膜或骨外膜增厚。硬化性RFL患者的平均年齡為69歲，其中16例（94.1%）有雙磷酸鹽使用史，1例曾接受地舒單抗治療。抗骨質吸收治療的平均持續時間為66個月。3例（17.6%）進展為完全性骨折，6例（35.3%）需接受預防性內固定。三組患者在人口統計學特徵、抗骨質吸收治療或手術介入方面均無顯著差異。

結論：我們描述了病灶周圍硬化，此為一種先前未被識別的AFF中RFL附近之放射學特徵，具有獨特的表現形式。其發生率約佔RFL病例的三分之一。需進一步研究以闡明其病理生理機制及預後意義。

INTRODUCTION

Atypical femoral fractures (AFFs) were first recognised as a distinct clinical entity following multiple clinical reports, yet their pathophysiology and clinical characteristics remain incompletely understood.^{1,2} Over time, our understanding of AFFs has evolved, as reflected in ongoing efforts by a task force of the American Society for Bone and Mineral Research (ASBMR) to refine diagnostic criteria.^{1,2} Major features used to define AFFs were first established in 2010 and included fractures following low-energy or no trauma, transverse fractures originating from the lateral cortex which may become oblique medially, complete fractures with a medial spike, and incomplete fractures involving only the lateral cortex, with minimal or no comminution and localised periosteal or endosteal thickening of the lateral cortex.¹ Minor features associated but not required for diagnosis include generalised femoral diaphyseal cortical thickening, unilateral or bilateral prodromal pain in the groin or thigh, incomplete or complete fractures of both femoral diaphyses, and delayed fracture healing.¹ In 2014, new epidemiological studies and clinical data prompted the ASBMR to revise the definition of AFFs,

emphasising their diaphyseal location and requiring at least four of the five major features for diagnosis.² This refined definition provides a more precise framework for identifying AFFs and distinguishing them from typical osteoporotic femoral fractures.² This reflects the dynamic and evolving nature of our understanding of AFFs and highlights that much remains unknown, including the identification of potential novel clinical and radiological features and their implications for patient management.

Radiological studies have also expanded our understanding of AFFs, particularly when Mohan et al³ described multifocal endosteal thickening along the femoral diaphysis in bisphosphonate-related AFFs, highlighting its association with a periosteal beak and/or a 'dreaded black line', also referred to as a radiolucent fracture line (RFL). These features were associated with an increased risk of progression to fracture.³ A subsequent study by Png et al⁴ demonstrated that when an RFL is present, the lesion is likely to persist, either remaining static or progressing to a displaced fracture. The significance of RFLs was also emphasised in the 2015 position statement by the Korean Society for Bone

and Mineral Research, which recommended prophylactic femoral nailing in the presence of an RFL, especially when located in the subtrochanteric region.⁵

Despite these insights, gaps remain in the literature, as not all RFLs progress to complete fractures and there are no clear discerning features to guide when prophylactic fixation is indicated. During our review of patients with AFFs, we observed a previously undescribed radiological feature: perilesional sclerosis—an area of sclerosis closely associated with the presence of an RFL seen in an incomplete AFF. This finding, distinct from previously reported radiological features of AFFs, may have implications for understanding bone stability, fracture progression, and management strategies, as sclerosis has previously been suggested to be associated with fatigue fractures and delayed fracture healing.⁶

Although with established diagnostic criteria and the recognition of RFLs as high-risk markers, it remains unclear why not all RFLs progress to complete fractures or ultimately require intervention. To date, no study has described the presence or significance of perilesional sclerosis in relation to RFLs in AFFs. Our study aimed to address this gap by identifying and characterising this radiological feature in association with RFLs in incomplete AFFs, and by exploring its potential clinical implications.

METHODS

Study Cohort

We retrospectively reviewed plain radiographs of cases of incomplete AFFs in patients presenting to our institution, Singapore General Hospital in Singapore, while receiving bisphosphonate therapy between 2004 and 2020. These cases were retrieved from our institutional AFF registry, which includes patients exhibiting features of AFF that have not yet progressed to a complete fracture.

We reviewed all available plain radiographs of the AFFs, as well as those of the contralateral femur when available. Perilesional sclerosis was defined as a linear area of sclerosis observed on either side of an RFL. All anteroposterior and lateral views were obtained using standard radiographic techniques, and all analysed fractures met the ASBMR criteria for an AFF.^{3,4}

The study cohort of 100 AFFs was subsequently divided into three groups: Group 1A included AFFs with an RFL and perilesional sclerosis; Group 1B included AFFs with

an RFL but without perilesional sclerosis; and Group 2 included AFFs without an RFL.

We also analysed age data and collected information on the type and duration of bisphosphonate therapy. Patients were followed up for sequelae, including progression to complete fracture or subsequent prophylactic fixation. Prophylactic fixation was performed in cases of persistent pain at the site of AFFs, while surgical fixation was performed for patients who progressed to complete fractures.

Image Analysis

All radiographs were reviewed for the presence of RFLs with adjacent sclerosis using Vue Motion (Carestream Health, Rochester [NY], US), and independently assessed by two authors (SBK and TSH), each with over 20 years of clinical orthopaedic experience. RFLs were categorised into one of four patterns: (1) RFL without sclerosis (Figure 1); (2) RFL with linear sclerosis (Figure 2); (3) RFL with patchy continuous sclerosis (Figure 3); and (4) RFL with patchy non-continuous sclerosis (Figure 4).

We recorded the location of each lesion, along with the presence or absence of focal endosteal or periosteal thickening. Cases were followed up until fixation was required or a complete fracture occurred. Lesions were classified as being located in either the subtrochanteric or diaphyseal region, and further subdivided into proximal, middle, or distal thirds. Observations were collected independently by each of the same two authors and correlated. In the event of any discrepancies, a senior radiologist was consulted to provide a final decision.

Statistical Analyses

Pearson's Chi squared test was used to compare categorical data, while one-way analysis of variance was employed to analyse continuous variables. Statistical analyses were performed using SPSS (Windows version 23.0; IBM Corp, Armonk [NY], US). Statistical significance was defined as $p < 0.05$.

RESULTS

There were 100 radiographs of AFFs from 80 cases available for review. Demographic and clinical data of the study cohort are summarised in Table 1. There were 17 femurs in Group 1A, 35 femurs in Group 1B, and 48 femurs in Group 2. All 17 femurs with perilesional sclerosis were independently identified by the two authors previously described. There were no significant differences among the three groups in terms of patient

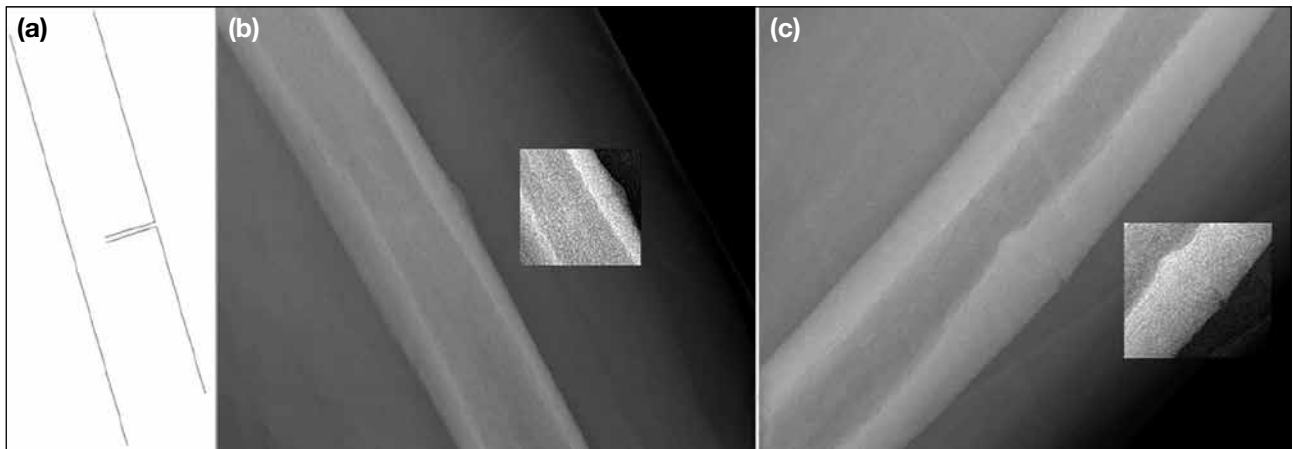


Figure 1. (a) Illustration of radiolucent fracture line (RFL) without sclerosis. (b) Anteroposterior and (c) lateral radiographs of the left femur showing an RFL without sclerosis.

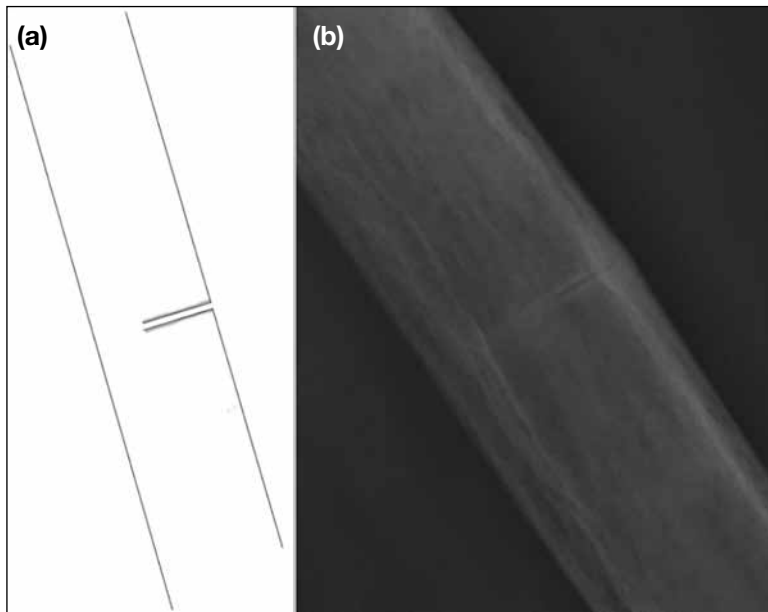


Figure 2. (a) Illustration of radiolucent fracture line (RFL) showing linear sclerosis. (b) Lateral radiograph of the left femur showing an RFL with linear sclerosis.

demographics (age: $p = 0.979$); the patients were predominantly female and Asian. All had a history of bisphosphonate use, except for two AFF cases with a history of denosumab use only (one in Group 1A and one in Group 2). There were no significant differences in the duration of antiresorptive therapy ($p = 0.418$), progression to complete fracture ($p = 0.078$), or subsequent prophylactic fixation ($p = 0.076$) among the three groups. The radiographic finding of perilesional sclerosis was observed in 17 of the 100 femurs (17%), with bilateral involvement in three patients who were all female with a mean age of 66 years; two were Chinese

(88.2%) and the remaining patient was of Indian descent. The mean (\pm standard deviation) duration of bisphosphonate use was 66 ± 31 months (range, 4-120). Only one femur in Group 1A was from a patient with a history of denosumab use without prior bisphosphonate therapy. Bisphosphonate treatment was discontinued upon diagnosis of AFF in all patients. Three femurs (17.6%) subsequently progressed to complete fractures, while six incomplete fractures required prophylactic fixation (35.3%). The mean time to surgical fixation or prophylactic fixation from the date of presentation with perilesional sclerosis was 9 ± 12 months.

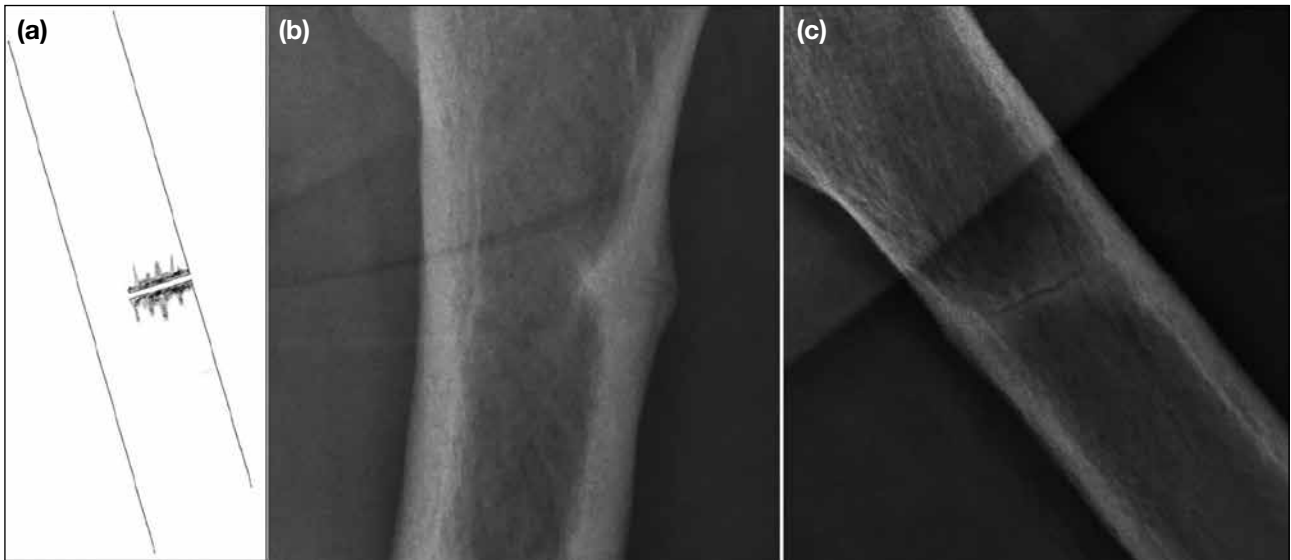


Figure 3. (a) Illustration of radiolucent fracture line (RFL) with patchy continuous sclerosis. (b) Anteroposterior and (c) lateral radiographs of the left femur showing an RFL with patchy continuous sclerosis.

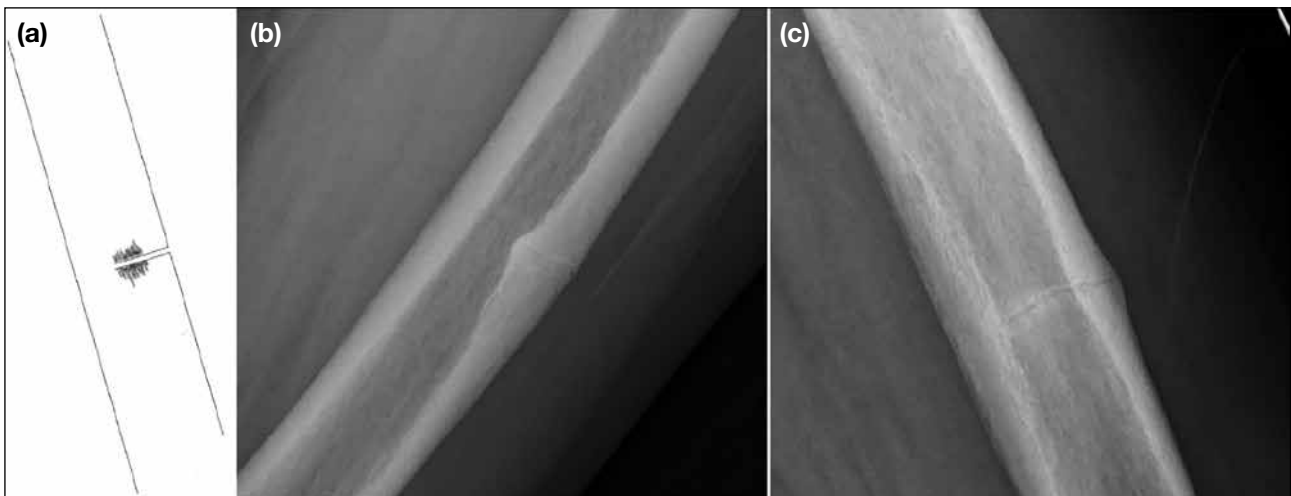


Figure 4. (a) Illustration of radiolucent fracture line (RFL) with patchy non-continuous sclerosis. (b) Anteroposterior and (c) lateral radiographs of the left femur of the same patient in Figure 2 showing RFL with patchy non-continuous sclerosis.

Table 1. Clinical data of the study cohort (n = 100).*

	Incomplete AFFs with RFLs		Incomplete AFFs without RFLs	p Value
	Group 1A (n = 17)	Group 1B (n = 35)	Group 2 (n = 48)	
Perilesional sclerosis	17 (100%)	0	0	N/A
Age, y	69 ± 11	69 ± 10	69 ± 11	0.979
Female sex	17 (100%)	34 (97.1%)	47 (97.9%)	0.787
History of bisphosphonate therapy	16 (94.1%)	35 (100%)	47 (97.9%)	0.364
Duration of antiresorptive therapy, mo	66 ± 31	51 ± 45	58 ± 33	0.418
Progression to complete fracture	3 (17.6%)	13 (37.1%)	8 (16.7%)	0.078
Prophylactic fixation	6 (35.3%)	10 (28.6%)	6 (12.5%)	0.076

Abbreviations: AFF = atypical femoral fracture; N/A = not applicable; RFL = radiolucent fracture line.

* Data are shown as No. (%) or mean ± standard deviation, unless otherwise specified.

Table 2. Radiographic features of perilesional sclerosis (n = 17).

	No. (%)
Non-linear	16 (94.1%)
Non-continuous	10 (58.8%)
Seen on lateral view	15 (88.2%)
Seen on anteroposterior view	9 (52.9%)
Presence of endosteal or periosteal thickening	17 (100%)

The radiographic features of perilesional sclerosis in Group 1A are summarised in Table 2. Each sclerotic lesion was observed in an incomplete AFF and only in the presence of an RFL. Perilesional sclerosis was identified on lateral views in 15 femurs (88.2%), while only nine femurs (52.9%) demonstrated sclerosis on anteroposterior views. The lesions were mainly located in the subtrochanteric region (n = 7, 41.2%), followed by the proximal diaphyseal region (n = 6, 35.3%) and the mid-diaphyseal region (n = 4, 23.5%). All lesions were associated with either adjacent endosteal thickening or periosteal thickening. Of the 17 lesions with perilesional sclerosis, 16 (94.1%) were RFLs with patchy sclerosis of varying widths along either side of the fracture line, and 10 (58.8%) demonstrated patchy non-continuous sclerosis.

Among the 17 femurs with sclerotic RFLs, three had earlier radiographs (mean, 56.4 months; range, 0.5-96.3) showing an RFL without adjacent sclerosis, indicating that perilesional sclerosis developed later. Once sclerosis appeared, it persisted in all subsequent follow-up radiographs. For the eight femurs that did not undergo surgery, the mean duration between the first presentation of RFL with perilesional sclerosis and the last available radiograph was 31 ± 22 months (range, 0-57.6). Follow-up was achieved for 100% of the 17 lesions, with a mean follow-up duration of 72 ± 45 months (range, 8-184). Regarding inter-observer variability, there was complete agreement between both readers on the presence and pattern of sclerosis.

DISCUSSION

Our study describes the presence of perilesional sclerosis adjacent to the RFL, previously described by Png et al,⁴ and the radiological progression of AFFs in which the RFL is recognised as the penultimate radiological feature before progression to a complete fracture. We observed that an RFL can be associated with, or may later develop, perilesional sclerosis. This radiological feature has not previously been documented in AFFs, which are predominantly located between the subtrochanteric

region and mid-diaphyseal regions of the femur, may be bilateral and are consistently associated with endosteal or periosteal thickening. In our study, perilesional sclerosis appears to occur in approximately one-third of AFFs with an RFL, and is usually seen on lateral radiographic views, and occasionally on anteroposterior radiographic views. While the variability in its appearance and its significance remain largely unstudied, and descriptions in the literature are scarce, our study presents observations that may enhance our understanding of this entity.

AFFs are considered to be ‘tensional’ stress fractures, typically initiating along the upper two-thirds of the lateral femoral shaft corresponding to regions subjected to greater tensional forces.⁷ Accordingly, RFLs are better observed as linear structures across the femoral diaphysis on lateral views. As perilesional sclerosis appears to occur in association with RFLs, this may account for its notably high prevalence on lateral views of the femoral shaft.

In the majority of our cases, perilesional sclerosis was observed only on the lateral views. In two cases with both anterior and lateral cortical thickening, sclerosis was visible on both anteroposterior and lateral views. These findings suggest that, in most cases, perilesional sclerosis may be related to viewing cortical thickening at right angles to its long axis. However, in two cases, perilesional sclerosis was seen on the anteroposterior views despite cortical thickening being confined to the lateral cortex. This suggests that, in these cases, there was focal sclerosis at the intracortical fracture margins.

Radiologically, sclerosis at fracture sites has been described as a feature of fracture non-union.⁸ Although sclerosis has been postulated to be associated with avascular necrosis or reduced metabolic bone activity,⁹ it has also been linked to prolonged time to union.¹⁰ Perilesional sclerosis has been mentioned in some cases of insufficiency fractures but is rarely described in AFFs. Only a single study by McKenna et al¹¹ described sclerosis in relation to AFFs, but only on computed tomography scans without specific reference to its relationship with RFLs. The fact that this feature is observed only in a subset of incomplete AFFs with variable continuity along the RFL, suggests that it may represent a phase in the pathophysiological progression of AFFs.

Perilesional sclerosis associated with cortical thickening may resemble that seen in stress or fatigue fractures.

However, cases with intracortical perilesional sclerosis may represent an early phase of the process leading to non-union. Fracture non-union is usually associated with sclerosis at the fracture margins, and the two cases in our cohort where sclerosis was confined to the lateral cortex may represent non-union of the incomplete fracture, akin to hypertrophic non-union involving the lateral cortex. This may be the result of persistent tensile stresses that inhibit bony union.¹² These lesions also appeared to progress from an isolated RFL to an RFL with adjacent sclerosis, with this radiographic feature persisting for a mean duration of 31 ± 22 months. Perilesional sclerosis may take considerable time to develop but can persist long after initial presentation. We postulate that it could represent the development of a chronic non-union state in incomplete AFFs. Bisphosphonates such as alendronate are known to have prolonged effects on osteoclast function, and these may continue long after cessation of therapy.¹³

Although there were no significant differences in the proportion of cases that progressed to complete fracture or required prophylactic fixation between Group 1A and Group 1B, a higher rate of surgical fixation in Group 1B was noted (65.7% vs. 52.9%). A histological study by Schilcher et al¹⁴ demonstrated signs of attempted healing at the site of AFFs; however, the current literature does not explain the pathological differences between AFFs that eventually heal and those that do not. Future histological studies could examine samples of perilesional sclerosis to explore the underlying pathology and provide insights into its clinical significance.

Strengths and Limitations

A strength of this study is the 100% follow-up rate over a mid-term duration for a previously undescribed radiological finding in AFFs. The main limitation is the limited sample size of patients with perilesional sclerosis, although this may reflect the low prevalence of AFFs among patients on antiresorptive therapy. Additionally, the predominance of female patients in the cohort limited our ability to assess potential gender-related differences. Another limitation is the irregular follow-up of patients due to variation in individual physicians' clinical practices and the retrospective nature of the study. Longer-term, regularly scheduled follow-up with standardised radiographic imaging should be considered in future studies to better evaluate the relationship between these lesions and fracture outcomes.

CONCLUSION

We describe perilesional sclerosis as a previously unrecognised radiological feature along the RFL, in incomplete AFFs with distinctive characteristics. Its presence may suggest a state of non-union and was observed in approximately one-third of cases with an RFL. Further research involving larger cohorts could shed light on its pathophysiological and prognostic significance.

REFERENCES

1. Shane E, Burr D, Ebeling PR, Abrahamsen B, Adler RA, Brown TD, et al. Atypical subtrochanteric and diaphyseal femoral fractures: report of a task force of the American Society for Bone and Mineral Research. *J Bone Miner Res.* 2010;25:2267-94.
2. Shane E, Burr D, Abrahamsen B, Adler RA, Brown TD, Cheung AM, et al. Atypical subtrochanteric and diaphyseal femoral fractures: second report of a task force of the American Society for Bone and Mineral Research. *J Bone Miner Res.* 2014;29:1-23.
3. Mohan PC, Howe TS, Koh JS, Png MA. Radiographic features of multifocal endosteal thickening of the femur in patients on long-term bisphosphonate therapy. *Eur Radiol.* 2013;23:222-7.
4. Png MA, Mohan PC, Koh JS, Howe CY, Howe TS. Natural history of incomplete atypical femoral fractures in patients after a prolonged and variable course of bisphosphonate therapy—a long-term radiological follow-up. *Osteoporos Int.* 2019;30:2417-28.
5. Yang KH, Min BW, Ha YC. Atypical femoral fracture: 2015 position statement of the Korean Society for Bone and Mineral Research. *J Bone Metab.* 2015;22:87-91.
6. Hedge G, Thaker S, Botchu R, Fawcett R, Gupta H. Atraumatic fractures of the femur. *Br J Radiol.* 2021;94:20201457.
7. Koh JS, Goh SK, Png MA, Ng AC, Howe TS. Distribution of atypical fractures and cortical stress lesions in the femur: implications on pathophysiology. *Singapore Med J.* 2011;52:77-80.
8. Gharu E, John B. Nonunion of fractures: a review of epidemiology, diagnosis, and clinical features in recent literature. *Indian J Orthop.* 2024;58:1680-5.
9. Jones W, Roberts RE. Pathological calcification and ossification in relation to Leriche and Policard's theory. *Proc R Soc Med.* 1933;26:853-9.
10. Schmidle G, Ebner HL, Klauser AS, Fritz J, Arora R, Gabl M. Correlation of CT imaging and histology to guide bone graft selection in scaphoid non-union surgery. *Arch Orthop Trauma Surg.* 2018;138:1395-405.
11. McKenna MJ, Heffernan E, Hurson C, McKiernan FE. Clinician approach to diagnosis of stress fractures including bisphosphonate-associated fractures. *QJM.* 2014;107:99-105.
12. Andrzejowski P, Giannoudis PV. The 'diamond concept' for long bone non-union management. *J Orthop Traumatol.* 2019;20:21.
13. Stock JL, Bell NH, Chesnut CH 3rd, Ensrud KE, Genant HK, Harris ST, et al. Increments in bone mineral density of the lumbar spine and hip and suppression of bone turnover are maintained after discontinuation of alendronate in postmenopausal women. *Am J Med.* 1997;103:291-7.
14. Schilcher J, Sandberg O, Isaksson H, Aspenberg P. Histology of 8 atypical femoral fractures: remodeling but no healing. *Acta Orthop.* 2014;85:280-6.

CASE REPORT

Perineural and Muscular Involvement in Recurrent Diffuse Large B-Cell Lymphoma Detected by Fluorine-18 Fluorodeoxyglucose Positron Emission Tomography/Computed Tomography: A Case Report

JHY Lau, KK Ng, BT Kung

Nuclear Medicine Unit, Department of Diagnostic and Interventional Radiology, Queen Elizabeth Hospital, Hong Kong SAR, China

CASE PRESENTATION

A 79-year-old female with a past medical history of hypertension and impaired fasting glucose presented to our institution in April 2020 with a neck mass and fever. She was an ex-smoker with no known drug allergies. Following an ear, nose, and throat consultation, she was diagnosed with stage 4B diffuse large B-cell lymphoma (DLBCL). A biopsy of the left tonsil revealed high-grade B-cell lymphoma, consistent with DLBCL. Further evaluation including bilateral bone marrow aspiration and bilateral trephine biopsy showed no evidence of lymphoma involvement.

Staging fluorine-18 fluorodeoxyglucose positron emission tomography/computed tomography (¹⁸F-FDG PET/CT) revealed hypermetabolic lymphadenopathy on both sides of the diaphragm, consistent with the biopsy-proven lymphoma, as well as hypermetabolic lesions in bilateral tonsils, confirming lymphomatous involvement (Figure 1).

The patient commenced R-CHOP chemotherapy (rituximab, cyclophosphamide, doxorubicin, vincristine, and prednisone), receiving six cycles over 5 months. The first cycle was administered at 50% dosage, with subsequent cycles adjusted for tolerance and side-effects. Following completion of the last cycle, an end-of-treatment ¹⁸F-FDG PET/CT scan demonstrated complete metabolic remission, with a Deauville score of 2 (Figure 2).

Five months after completing R-CHOP chemotherapy, the patient developed a right neck mass and numbness over the right side of her neck and right lower limb, with muscle power graded at 2 out of 5. A CT scan revealed a large soft tissue mass on the right side of the oropharynx, and biopsy confirmed DLBCL with CD20 positivity. A subsequent ¹⁸F-FDG PET/CT scan for restaging revealed a new hypermetabolic soft tissue mass in the right side of the oropharynx, consistent with lymphomatous involvement, with a Deauville score of 5. Notably,

Correspondence: Dr JHY Lau, Nuclear Medicine Unit, Department of Diagnostic and Interventional Radiology, Queen Elizabeth Hospital, Hong Kong SAR, China
Email: hugh.lau@ha.org.hk

Submitted: 16 December 2024; Accepted: 5 September 2025.

Contributors: All authors designed the study. JHYL acquired the data. All authors analysed the data. JHYL drafted the manuscript. KKN and BTK critically revised the manuscript for important intellectual content. All authors had full access to the data, contributed to the study, approved the final version for publication, and take responsibility for its accuracy and integrity.

Conflicts of Interest: All authors have disclosed no conflicts of interest.

Funding/Support: This study received no specific grant from any funding agency in the public, commercial, or not-for-profit sectors.

Data Availability: All data generated or analysed during the present study are available from the corresponding author on reasonable request.

Ethics Approval: This study was approved by the Central Institutional Review Board of Hospital Authority, Hong Kong (Ref No.: CIRB-2024-313-4). The requirement for patient consent was waived by the Board as the patient was deceased and no contact information for next of kin was available. The study involved retrospective review of anonymised clinical data only and posed no risk to subjects. All data were handled in accordance with Hospital Authority policies on data privacy and security.

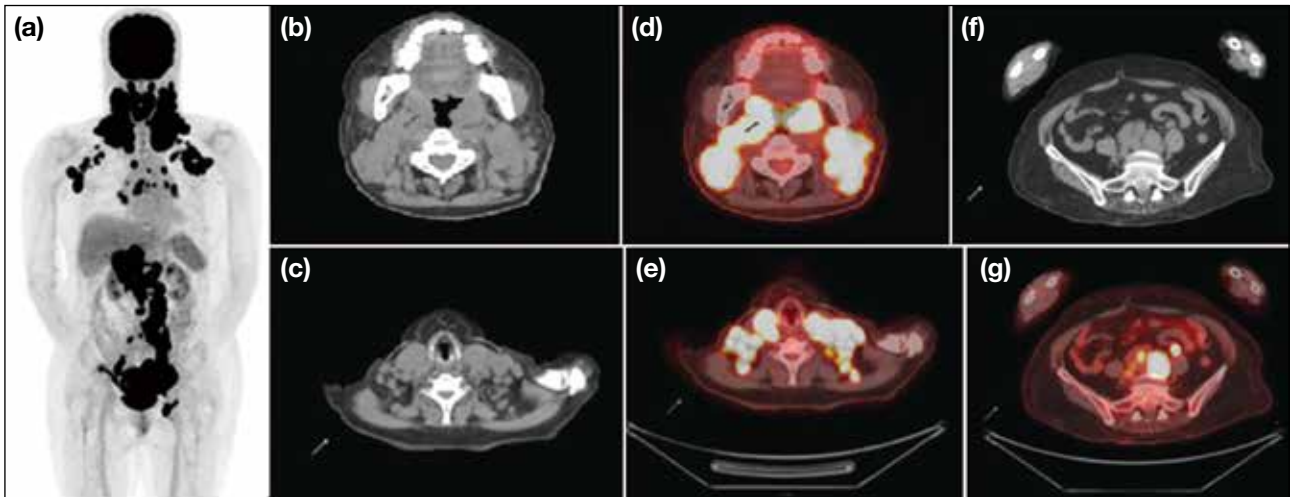


Figure 1. Staging fluorine-18 fluorodeoxyglucose positron emission tomography/computed tomography (^{18}F -FDG PET/CT) in a patient with biopsy-proven diffuse large B-cell lymphoma. (a) Maximum intensity projection shows multiple hypermetabolic, enlarged lymph nodes on both sides of the diaphragm. Transaxial (b and c) plain CT and (d and e) fused PET/CT images show supradiaphragmatic involvement, and transaxial (f) plain CT and (g) fused PET/CT images show infradiaphragmatic involvement.

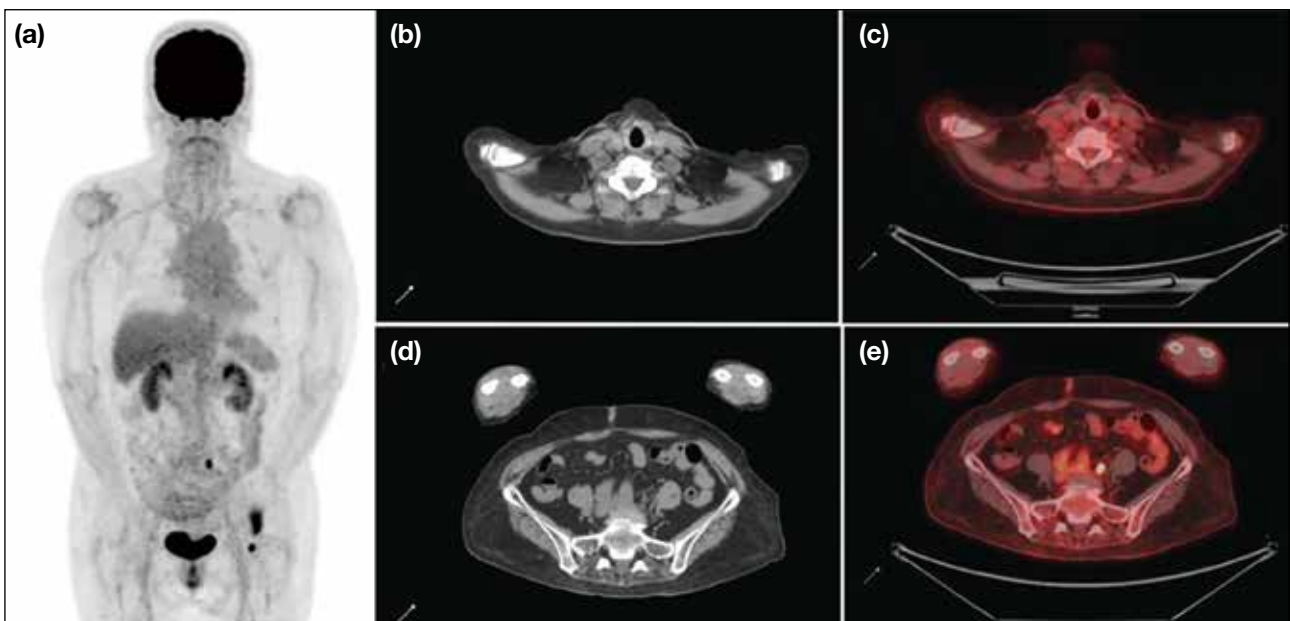


Figure 2. Fluorine-18 fluorodeoxyglucose positron emission tomography/computed tomography (^{18}F -FDG PET/CT) following treatment with R-CHOP chemotherapy (rituximab, cyclophosphamide, doxorubicin, vincristine, and prednisone). (a) Maximum intensity projection shows significant metabolic improvement or resolution on both sides of the diaphragm. Transaxial (b) plain CT and (c) fused PET/CT images show resolved supradiaphragmatic lymph nodes, and transaxial (d) plain CT and (e) fused PET/CT images show resolved infradiaphragmatic lymph nodes.

the scan also revealed new, multiple hypermetabolic foci involving perineural and muscular involvements in the bilateral head and neck regions and the right proximal lower limb, raising suspicion for perineural lymphomatous infiltration (Figure 3).

The patient subsequently received six cycles of

R-IMVP-16 (rituximab, ifosfamide, methotrexate, etoposide, and prednisone) over 5 months. End-of-treatment ^{18}F -FDG PET/CT showed metabolic resolution of the right tonsillar/oropharyngeal mass and other infiltrative perineural lesions in the neck region and right lower limb, indicating a favourable treatment response (Figure 4). Clinically, her numbness subsided,

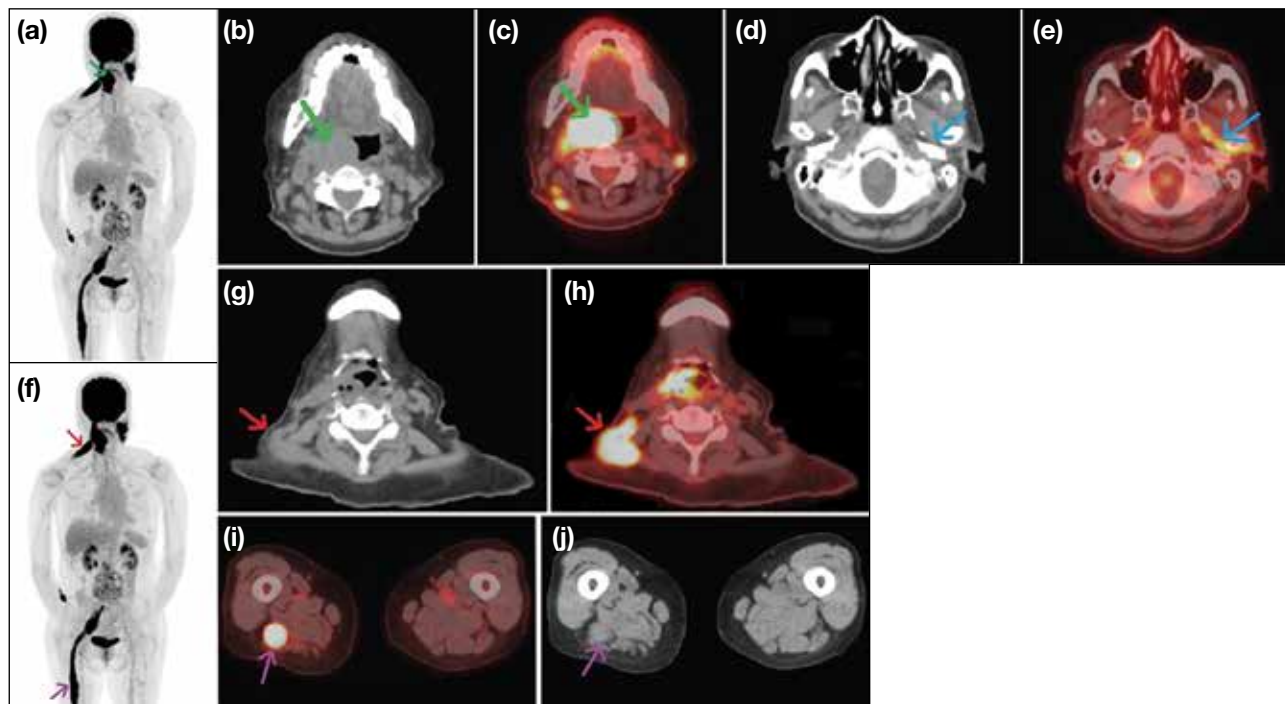


Figure 3. Recurrence and suspected atypical lymphomatous involvement in neuromuscular regions. (a) Maximum intensity projection of the fluorine-18 fluorodeoxyglucose positron emission tomography/computed tomography (^{18}F -FDG PET/CT) shows a hypermetabolic right oropharyngeal lesion (arrow). Transaxial (b) plain CT and (c) fused PET/CT images show the corresponding hypermetabolic lesion (arrows). Transaxial (d) plain CT and (e) fused PET/CT images show hypermetabolic left perineural involvement along the distribution of the left trigeminal branches (arrows). (f) Maximum intensity projection shows a hypermetabolic right neck perineural and muscular lesion (red arrow) and a right lower limb perineural and muscular lesion (purple arrow). Transaxial (g) plain CT and (h) fused PET/CT images show a hypermetabolic right neck neuromuscular lesion over the right trapezius muscle and accessory nerve region (arrows). Transaxial (i) plain CT and (j) fused PET/CT images show a hypermetabolic right lower limb neuromuscular lesion in the region of the right sciatic nerve (arrows).

with improved sensation in the previously affected regions and right lower limb power improved to 4 out of 5, consistent with the ^{18}F -FDG PET/CT findings. Both clinical and imaging findings favoured a positive treatment response of the perineural and muscular lymphomatous involvement in this patient with recurrent lymphoma.

DISCUSSION

Perineural and muscular involvement in DLBCL is rare, with only a limited number of cases reported in the literature.¹ The underlying mechanisms are not fully understood, but it is believed that DLBCL may infiltrate muscle tissue either via a haematogenous route or through adjacent lymphatic structures.² Clinical manifestations can vary widely, with patients presenting with muscle weakness, myalgia, or neuropathic symptoms.³ Differential diagnoses for FDG-avid perineural and muscular lesions include polyneuritis, compartment-related compression radiculopathy, and tuberculosis. In polyneuritis, the pattern of increased FDG uptake is usually symmetrical and occurs without associated soft



Figure 4. Maximum intensity projection of fluorine-18 fluorodeoxyglucose positron emission tomography/computed tomography with significant metabolic improvements or resolutions of the oropharynx, right neck and right lower limb hypermetabolic lesions after treated with R-IMVP-16 (rituximab, ifosfamide, methotrexate, etoposide, and prednisone) chemotherapy.

tissue thickening.^{4,5} The significant soft tissue thickening in our case made compartment-related compression radiculopathy less likely. Active tuberculosis was excluded through microbiological investigations.

This case demonstrated that the patient's neuropathic symptoms and imaging findings were indicative of perineural and muscular involvement. The identification of hypermetabolic activity in the muscles on ¹⁸F-FDG PET/CT was crucial in establishing the diagnosis due to the asymmetrical metabolic distribution and soft tissue thickening in the affected regions. These abnormalities resolved in parallel with the biopsy-proven recurrent right oropharynx DLBCL, both metabolically and morphologically. Such findings are often mistaken for primary myopathies or neuropathies.

In our case, ¹⁸F-FDG PET/CT not only confirmed the recurrence of DLBCL but also revealed the unusual sites of perineural and muscular involvement. This underscores the importance of considering extranodal manifestations of DLBCL, as it ultimately guided treatment decisions. Furthermore, the most recent ¹⁸F-FDG PET/CT showed both metabolic and morphological resolution of the hypermetabolic perineural and muscular lesions, supporting the diagnosis of atypical lymphomatous involvement and reflecting a significant treatment response.

Previous studies^{6,7} revealed that perineural and muscular involvement in DLBCL is largely underreported, with only a limited number of cases documented—primarily in patients with advanced-stage disease—and highlighted the importance of recognising ¹⁸F-FDG PET/CT findings in atypical sites of lymphomatous involvement to avoid misdiagnosis and ensure appropriate management. Primary muscular lymphoma⁶ and other atypical sites of DLBCL involvement^{6,7} have also been reported.

The utility of ¹⁸F-FDG PET/CT in the staging and treatment monitoring of DLBCL has been examined,^{8,9} which concluded that this imaging modality provides valuable insights into disease burden and can identify sites of active disease that may not be evident on conventional imaging. This aligns with our case, in which ¹⁸F-FDG PET/CT played a pivotal role in diagnosing perineural and muscular involvement in a one-stop-shop manner.

The management of DLBCL with perineural and muscular involvement is complex and often requires

a multidisciplinary approach.^{10,11} Treatment options may include chemotherapy, radiotherapy, and targeted therapies, depending on the extent of disease and the patient's overall health.

In our case, the patient was commenced on a salvage chemotherapy regimen following relapse of DLBCL. Given the aggressive nature of her disease, close monitoring with repeat ¹⁸F-FDG PET/CT was planned to assess treatment response. The prognosis for patients with perineural and muscular involvement in DLBCL varies, but early detection and timely intervention can significantly improve clinical outcomes.

CONCLUSION

This case highlights the importance of ¹⁸F-FDG PET/CT in detecting perineural and muscular involvement in patients with recurrent DLBCL. Early detection of the disease involvement using ¹⁸F-FDG PET/CT can guide biopsy targeting, inform appropriate treatment strategies and serve as a reference for assessing treatment response on end-of-treatment imaging, all of which are crucial for improving patient outcomes.

REFERENCES

1. Lim AT, Clucas D, Khoo C, Parameswaran BK, Lau E. Neurolymphomatosis: MRI and ¹⁸F-FDG-PET features. *J Med Imaging Radiat Oncol*. 2016;60:92-5.
2. Murthy NK, Amrami KK, Broski SM, Johnston PB, Spinner RJ. Perineural spread of peripheral neurolymphomatosis to the cauda equina. *J Neurosurg Spine*. 2021;36:464-9.
3. Broski SM, Bou-Assaly W, Gross MD, Fig LM. Diffuse skeletal muscle F-18 fluorodeoxyglucose uptake in advanced primary muscle non-Hodgkin's lymphoma. *Clin Nucl Med*. 2009;34:251-3.
4. Xie X, Cheng B, Han X, Liu B. Findings of multiple neuritis on FDG PET/CT imaging. *Clin Nucl Med*. 2013;38:67-9.
5. Ankrah AO, Glaudemans AW, Maes A, Van de Wiele C, Dierckx RA, Vorster M, et al. Tuberculosis. *Semin Nucl Med*. 2018;48:108-30.
6. Iioka F, Tanabe H, Honjo G, Misaki T, Ohno H. Resolution of bone, cutaneous, and muscular involvement after haploidentical hematopoietic stem cell transplantation followed by post-transplant cyclophosphamide in adult T-cell leukemia/lymphoma. *Clin Case Rep*. 2020;8:1553-9.
7. Belmonte G, Caldarella C, Hohaus S, Manfredi R, Minordi LM. Muscle recurrence of a primarily nodal follicular lymphoma studied by contrast-enhanced ¹⁸F-FDG PET/CT. *Clin Nucl Med*. 2020;45:65-7.
8. Kostakoglu L, Cheson BD. Current role of FDG PET/CT in lymphoma. *Eur J Nucl Med Mol Imaging*. 2014;41:1004-27.
9. Jing F, Liu Y, Zhao X, Wang N, Dai M, Chen X, et al. Baseline ¹⁸F-FDG PET/CT radiomics for prognosis prediction in diffuse large B cell lymphoma. *EJNMMI Res*. 2023;13:92.
10. Adams HJ, Kwee TC. Prognostic value of interim FDG-PET in R-CHOP-treated diffuse large B-cell lymphoma: systematic review and meta-analysis. *Crit Rev Oncol Hematol*. 2016;106:55-63.
11. Wai SH, Lee ST, Cliffer ER, Bei M, Lee J, Hawkes EA, et al. Utility of FDG-PET in predicting the histology of relapsed or refractory lymphoma. *Blood Adv*. 2024;8:736-45.

CASE REPORT

Urachal Adenocarcinoma in a Young Adult: A Rare Case Report

LLA Chan, IS Bandong

Institute of Radiology, St Luke's Medical Center–Quezon City, Quezon City, The Philippines

CASE PRESENTATION

A 19-year-old female presented to our institution in February 2023 with intermittent gross haematuria and dysuria for 2 months without seeking medical consultation. She then experienced a syncopal attack, prompting consultation and eventual admission. Her medical history included recurrent untreated urinary tract infections since childhood. No family history of malignancy or prior abdominal surgery was noted.

Initial transvaginal ultrasound revealed a solid, slightly irregular ovoid mass measuring $6.9 \times 5.9 \times 4.7 \text{ cm}^3$, located in the posterior bladder wall (Figure 1a). The mass exhibited heterogeneous echogenicity with punctate calcifications. Doppler ultrasound revealed moderate vascularity (Figure 1b). The ovaries, adnexa, and uterus appeared unremarkable.

A subsequent computed tomography (CT) urography (Figure 2) revealed a lobulated, heterogeneously enhancing mass in the supravescical region with associated calcifications. The mass abutted the bladder dome with obliteration of the fat plane, suggesting infiltration. A 1.8-cm enlarged lymph node was also noted in the right paravesical region. A urachal neoplasm was considered.

The patient underwent radical cystectomy and total abdominal hysterectomy with bilateral salpingectomy, all of which were well tolerated without complications. Histopathological examination of the excised mass revealed a moderately differentiated mucinous adenocarcinoma, consistent with urachal carcinoma.

Histopathological Findings

The mass was located approximately 6 cm from the umbilicus, with smooth external surfaces and yellow-tan friable content. Histological analysis showed malignant epithelial cells arranged in glandular and cribriform patterns, with extensive extracellular mucin and areas of tumour necrosis (Figure 3). The tumour infiltrated the bladder's lamina propria, muscularis propria, and perivesical fat. These findings were consistent with mucinous adenocarcinoma, a type of urachal carcinoma.

Postoperative Course and Outcome

Following surgery, the patient's recovery was uneventful. She was eventually discharged and underwent three cycles of chemotherapy comprising FOLFOX (leucovorin, 5-fluorouracil, and oxaliplatin). Eighteen months after surgery, she was frequently admitted with recurrent urinary tract infections that were found to be

Correspondence: Dr LLA Chan, Institute of Radiology, St Luke's Medical Center–Quezon City, Quezon City, The Philippines
Email: llachan@stlukes.com.ph

Submitted: 12 February 2025; Accepted: 28 April 2025.

Contributors: LLAC designed the study, acquired and analysed the data, and drafted the manuscript. ISB critically revised the manuscript for important intellectual content. Both authors had full access to the data, contributed to the study, approved the final version for publication, and take responsibility for its accuracy and integrity.

Conflicts of Interest: Both authors have disclosed no conflicts of interest.

Funding/Support: This study received no specific grant from any funding agency in the public, commercial, or not-for-profit sectors.

Data Availability: All data generated or analysed during the present study are available from the corresponding author on reasonable request.

Ethics Approval: This study was approved by the Institutional Ethics Review Committee of St Luke's Medical Center–Quezon City, The Philippines (Ref No.: SL-21346). The patient was treated in accordance with the Declaration of Helsinki. Informed consent for publication of this case report and the accompanying images was obtained from the patient's mother, as the patient is deceased.

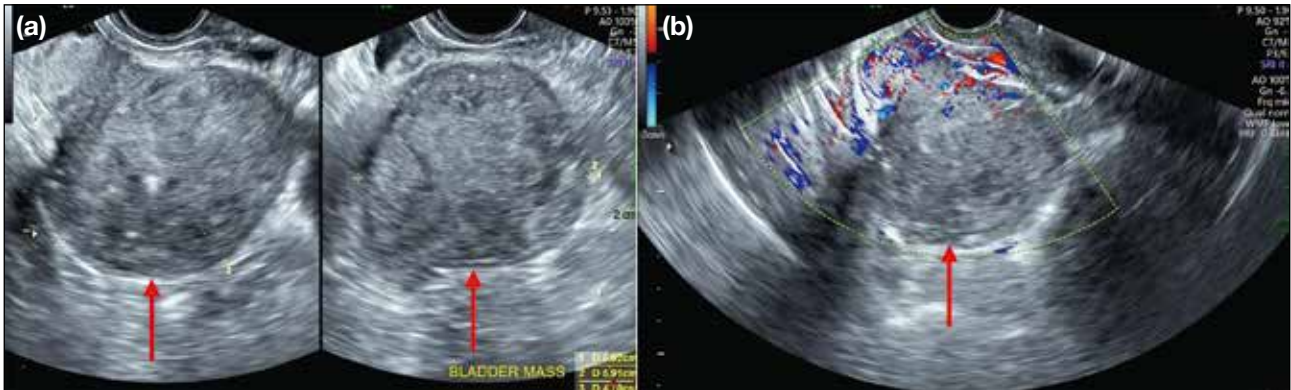


Figure 1. Transvaginal ultrasonography. (a) Slightly irregular ovoid solid mass (arrows) extending from the posterior urinary bladder wall, measuring $6.9 \times 5.9 \times 4.7$ cm³. (b) Doppler interrogation showing moderate vascularity of the mass (arrow).

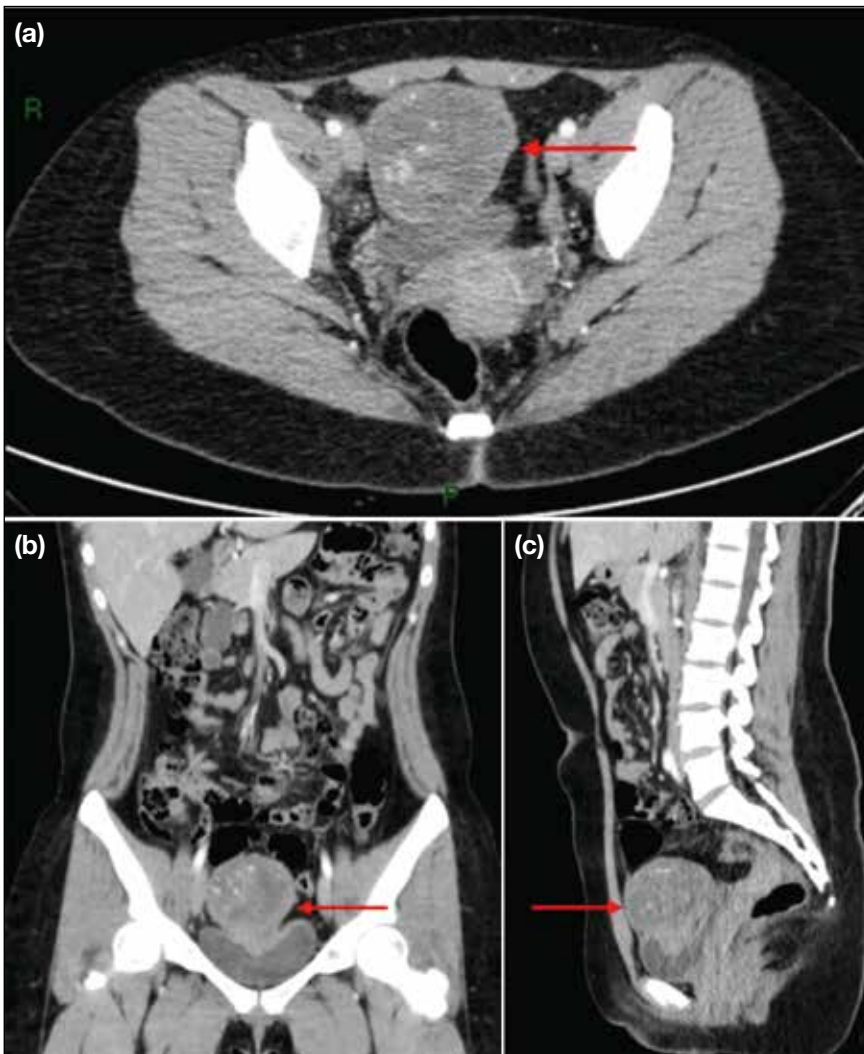


Figure 2. Contrast-enhanced multi-slice computed tomography urography in (a) axial, (b) coronal, and (c) sagittal views. A well-defined lobulated non-enhancing mass with intrinsic punctate calcifications (arrows) is seen at the supravescical region with involvement of the bladder dome. The mass is slightly less attenuating than the adjacent soft tissue, a finding suggestive of a mucus-filled structure.

caused by a newly discovered metastatic growth on the anterior pelvic wall, compressing the urinary collecting system. The patient underwent palliative care and eventually deceased within a year.

DISCUSSION

Urachal adenocarcinoma is a very rare primary bladder neoplasm, accounting for only 0.35% to 0.7% of all primary bladder cancers.¹ This malignancy tends to

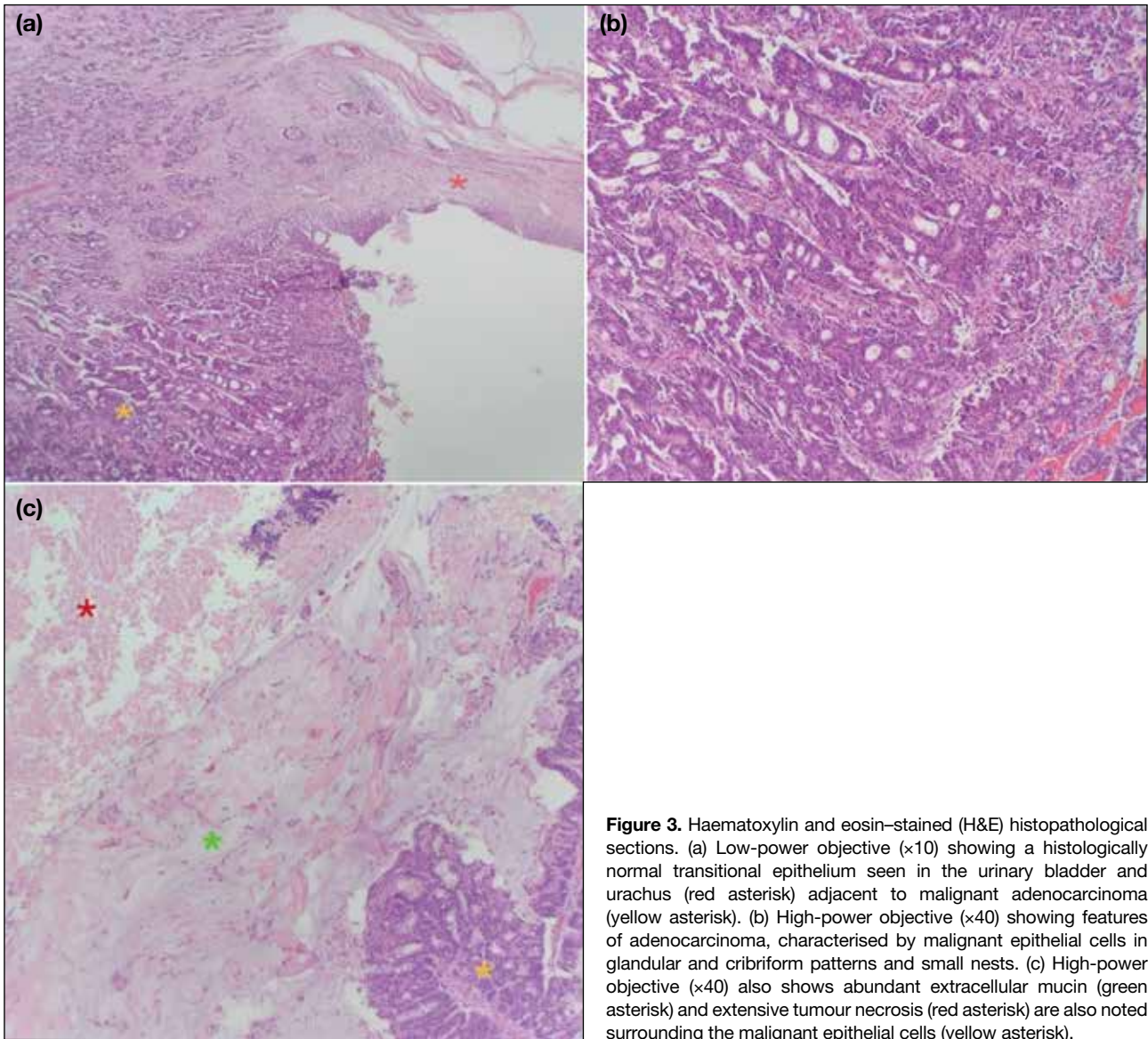


Figure 3. Haematoxylin and eosin-stained (H&E) histopathological sections. (a) Low-power objective (x10) showing a histologically normal transitional epithelium seen in the urinary bladder and urachus (red asterisk) adjacent to malignant adenocarcinoma (yellow asterisk). (b) High-power objective (x40) showing features of adenocarcinoma, characterised by malignant epithelial cells in glandular and cribriform patterns and small nests. (c) High-power objective (x40) also shows abundant extracellular mucin (green asterisk) and extensive tumour necrosis (red asterisk) are also noted surrounding the malignant epithelial cells (yellow asterisk).

have a male predilection and typically occurs in adults between 40 and 70 years old. The most common clinical feature is haematuria, as seen in the index patient. Other signs and symptoms include dysuria, abdominal pain, a suprapubic mass, and discharge of blood, pus, or mucus from the umbilicus.² Only six adult cases of urachal adenocarcinoma diagnosed before the age of 30 years have been reported in the English literature, with the youngest diagnosed at age 26 years.^{1,3-6}

Ultrasonography is often performed as the initial imaging modality and can provide a general impression of the lesion, including its location and characteristics.⁷ Sonographic imaging features of urachal adenocarcinoma

include: (1) a solid mass extending between the dome of the bladder and the abdominal wall, with an irregular shape and bladder wall invasion; (2) a hypoechoic, heterogeneous echo pattern with a small amount of calcification; and (3) patchy, short-line blood flow signals within the mass.⁸ These characteristic features were analogous to those seen on the initial ultrasonography performed in our patient.

CT imaging can be used to confirm the ultrasonographic findings or serve as the first-line imaging to evaluate local disease, tumour extension, and the presence of pelvic lymph node involvement or distant metastases.⁷ A key diagnostic feature of urachal adenocarcinoma

on CT is its supravescical midline location. The mass often demonstrates predominantly low attenuation, attributable to its mucinous content found on pathological examination. Calcifications are also commonly seen in mucinous tumours.⁹ These findings closely correspond to the appearance and location of the tumour in the index patient's CT urography.

Although urachal remnants are lined by urothelial epithelium, 80% of urachal cancers are adenocarcinomas, including mucin-producing (69%) and mucin-negative (15%) subtypes.⁷ The reason why adenocarcinoma is the predominant malignant epithelial type in urachal cancers remains unclear, but it has been hypothesised that chronic irritation may induce malignant transformation of transitional epithelium into columnar epithelium.⁷ Another theory proposes that intestinal metaplasia in the urinary bladder is associated with cytogenetic abnormalities and significant telomere shortening relative to telomere length in adjacent normal urothelial cells.¹⁰ These theories may help explain how urachal adenocarcinoma can, albeit rarely, present in a younger demographic, such as in the case of the index patient who experienced recurrent urinary tract infections and was therefore subject to d from childhood.

Differential diagnoses for urachal adenocarcinoma include ovarian malignancies and other types of urinary bladder cancer. Sonographic and CT findings of these malignancies may reveal large, complex masses similar to the radiographic findings of urachal adenocarcinoma.¹¹⁻¹³ Nonetheless, the key feature that supports a diagnosis of urachal adenocarcinoma over other possibilities is the supravescical midline location of the mass.

Surgery remains the mainstay of treatment for urachal adenocarcinoma. For muscle-invasive disease, radical cystectomy with en bloc resection of the urachal ligament may be the only curative option. Nonetheless, survival still strongly correlates with the stage and grade of the disease. A study reported a 5-year survival rate of 50% for stage I to III tumours, while no stage IV patients survived beyond 2 years.¹¹ Urachal adenocarcinoma has also been found to be resistant to chemotherapy and

radiotherapy; therefore, early definitive diagnosis and radical resection are essential for a better outcome.¹¹

CONCLUSION

Urachal carcinoma is a rare and aggressive malignancy that should be considered in the differential diagnosis of pelvic masses, even in young patients. The rarity of this condition highlights the importance of radiological imaging in early detection. Ultrasonography and CT are essential for identifying the tumour and assessing its extent. Although surgical resection remains the treatment of choice, the prognosis is generally poor, underscoring the need for further research into effective therapies for this rare and challenging type of cancer.

REFERENCES

1. Gopalan A, Sharp DS, Fine SW, Tickoo SK, Herr HW, Reuter VE, et al. Urachal carcinoma: a clinicopathologic analysis of 24 cases with outcome correlation. *Am J Surg Pathol*. 2009;33:659-68.
2. Chen X, Kang C, Zhang M. Imaging features of urachal cancer: a case report. *Front Oncol*. 2019;9:1274.
3. Henly DR, Farrow GM, Zincke H. Urachal cancer: role of conservative surgery. *Urology*. 1993;42:635-9.
4. Lee SR, Kang H, Kang MH, Yu YD, Choi CI, Choi KH, et al. The youngest Korean case of urachal carcinoma. *Case Rep Urol*. 2015;2015:707456.
5. Pinthus JH, Haddad R, Trachtenberg J, Holowaty E, Bowler J, Herzenberg AM, et al. Population based survival data on urachal tumors. *J Urol*. 2006;175:2042-7.
6. Machida H, Ueno E, Nakazawa H, Fujimura M, Kihara T. Computed tomographic appearance of urachal carcinoma associated with urachal diverticulum misdiagnosed by cystoscopy. *Abdom Imaging*. 2008;33:363-6.
7. Parada Villavicencio C, Adam SZ, Nikolaidis P, Yaghmai V, Miller FH. Imaging of the urachus: anomalies, complications, and mimics. *Radiographics*. 2016;36:2049-63.
8. Koster IM, Cleyndert P, Giard RW. Best cases from the AFIP: urachal carcinoma. *Radiographics*. 2009;29:939-42.
9. Brick SH, Friedman AC, Pollack HM, Fishman EK, Radecki PD, Siegelbaum MH, et al. Urachal carcinoma: CT findings. *Radiology*. 1988;169:377-81.
10. Lim H, Lusaya D. Urachal mucinous adenocarcinoma of the bladder. *Philipp J Urol*. 2020;28:115-7.
11. Marko J, Marko KI, Pachigolla SL, Crothers BA, Mattu R, Wolfman DJ. Mucinous neoplasms of the ovary: radiologic-pathologic correlation. *Radiographics*. 2019;39:982-97.
12. Wong-You-Cheong JJ, Woodward PJ, Manning MA, Sesterhenn IA. From the Archives of the AFIP: neoplasms of the urinary bladder: radiologic-pathologic correlation. *Radiographics*. 2006;26:553-80.
13. Varma V, Myers DT. Urachal adenocarcinoma. *Appl Radiol*. 2019;48:44-5.

CASE REPORT

Salvaging Inadvertent Subintimal Stenting with Double-Barrel Subintimal Stenting: A Case Report

ES Lo¹, SC Woo¹, SKH Wong¹, LF Cheng¹, KM Chan², WK Ng²

¹*Department of Radiology, Princess Margaret Hospital, Hong Kong SAR, China*

²*Vascular Surgery Department, Princess Margaret Hospital, Hong Kong SAR, China*

CASE PRESENTATION

A 59-year-old male patient with a history of smoking, metabolic syndrome, ischaemic heart disease, and long-standing peripheral arterial disease presented to our institution in October 2022 with recurrent claudication. He had previously undergone multiple lower limb angioplasties and stenting procedures at various institutions between 2018 and 2021 for recurrent in-stent restenosis. These included an EverFlex stent (Medtronic, Plymouth [MN], US) in the left external iliac artery (EIA), a Protégé stent (Medtronic, Plymouth [MN], US) in the left common iliac artery (CIA), an EverFlex stent in the right EIA, a Supera stent (Abbott, Santa Clara [CA], US) from the right common femoral artery to the proximal superficial femoral artery (CFA-pSFA), a Zilver stent (Cook Medical, Limerick, Ireland) in the

right mid superficial femoral artery (mid-SFA), and a Supera stent from the right distal superficial femoral artery to the popliteal artery (dSFA-pop) [Figure 1].

The patient presented in 2022 with recurrent claudication following placement of a bridging CFA-pSFA stent between the right EIA and mid-SFA stents, with claudication distance reduced to 10 metres. In view of his recurrent symptoms, the authors were consulted for suspected stent occlusion of the previously placed multi-stent system. Computed tomography angiography revealed an in-stent occlusion due to misalignment of the CFA-pSFA and mid-SFA stents (Figure 2), likely resulting from subintimal placement of the CFA-pSFA stent.

Correspondence: Dr ES Lo, Department of Radiology, Princess Margaret Hospital, Hong Kong SAR, China
Email: les474@ha.org.hk

Submitted: 9 July 2025; Accepted: 29 September 2025.

Contributors: ESL, SCW and LFC designed the study. All authors acquired and analysed the data. ESL and SKHW drafted the manuscript. All authors critically revised the manuscript for important intellectual content. All authors had full access to the data, contributed to the study, approved the final version for publication, and take responsibility for its accuracy and integrity.

Conflicts of Interest: All authors have disclosed no conflicts of interest.

Funding/Support: This study received no specific grant from any funding agency in the public, commercial, or not-for-profit sectors.

Data Availability: All data generated or analysed during the present study are available from the corresponding author on reasonable request.

Ethics Approval: This study was approved by the Central Institutional Review Board of Hospital Authority, Hong Kong (Ref No.: CIRB-2024-555-4). The patient was treated in accordance with the Declaration of Helsinki and provided written informed consent for all treatments, procedures, and the publication of all clinical images.

Declaration: Part of this study was presented as a poster at the 18th Annual Scientific Meeting of Asia Pacific Society of Cardiovascular and Interventional Radiology, 3-5 May 2024, Bangkok, Thailand.

Supplementary Material: The supplementary material was provided by the authors and some information may not have been peer reviewed. Any opinions or recommendations discussed are solely those of the author(s) and are not endorsed by the Hong Kong College of Radiologists. The Hong Kong College of Radiologists disclaims all liability and responsibility arising from any reliance placed on the content. To view the file, please visit the journal online (<https://doi.org/10.12809/hkjr2518009>).

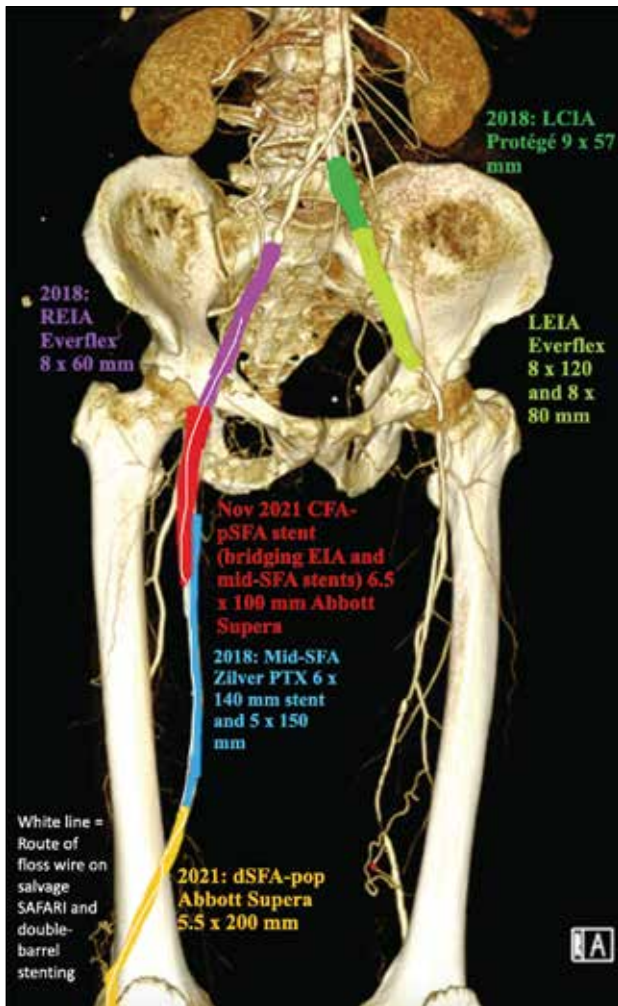


Figure 1. A summary of stents previously placed in the patient between 2018 and 2021 at various institutions. Left common iliac artery (LCIA), left external iliac artery (LEIA), right external iliac artery (REIA), and mid superficial femoral artery (mid-SFA) stents were placed in 2018 for peripheral vascular disease. A distal superficial femoral artery–popliteal artery (dSFA-pop) stent was placed in early 2021. A common femoral artery to proximal superficial femoral artery (CFA-pSFA) stent was placed in November 2021 to bridge the REIA and mid-SFA stents. A thin white line depicts the course of the retrograde guidewire during the 2023 SAFARI (subintimal arterial flossing with antegrade-retrograde intervention) double-barrel stenting procedure. The intraluminal position within the dSFA-pop stent, subintimal position outside the lumen of the mid-SFA stent, and subsequent intraluminal re-entry into the CFA-pSFA stent were confirmed by fluoroscopy and intravascular ultrasound. The retrograde wire was subsequently advanced into a long sheath to establish a floss wire between the right ankle and left groin access.

Digital subtraction angiography images in the anteroposterior projection from the previous procedure in November 2021 revealed apparent alignment of the CFA-pSFA and mid-SFA stents, with improved runoff post-stenting (Figure 3). Lateral views were unavailable.

In view of the recurrent claudication and the in-stent occlusion, repeat angioplasty was performed in October 2023. Left CFA access with crossover was performed. A 6-Fr Destination long sheath (Terumo, Somerset [NJ], US) was placed in the right CIA. A 0.035-inch guidewire (Terumo, Tokyo, Japan) was advanced through the lumen of the occluded right CFA-pSFA stent, encountering resistance (Figure 4a). Inability to negotiate the wire into the right mid-SFA stent led to a decision to obtain retrograde access via the right posterior tibial artery (PTA). With the aid of a 2.6-Fr CXI microcatheter (Cook Medical, Bloomington [IN], US), a 0.018-inch Advantage wire (Terumo, Tokyo, Japan) was advanced retrogradely through the PTA and the dSFA-pop Supera stent intraluminally. The wire was manipulated at the junction of the mid-SFA Zilver stent and dSFA-pop Supera stent, entering the subintimal space. After further subintimal manipulation, re-entry of the retrograde wire into the lumen of the occluded CFA-pSFA stent was achieved. The wire was then advanced into the right EIA/CIA stent lumen (Figures 1 and 4b). Wire position was confirmed by intravascular ultrasound (IVUS) [Visions PV 0.018-inch catheter (Phillips, Rancho Cordova [CA], US)] and angiography. The retrograde wire was externalised through the 6-Fr crossover sheath and retrieved via the left groin access to establish through-and-through access.

Angioplasty was performed along the wire path from the right popliteal artery stent to the left EIA stent with an Armada 6 × 200 mm² balloon (Abbott, Santa Clara [CA], US), expanding the subintimal space for subsequent stenting. Following IVUS sizing, double-barrel subintimal stenting was performed by deploying a Supera 5.5 × 80 mm² stent to bridge the CFA-pSFA and dSFA-pop stents (Figure 4c). Additional angioplasty of the newly deployed stent, as well as the PTA and tibioperoneal trunk, was performed with an Armada 2.5 × 200 mm² balloon. Completion angiography demonstrated re-establishment of flow through the double-barrel subintimal stent, with a patent intraluminal-subintimal-intraluminal channel and crush exclusion of the Zilver mid-SFA stent (Figure 4d and e). Postoperatively, the patient resumed apixaban 5 mg twice daily and aspirin 80 mg daily.

At 1-month follow-up, symptoms improved from claudication after walking 20 steps (Rutherford grade III) to no claudication (Rutherford grade 0). There was no evidence of tissue loss or vascular compromise. At 8 months, follow-up computed tomography showed

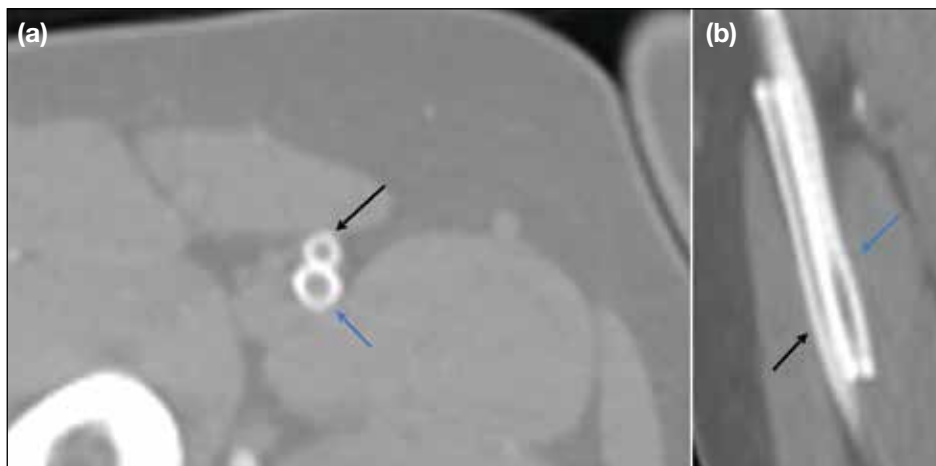


Figure 2. Computed tomography angiogram in 2022 showing stent occlusion, likely resulting from malalignment of the common femoral artery to the Supera stent (blue arrows) of the proximal superficial femoral artery (CFA-pSFA) and the Zilver stent (black arrows) of the mid superficial femoral artery (mid-SFA). The distal margin of the CFA-pSFA stent is seen within the subintimal space, external to the mid-SFA stent. (a) Axial view. (b) Sagittal reconstruction.



Figure 3. Retrospective review of prior common femoral artery to proximal superficial femoral artery bridging stent placement in 2021 showing (a) apparent stent alignment (black arrow) and (b) acceptable runoff on completion angiography.

successful crush exclusion of the mid-SFA Zilver stent (Figure 5). There was complete alignment of the mid-SFA Supera stent with adjacent proximal and distal

stents, with preserved patency and no significant in-stent restenosis (Figure 5). However, mild-to-moderate in-stent restenosis was noted in the previously implanted popliteal and iliac stents. The patient remains under surveillance and is scheduled for repeat angioplasty to preserve the patency of the multi-stent system (online supplementary Figure).

DISCUSSION

Our case highlights several important considerations for interventionists. In retrospect, inadvertent subintimal stent placement could have been avoided through several measures. First, routine biplanar imaging could prevent false assurance from a single anteroposterior projection and detect stent misalignment. Attention should also be paid to contrast pooling around the stent tips and the rate of contrast runoff; delayed clearance may alert the operator to possible distal outflow impairment or subintimal entry. Second, careful observation of the guidewire tip behaviour and mobility may alert interventionists to inadvertent subintimal entry. In cases of initial intimal dissection and subintimal entry, the tip load of the guidewire may be exceeded with the wire tip bending in the reverse direction and a ‘crushing’ sensation commonly reported.¹ Initial entry into the potential subintimal space may restrict free wire rotation. Nonetheless, where manipulation continues and the wire tracks further into an enlarging subintimal space, guidewire rotation may become freer, with loss of resistance. Prolonged manipulation should be avoided if early intraluminal re-entry fails, as this may enlarge the subintimal space and further complicate luminal re-entry. Third, in cases of equivocal wire position,

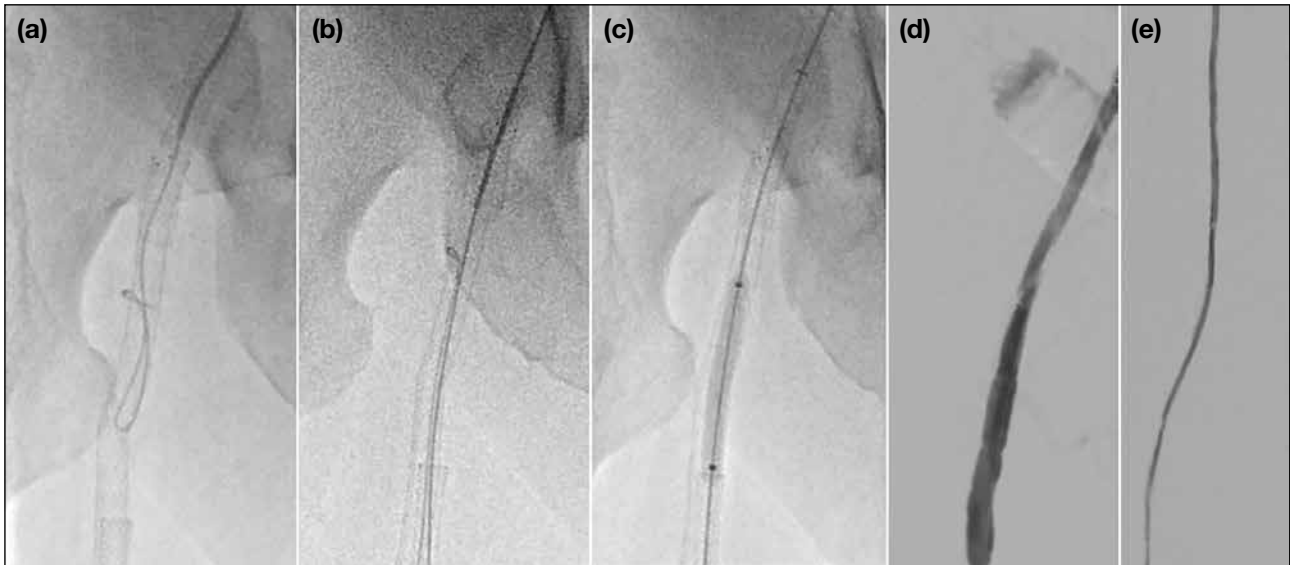


Figure 4. Digital subtraction angiography images of angioplasty and double-barrel stenting performed in November 2023. (a) Crossover wire from left femoral access, with the tip positioned within the right common femoral artery to the proximal superficial femoral artery (CFA-pSFA) stent, encountering resistance due to occlusion. The occlusion was eventually navigated; however, in view of failure to re-enter the mid superficial femoral artery (mid-SFA) stent lumen, a retrograde approach was employed. (b) A 0.018-inch retrograde wire via right posterior tibial artery access was advanced intraluminally through the occluded distal superficial femoral artery popliteal artery stent, with subsequent entry into the subintimal space outside the Zilver SFA stent and re-entry into the intraluminal occluded CFA stent. The long sheath from the left groin access was cannulated by the retrograde wire and subsequently externalised, establishing a through-and-through floss wire. Position was confirmed by intravascular ultrasound (Figure 6). (c) After establishment of the floss wire, angioplasty of the intraluminal-subintimal-intraluminal wire tract was performed. (d, e) Angioplasty of the posterior tibial artery and tibioperoneal trunk was performed, followed by mid-SFA stenting with double-barrel exclusion of the Zilver stent. Completion angiography showed significant restoration of flow between the newly deployed mid-SFA stent and adjacent stents.

familiarity with IVUS may assist operators in accurately stenting within the true lumen. The IVUS images from our salvage procedure are shown (Figure 6). Although resource-intensive and operator-dependent, IVUS enables more accurate visualisation of the vascular and subintimal spaces with applications not only in stent positioning but also in the accurate arterial stent sizing.^{2,3}

In cases of inadvertent subintimal entry or dissection, achieving luminal re-entry remains a major challenge, and familiarity with re-entry techniques is essential for interventionists. If spontaneous re-entry cannot be achieved with a standard wire, specific re-entry devices such as the Outback (Cordis, Miami Lakes [FL], US) may be utilised. Promising data demonstrated technical success and primary stent patency rates of up to 92.3% at 12 months with the Outback, as subintimal angioplasty gains increasing recognition in the treatment of long-segment TransAtlantic Inter-Society Consensus II class C/D lesions.⁴ Where such devices are unavailable, several alternative approaches may be considered, including retrograde access via the distal artery with

establishment of a through-and-through floss wire using the subintimal arterial flossing with antegrade-retrograde intervention (the SAFARI [subintimal arterial flossing with antegrade-retrograde intervention] technique⁵ as in our case), the parallel wire technique,⁶ the wire rendezvous technique with ballooning of subintimal space as seen in CART (controlled antegrade and retrograde subintimal tracking), reverse CART, or the double-balloon technique.^{7,8}

In our experience, SAFARI can be performed in several ways once luminal re-entry has been achieved. First, a nitinol snare system may be deployed via antegrade access to capture the retrograde wire intraluminally and establish a through-and-through access.⁹ Alternatively, retrograde manipulation of the wire tip within the sheath or catheter via groin access may be performed (as in our current case).

To the best of our knowledge, cases of double-barrel subintimal stenting are sparsely reported in the literature and have not been reported locally. Several case reports

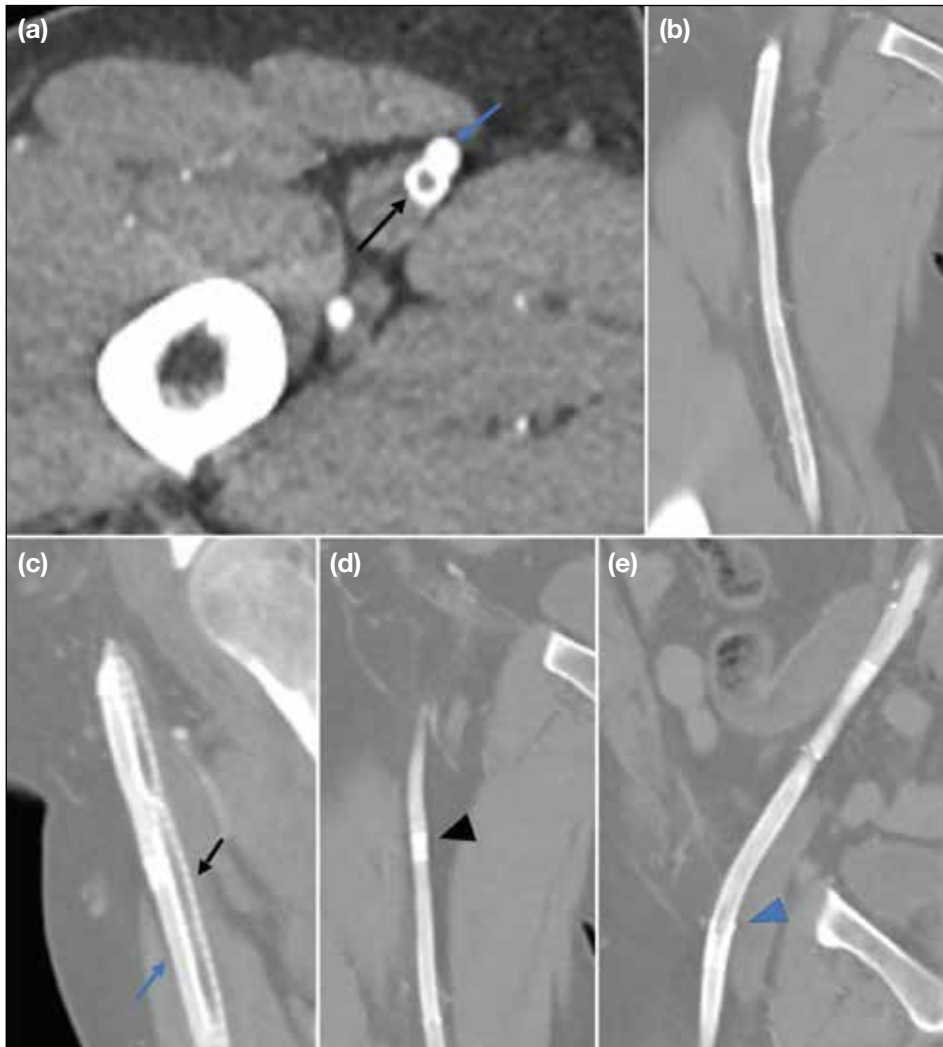


Figure 5. Follow-up computed tomography angiogram at 8 months postprocedure showing successful double-barrel stenting with exclusion of the mid superficial femoral artery (mid-SFA) Zilver stent (black arrows in [a] and [c]) and a patent new Supera mid-SFA stent (blue arrows in [a] and [c]): (a) axial view; (c) oblique sagittal view. Oblique coronal reconstruction showing patency throughout the intraluminal-subintimal-intraluminal multi-stent system (b), including the distal overlapping stent segments (black arrowhead in [d]) and the proximal overlapping stent segments (blue arrowhead in [e]).

describe double-barrel stenting (DBS) for exclusion of occluded stents in salvage procedures for lower limb and coronary arterial occlusions,¹⁰⁻¹² although this remains an uncommonly utilised technique. One case series of three patients with peripheral arterial disease following DBS reported varying degrees of success, with the longest assisted secondary patency of up to 85 months,¹³ supporting its feasibility and long-term patency.

CONCLUSION

We report a case of prior inadvertent subintimal stenting of a bridging CFA-pSFA stent, followed by successful salvage with subintimal DBS using the SAFARI technique within a multi-stent system. Methods to reduce the risk of inadvertent subintimal stenting are discussed. Subintimal manipulation and re-entry techniques with

antegrade-retrograde approaches are also discussed as important tools for interventionists. Although not commonly employed, DBS has been described in several case reports and small case series. Our case affirms the feasibility of this technique where salvage of inadvertent subintimal stenting is necessary.

REFERENCES

1. Dash D. Guidewire crossing techniques in coronary chronic total occlusion intervention: A to Z. *Indian Heart J.* 2016;68:410-20.
2. Loffroy R, Falvo N, Galland C, Fréquier L, Ledan F, Midulla M, et al. Intravascular ultrasound in the endovascular treatment of patients with peripheral arterial disease: current role and future perspectives. *Front Cardiovasc Med.* 2020;7:551861.
3. Ying LH, Fan YS, Lu Y, Xu K, Li CJ. Intravascular ultrasound guided retrograde guidewire true lumen tracking technique for chronic total occlusion intervention. *J Geriatr Cardiol.* 2018;15:199-202.

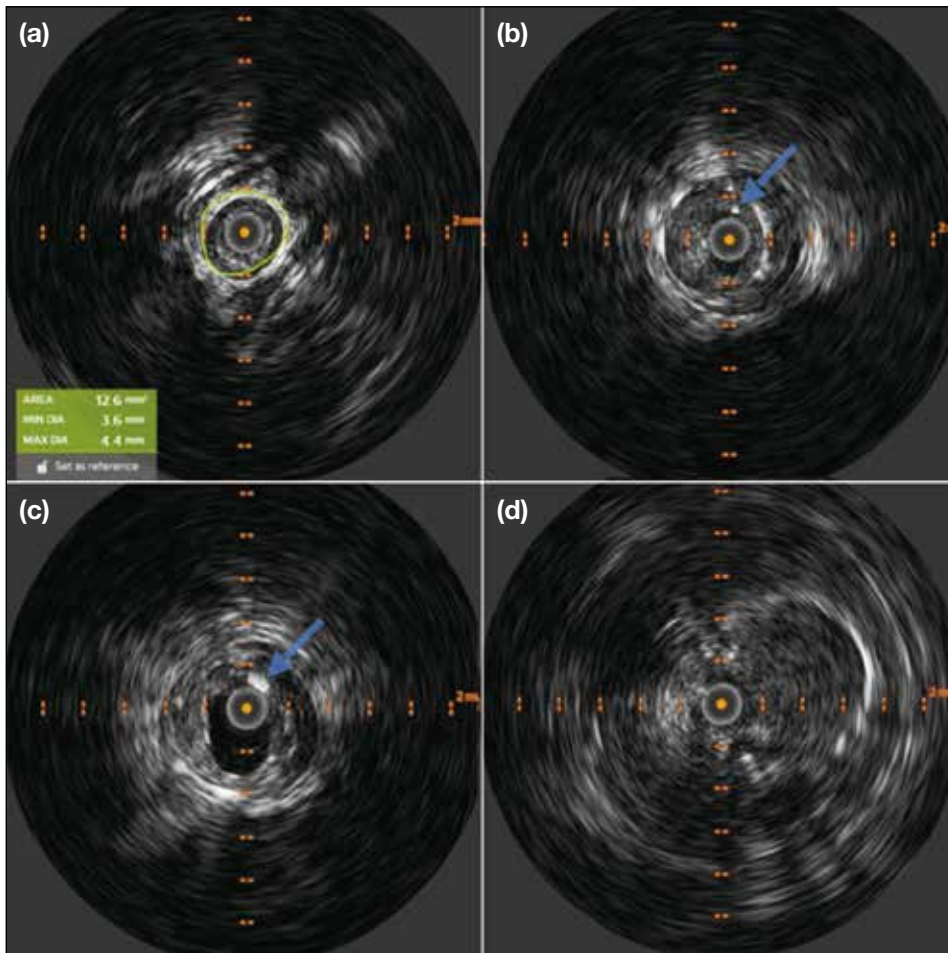


Figure 6. Intravascular ultrasound (IVUS) images confirming wire positioning from the 2023 SAFARI (subintimal arterial flossing with antegrade-retrograde intervention) double-barrel stenting procedure. (a) IVUS enables vessel sizing for selection of appropriate catheters and stents. (b) IVUS image showing the echogenic guidewire in the intraluminal space (arrow). (c) IVUS image showing echogenic guidewire in the subintimal space (arrow). (d) IVUS allows assessment of stent margins to prevent malalignment and inadvertent subintimal entry.

4. Gandini R, Fabiano S, Spano S, Volpi T, Morosetti D, Chiaravalloti A, et al. Randomized control study of the Outback LTD reentry catheter versus manual reentry for the treatment of chronic total occlusions in the superficial femoral artery. *Catheter Cardiovasc Interv.* 2013;82:485-92.
5. Zhuang KD, Tan SG, Tay KH. The “SAFARI” technique using retrograde access via peroneal artery access. *Cardiovasc Intervent Radiol.* 2012;35:927-31.
6. Taniguchi Y, Sakakura K, Ban S, Fujita H. IVUS-assisted parallel wiring for coronary chronic total occlusion. *Postępy Kardiologii Interwencyjnej.* 2022;18:79-80.
7. Michael TT, Papayannis AC, Banerjee S, Brilakis ES. Subintimal dissection/reentry strategies in coronary chronic total occlusion interventions. *Circ Cardiovasc Interv.* 2012;5:729-38.
8. Lee CH, Lee SW. Advancements in endovascular therapy for chronic limb-threatening ischemia: a focus on below-the-ankle interventions and wound healing strategies. *J Cardiovasc Interv.* 2023;2:220-31.
9. Spinosa DJ, Harthun NL, Bissonette EA, Cage D, Leung DA, Angle JF, et al. Subintimal arterial flossing with antegrade-retrograde intervention (SAFARI) for subintimal recanalization to treat chronic critical limb ischemia. *J Vasc Interv Radiol.* 2005;16:37-44.
10. Duterloo D, Lohle PN, Lampmann LE. Subintimal double-barrel restenting of an occluded primary stented superficial femoral artery. *Cardiovasc Intervent Radiol.* 2007;30:474-6.
11. Somsen YB, Nap A, Henriques JP, Knaapen P. Double barrel in CTO PCI. *PCRonline.com.* Available from: <https://www.pronline.com/Cases-resources-images/Images-interventional-cardiology/EuroIntervention-images/2024/Double-barrel-in-CTO-PCI>. Accessed 1 Jun 2025.
12. Capretti G, Mitomo S, Giglio M, Carlino M, Colombo A, Azzalini L. Subintimal crush of an occluded stent to recanalize a chronic total occlusion due to in-stent restenosis: insights from a multimodality imaging approach. *JACC Cardiovasc Interv.* 2017;10:e81-3.
13. Asfoura S, Farooq I, Siddiqui W, Khatib Y. Long-term patency of double-barrel endovascular stenting for occlusive peripheral vascular disease. Available from: <https://javelinjournal.org/long-term-patency-of-double-barrel-endovascular-stenting-for-occlusive-peripheral-vascular-disease/>. Accessed 1 Jun 2025.

PICTORIAL ESSAY

Revisiting Preoperative Evaluation of the Inferior Vena Cava in Abdominal Malignancies: A Pictorial Essay

A Mandava¹, V Koppula¹, M Kandati¹, AK Reddy¹, H Kacharagadla¹, SR Thammineedi²

¹Department of Radiodiagnosis, Basavatarakam Indo American Cancer Hospital and Research Institute, Hyderabad, India

²Department of Surgical Oncology, Basavatarakam Indo American Cancer Hospital and Research Institute, Hyderabad, India

INTRODUCTION

Inferior vena cava (IVC) is the largest vein in the body, draining blood from the lower extremities, pelvis, and abdomen into the right atrium. Accurate anatomical assessment is crucial when planning vascular interventions, resections, anastomoses, and reconstructions that form an integral part of the surgical management of abdominopelvic malignancies. Anomalies and variants can complicate access to the IVC and its tributaries during interventional procedures and filter placement. Given that abdominopelvic oncological surgeries require extensive dissections, unawareness of vascular involvement and congenital anomalies can lead to inadvertent injuries with catastrophic outcomes. Contrast-enhanced computed tomography with reconstruction is the gold-standard non-invasive investigation for presurgical mapping; ultrasound with

colour Doppler, magnetic resonance imaging, and positron emission tomography/computed tomography often play complementary roles in evaluating the IVC and its draining veins. This pictorial essay presents several illustrative cases from our experience at a tertiary care cancer centre in India.

ANATOMY AND VARIANTS

The embryogenesis and development of the IVC is a complex process, and multiple congenital variations can arise from abnormal persistence or regression of embryological veins (Table 1).¹⁻⁸ These congenital anomalies are collectively present in 4% of the population.²⁻⁸ The most common clinically significant variations include duplication of the IVC and absence or agenesis (interruption) of the IVC with prominent hemiazygos-azygos pathways² (Figures 1 to 5). Because

Correspondence: Dr A Mandava, Department of Radiodiagnosis, Basavatarakam Indo American Cancer Hospital and Research Institute, Hyderabad, India
Email: dranitha@basavatarakam.org

Submitted: 6 August 2025; Accepted: 23 November 2025.

Contributors: All authors designed the study, acquired the data, analysed the data, drafted the manuscript, and critically revised the manuscript for important intellectual content. All authors had full access to the data, contributed to the study, approved the final version for publication, and take responsibility for its accuracy and integrity.

Conflicts of Interest: All authors have disclosed no conflicts of interest.

Funding/Support: This study received no specific grant from any funding agency in the public, commercial, or not-for-profit sectors.

Data Availability: All data generated or analysed during the present study are available from the corresponding author on reasonable request.

Ethics Approval: The study was approved by the Institutional Ethics Committee of Basavatarakam Indo American Cancer Hospital and Research Institute, India (Ref No.: IEC/2021/55). A waiver of informed patient consent was granted by the Committee as the study involved minimal risk and non-identifiable data were used.

Declaration: A few of the images were presented as part of scientific exhibit in Radiological Society of North America Annual Meeting 2023, 26-30 November 2023, Chicago [IL], United States.

visceral thoracic and abdominal organs demonstrate left-right anatomical asymmetry, awareness of discrepancies in laterality and venous drainage into the IVC—such as in situs inversus and heterotaxy syndromes—is critical before undertaking biliary, hepatic, and gastric surgeries (Figure 6). Variations in renal vein anatomy are often asymptomatic and overlooked but are crucial during renal or adrenal surgeries and retroperitoneal

dissections. Anomalous veins and collateral vessels may be misdiagnosed as lymphadenopathy; hence, contrast imaging is essential in all cases of malignancy (Figures 7 to 9).

ACQUIRED PATHOLOGIES

The major acquired venous pathologies in abdominopelvic malignancies include external compression or infiltration of the IVC and its draining veins by neoplasms (Figures 10 and 11), metastatic lymph nodes (Figure 12), and/or intraluminal thrombosis.

Malignancies most commonly involving the IVC include those of the liver (4.0%-5.9%), kidney (4%-10%), and adrenal glands (9%-19%).^{4,8} Although the portal veins are more frequently involved, abnormalities of the hepatic artery, hepatic veins, and IVC may occur in hepatocellular carcinomas; accordingly, triphasic computed tomography should be performed in the evaluation of liver malignancies (Figure 13).

Table 1. Common congenital anomalies involving the inferior vena cava and their incidence.¹⁻⁹

	Incidence
Agenesis of IVC	0.0005% to 1%
Duplication of IVC	0.2% to 3.0%
Left-sided IVC	0.2% to 0.5%
Retroaortic left renal vein	1.2% to 2.4%
Circumaortic left renal vein	1.5% to 8.7%
Situs inversus totalis	0.01%

Abbreviation: IVC = inferior vena cava.

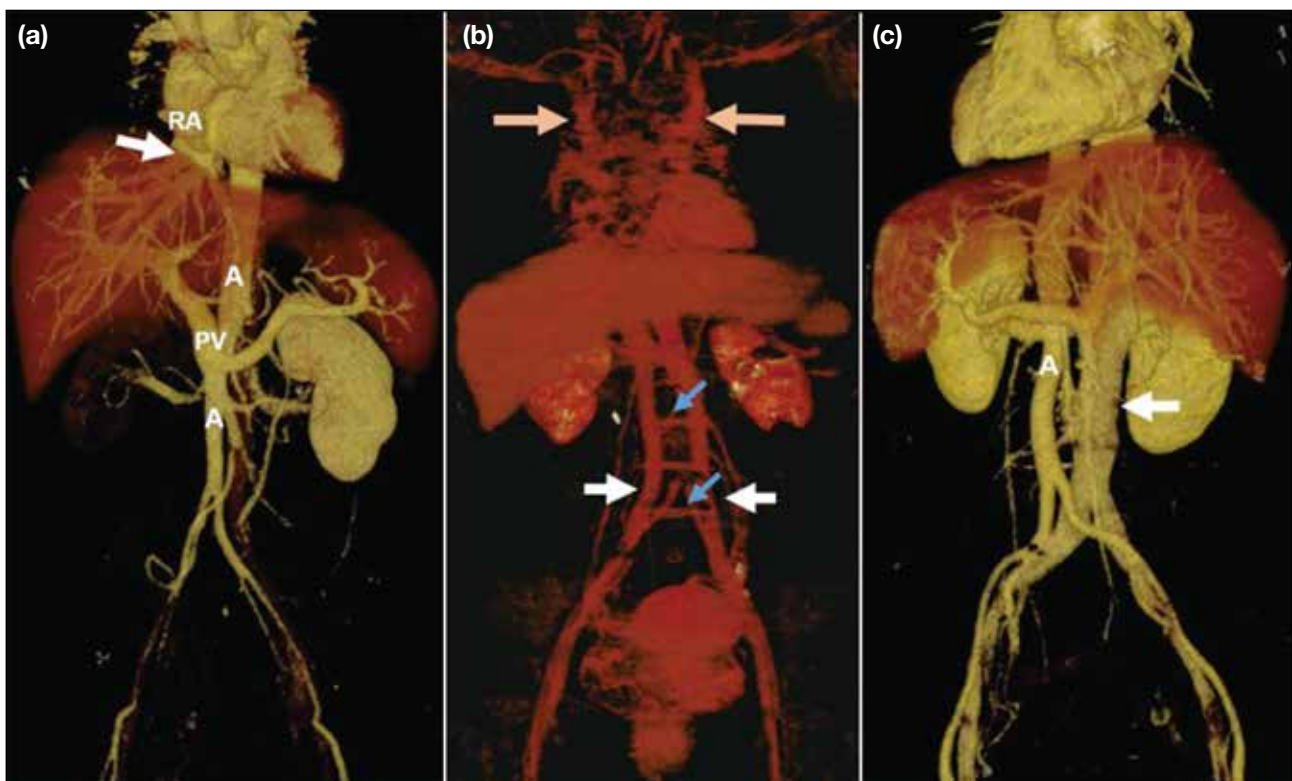


Figure 1. Volume-rendered contrast-enhanced computed tomography images. (a) Interrupted inferior vena cava (IVC) with absence of the infrahepatic IVC. The suprahepatic IVC (white arrow) drains into the right atrium (RA) of the heart. The normal portal vein (PV) and the aorta (A) are visible. (b) Rare case of complete duplication of the superior vena cava in the thorax (orange arrows) and the IVC in the abdomen (white arrows), with multiple bridging veins between duplicated segments (blue arrows). (c) The IVC (white arrow) lies to the left of the aorta (A), with dextrocardia in a patient with situs inversus totalis.

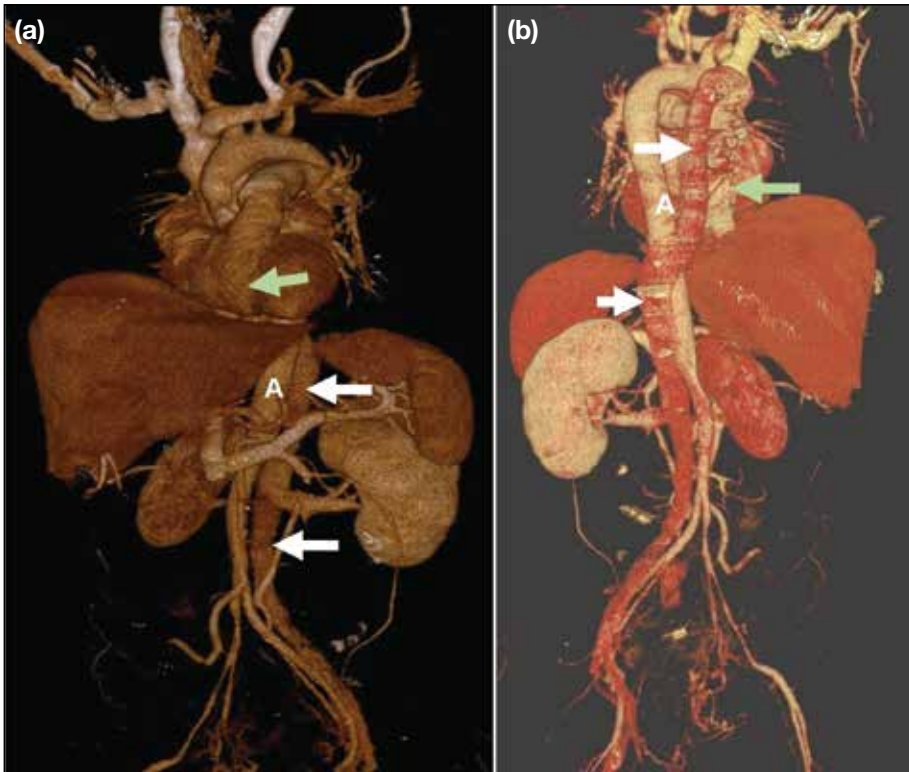


Figure 2. (a) Anterior and (b) posterior volume-rendered contrast-enhanced computed tomography images show a left inferior vena cava with hemiazygos continuation, crossing the midline posterior to the aorta (A) and draining into the azygos-superior vena cava pathway (white arrows). Hepatic veins are visible draining separately into the right atrium (green arrows).

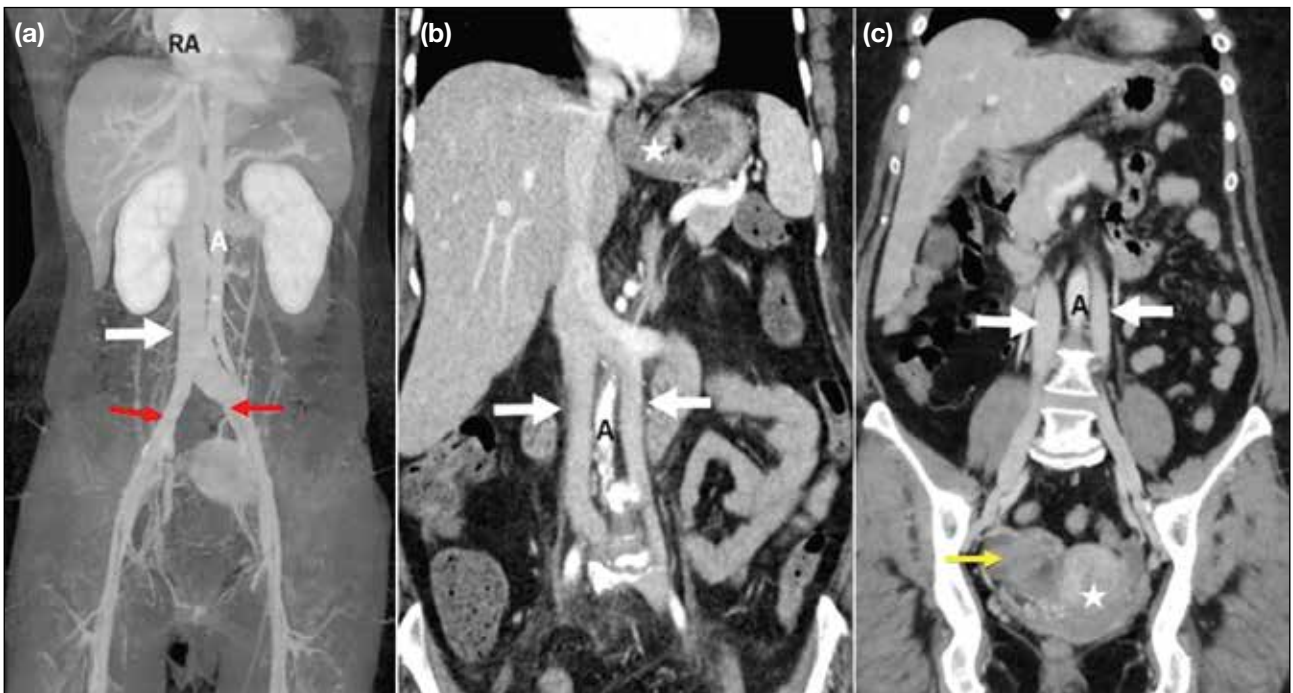


Figure 3. Coronal maximum intensity projection contrast-enhanced computed tomography images of the abdomen. (a) Normal inferior vena cava (IVC) [white arrow] to the right of the aorta (A), formed by the confluence of the bilateral common iliac veins (red arrows), draining into the right atrium (RA). (b) Duplication of the IVC (white arrows) in a patient with gastric malignancy (star). The left infrarenal IVC crosses the midline anterior to the aorta (A) and joins the right IVC. (c) Duplication of the IVC (white arrows) on both sides of the aorta (A) in a patient with endometrial malignancy (star) and a complex right ovarian cyst (yellow arrow).

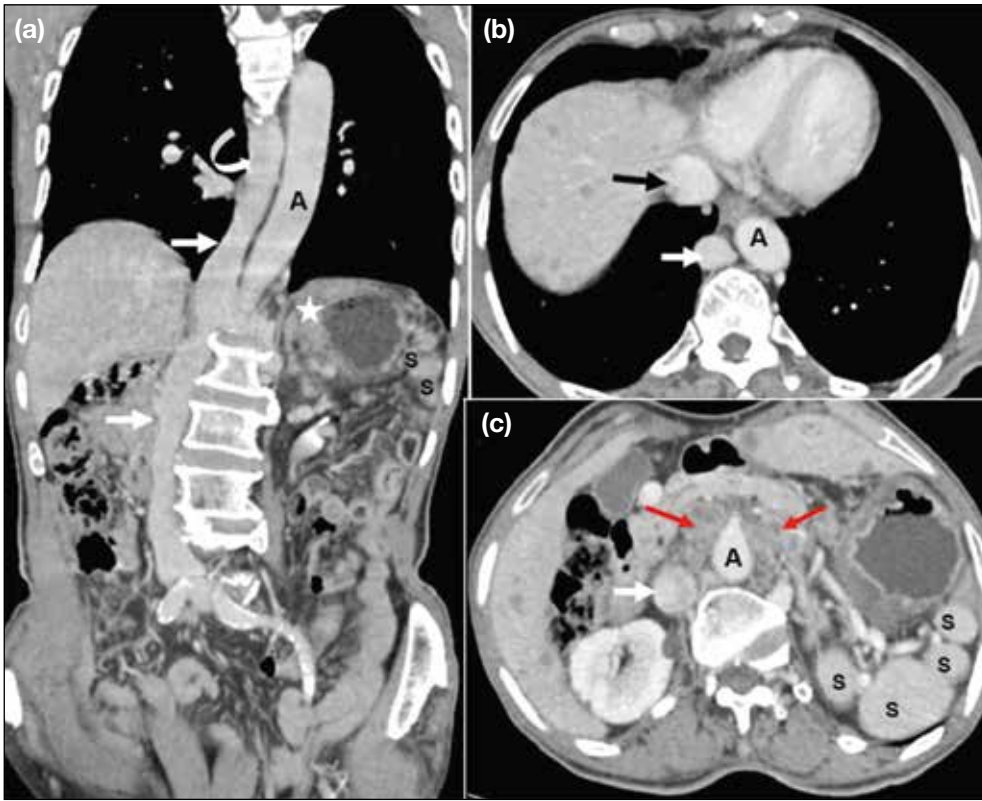


Figure 4. Coronal (a) and axial (b, c) contrast-enhanced computed tomography images in a patient with gastric malignancy (star in [a]) show polysplenia (S) and a right inferior vena cava with azygos continuation (white arrows) draining into the superior vena cava (curved arrow in [a]). Hepatic veins drain separately into the right atrium (black arrow in [b]), and para-aortic lymphadenopathy is also noted (red arrows in [c]). Abbreviation: A = aorta.

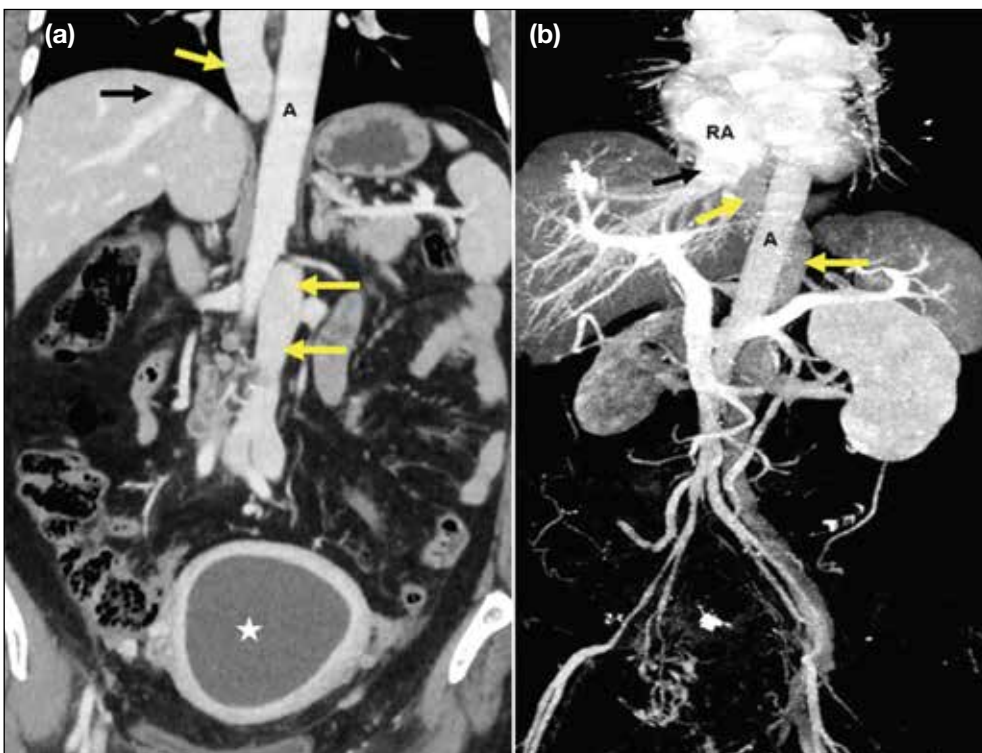


Figure 5. (a) Coronal contrast-enhanced computed tomography and (b) posterior maximum intensity projection images of a patient with cervical carcinoma and pyometra (star in [a]) show a left inferior vena cava crossing the midline posterior to the aorta (A), continuing as the azygos-superior vena cava pathway (yellow arrows). Hepatic veins (black arrows) drain separately into the right atrium (RA).

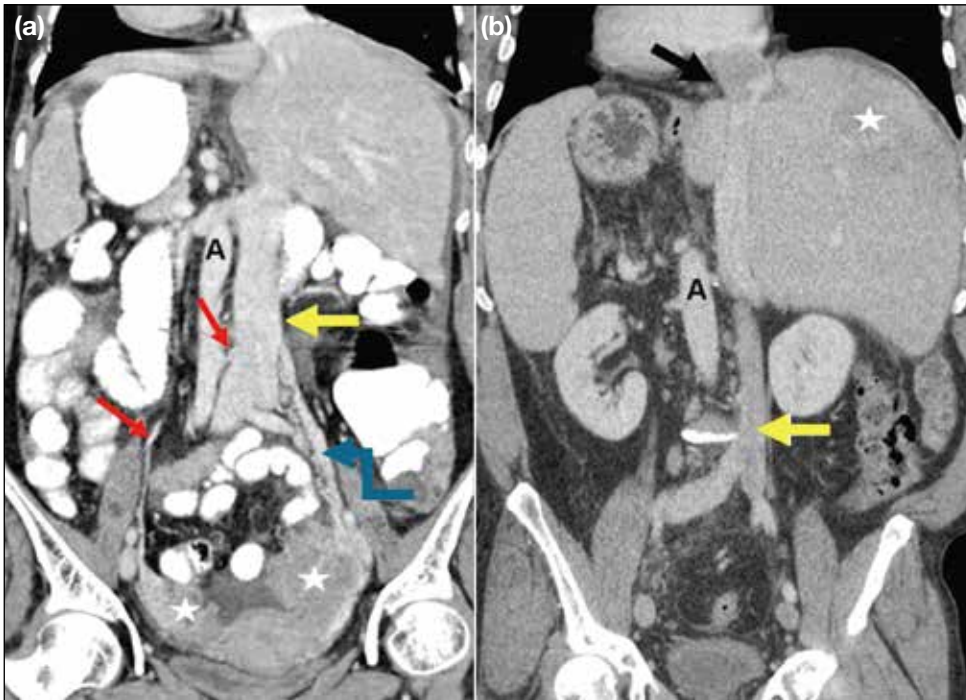


Figure 6. Two cases of situs inversus totalis. (a) A 48-year-old woman with bilateral ovarian malignancy (stars). The right ovarian vein (red arrows) crosses the midline posterior to the aorta (A) and drains into the inferior vena cava (IVC) [yellow arrow], while a prominent left ovarian vein drains directly into the left-sided IVC (blue elbow arrow). (b) A 55-year-old man with hepatocellular carcinoma (star). The IVC (yellow arrow) lies to the left of the aorta (A), with an intraluminal thrombus present in the hepatic and suprahepatic segments (black arrow).

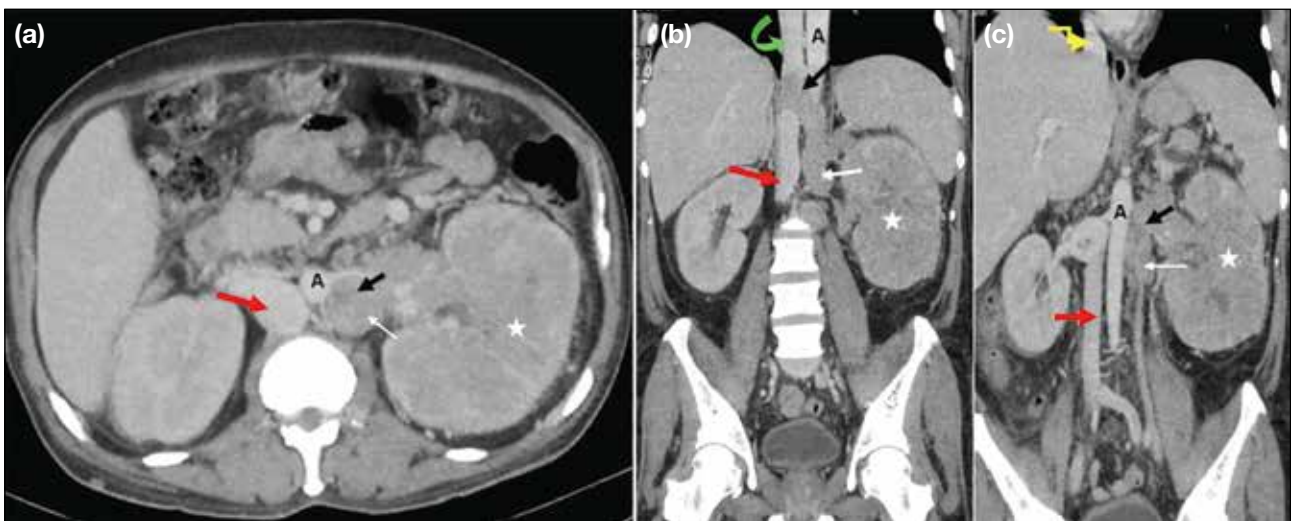


Figure 7. (a) Axial and (b, c) coronal contrast-enhanced computed tomography images of a patient with left renal cell carcinoma (stars) show a duplicated inferior vena cava (IVC) on either side of the aorta (A), with azygos continuation of the right IVC (red arrows). The left IVC (white arrows) crosses the midline and drains into the right IVC-azygos-superior vena cava pathway (green curved arrow in [b]). Tumour thrombus is present in the left renal vein and the left IVC, extending across the midline into the azygos continuation of the right IVC (black arrows). Hepatic veins drain separately into the right atrium (yellow elbow arrow in [c]).

Cancer-associated thrombosis is recognised as the most common complication of cancer and is attributed to several factors (Table 2).⁷⁻¹² Compared with the general population, patients with cancer have a 12-fold

increased risk of developing venous thrombosis, as well as a significantly worse prognosis^{9,10} (Figure 14). The IVC and its tributaries, especially the renal and gonadal veins, should be assessed in all abdominal malignancies

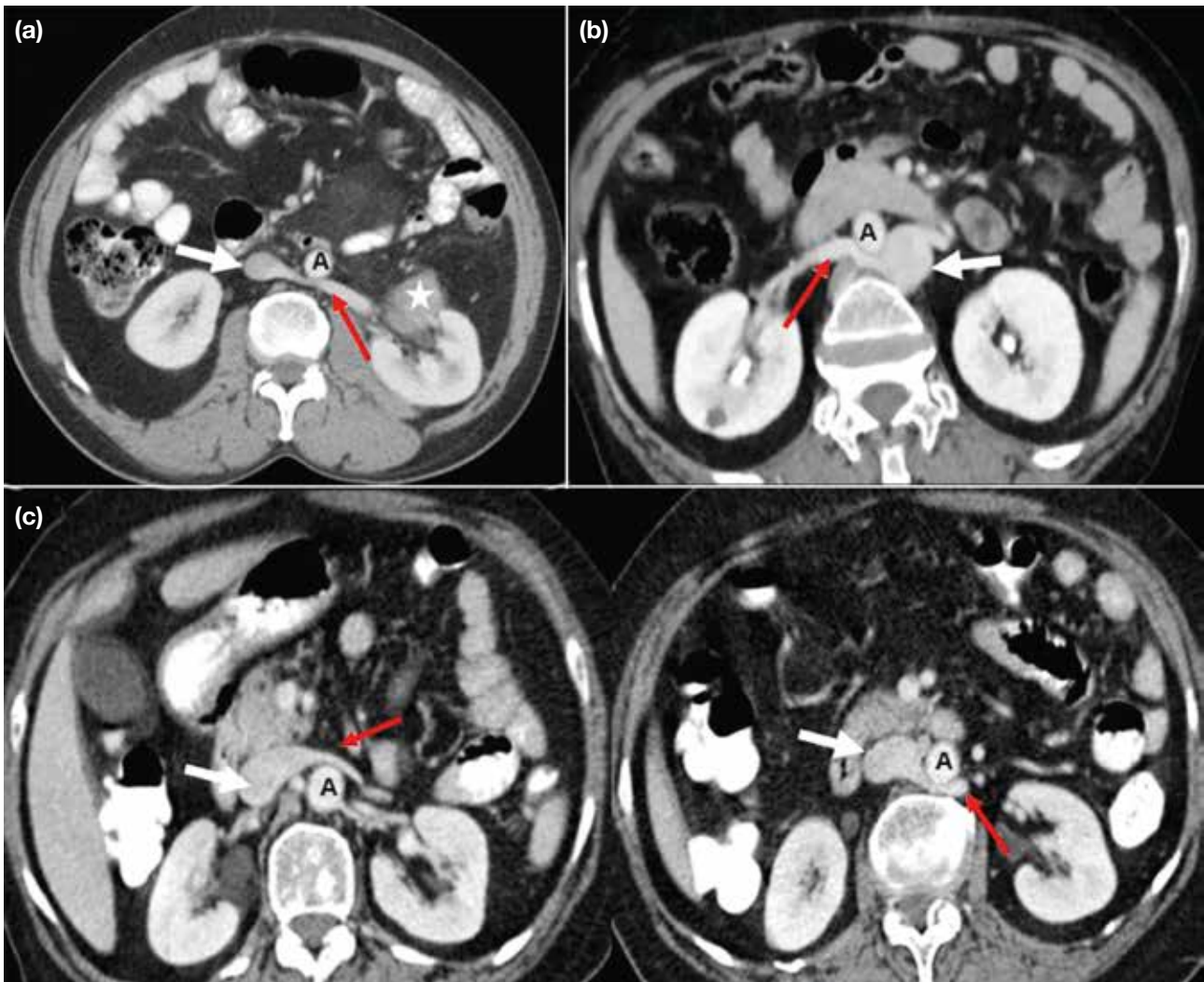


Figure 8. Contiguous axial contrast-enhanced computed tomography images showing anomalous renal veins. (a) Retroaortic left renal vein (red arrow) posterior to the aorta, draining into the normal right inferior vena cava (IVC) [white arrow] in a patient with abdominal liposarcoma (star). (b) Retroaortic right renal vein (red arrow) draining into the left IVC (white arrow). (c) Circumaortic left renal veins (red arrows) passing anterior and posterior to the aorta, draining into the right-sided IVC (white arrows). Abbreviation: A = aorta.

to exclude thrombosis (Figure 15). Postsurgical venous thromboembolism is the leading cause of postoperative death in cancer patients, and IVC thrombosis is associated with substantial morbidity and mortality.^{11,12}

Tumour thrombus results either from direct extension of the malignancy or embolisation of neoplastic cells into the abdominal veins and/or the IVC. Differentiation between bland and tumour thrombi is crucial for management: anticoagulation or catheter-directed thrombolysis is the mainstay of treatment for bland thrombus, whereas tumour thrombus may require surgical resection (Table

3).^{8,13-15} In addition to tumour thrombectomy, adherent tumour thrombus invading the IVC wall necessitates en bloc excision, segmental resection, and vascular reconstruction.¹⁵ Magnetic resonance imaging is superior to computed tomography in detecting and characterising tumour thrombus, as well as in identifying vessel wall invasion⁸ (Figure 16). The extent of tumour thrombus within the IVC and the right atrium, along with vessel wall invasion, determines staging and resectability. These two factors are also independent predictors of adverse prognosis and poor survival rates in abdominal malignancies.^{7,8}

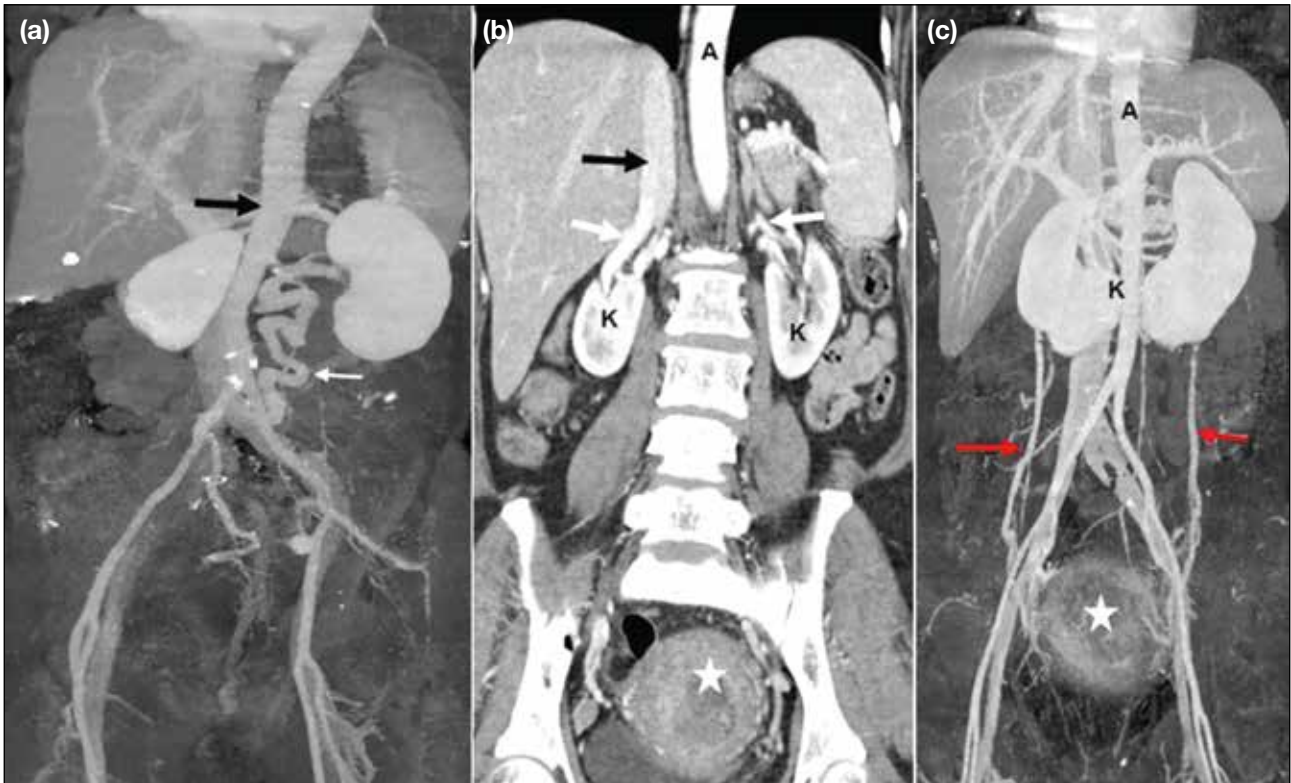


Figure 9. (a) Tortuous left renal vein draining into the left common iliac vein (white arrow) instead of the inferior vena cava (IVC) [black arrow]. (b) Anterior and (c) posterior views show 'horseshoe' kidneys (K) with vertically oriented renal veins (white arrows in [b]) and gonadal veins (red arrows in [c]) draining into the IVC (black arrow in [b]) in a patient with endometrial malignancy (stars).



Figure 10. Right adrenocortical malignancy. (a) Axial and (b) coronal contrast-enhanced computed tomography images of the abdomen show a large, heterogeneously enhancing hypoattenuating lesion (stars) invading the inferior vena cava (arrows).

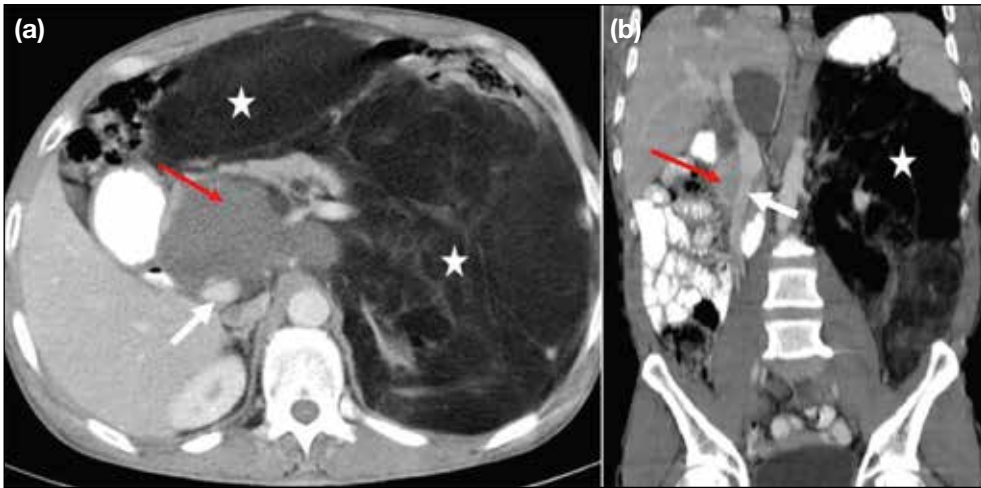


Figure 11. Retroperitoneal liposarcoma. (a) Axial and (b) coronal contrast-enhanced computed tomography images of the abdomen show large fatty component (stars) and small soft-tissue component (red arrows) encasing the inferior vena cava (white arrows).

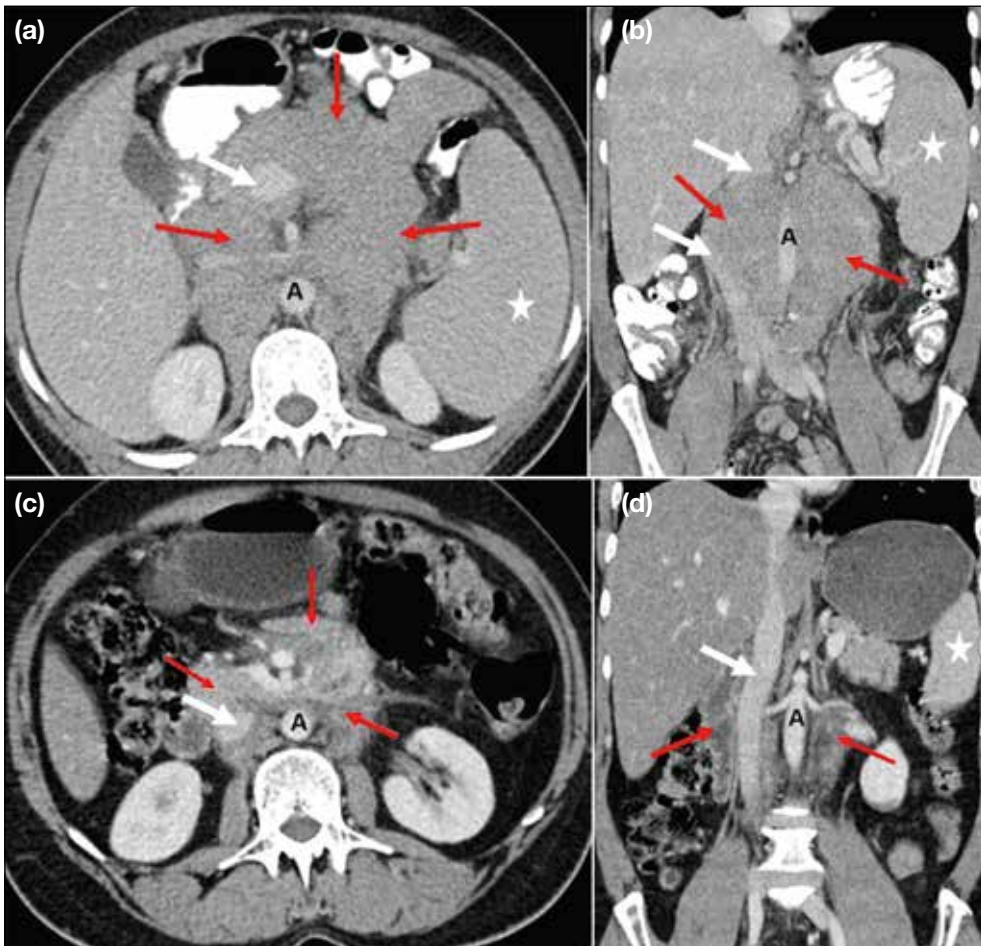


Figure 12. A 24-year-old man with lymphoma. (a) Axial and (b) coronal contrast-enhanced computed tomography images of the abdomen show splenomegaly (stars) and conglomerated nodal mass (red arrows) encasing and causing narrowing of the inferior vena cava (IVC) [white arrows], aorta, and their branches. (c, d) Corresponding post-chemotherapy images show a significant decrease in the size of the nodal mass (red arrows) and spleen (star in [d]), with expansion and visualisation of the IVC (white arrows). Abbreviation: A = aorta.

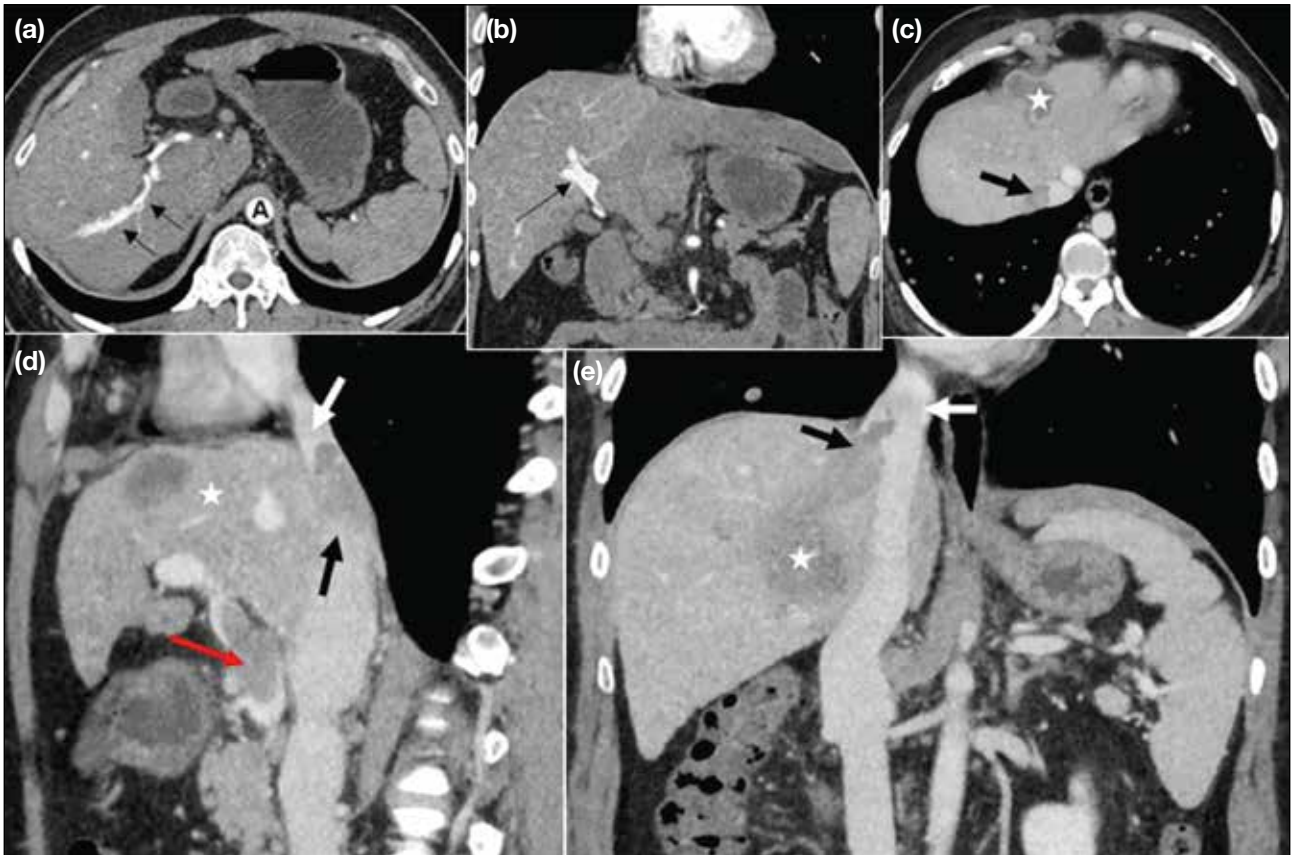


Figure 13. Hepatocellular carcinoma (HCC) in a 56-year-old man. (a) Axial and (b) coronal contrast-enhanced computed tomography (CECT) images in the early arterial phase show contrast opacification of the aorta (A), hepatic artery, and portal vein due to an arteriportal fistula in the right lobe of the liver (black arrows). (c) Axial CECT image shows HCC (star) with thrombus in the inferior vena cava (IVC) [black arrow]. (d, e) Coronal CECT images in the venous phase show HCC (stars), along with thrombus in the portal vein (red arrow in [d]) and hepatic veins (black arrows) extending into the IVC (white arrows).

Table 2. Risk factors associated with increased incidence of thrombosis in patients with cancer.⁷⁻¹²

	Increased incidence of thrombosis
General factors	<ul style="list-style-type: none"> • Increasing age: >70 years (2×), >85 years (10×) • Congenital variations in anatomy of the IVC and its draining veins • Co-morbidities: infection, renal failure, lung disease, cardiac disease, and obesity • History of thromboembolism (6-7×) • Immobilisation
Cancer-associated factors	<ul style="list-style-type: none"> • Time period: highest risk in first year after diagnosis • High-risk primary cancer sites: pancreas, gastrointestinal tract, ovary, uterus, kidney, brain, prostate, breast, and lung • Cancer stage: greater risk with advanced-stage cancers • Cancer histology: high risk in mucin-producing adenocarcinomas • Tumour grade: high-grade (Grade 3 and Grade 4) tumours (2×) compared with low-grade tumours • Vascular tumour invasion by malignancies such as renal cell carcinoma is an independent risk factor
Cancer therapy-related factors	<ul style="list-style-type: none"> • Surgery: high risk in abdominopelvic and general surgeries compared with urological surgeries • Prolonged hospitalisation • Indwelling central venous catheters, IVC filters • Chemotherapy (6-7×), blood transfusions, erythropoiesis-stimulating agents • Drugs associated with thrombosis: L-asparaginase, cisplatin, tamoxifen, angiogenesis inhibitors

Abbreviation: IVC = inferior vena cava.



Figure 14. (a) Coronal contrast-enhanced computed tomography (CECT) image of a 56-year-old man with adenocarcinoma of the stomach shows antropyloric gastric malignancy (stars), metastatic lymph nodes (white arrows), and multiple intraluminal tumour thrombi (black arrows) in the inferior vena cava (IVC) [red arrow], with extraluminal infiltration of the IVC by right iliac lymph nodes (yellow arrow). (b) Coronal and (c, d) axial CECT images of a 42-year-old woman with mucinous adenocarcinoma of the stomach show diffuse thickening of the gastric wall (stars in [b] and [c]) and widespread metastatic lymph nodes with multiple tiny calcifications (blue arrows in [b] and [c]). A focal intraluminal thrombus in the IVC (black arrows in [b] and [c]) and a long-segment thrombus in a dilated, non-enhancing right ovarian vein (green curved arrows in [b] and [d]) are evident. The left ovarian vein (yellow arrows in [b] and [d]) is compressed by retroperitoneal lymphadenopathy.

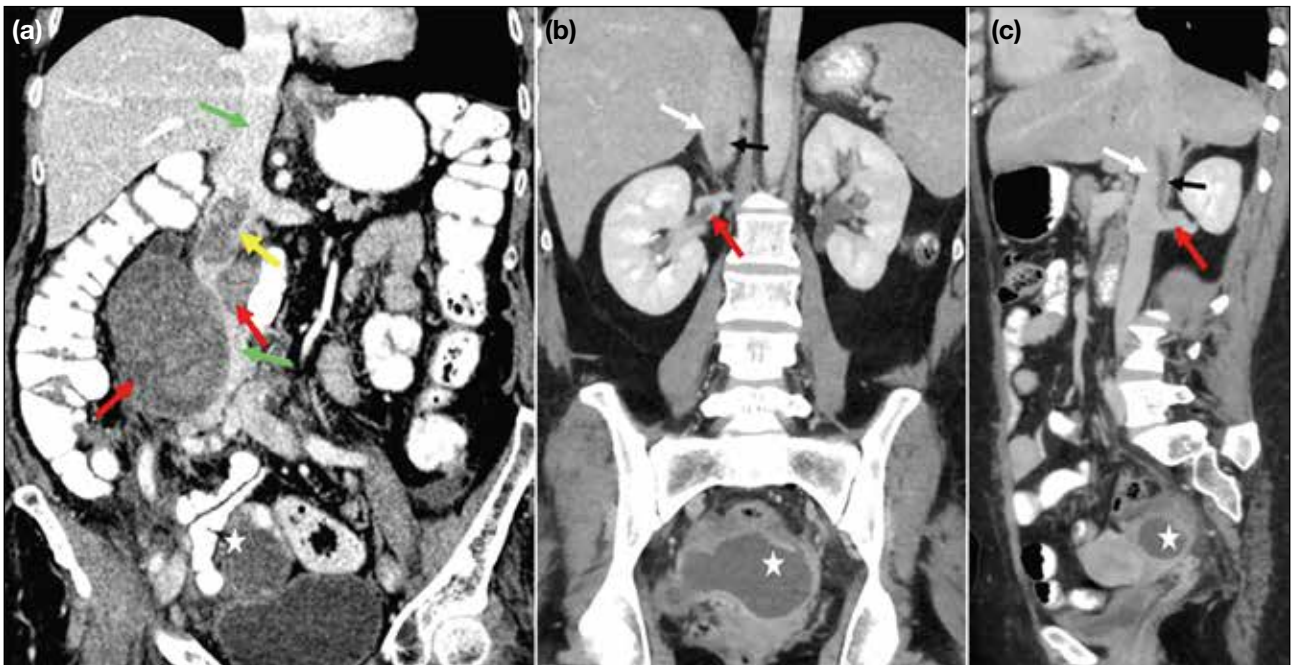


Figure 15. Two cases of ovarian cancer. (a) Coronal contrast-enhanced computed tomography (CECT) image of the abdomen of a 62-year-old patient shows right ovarian malignancy (star) with an intraluminal thrombus in the inferior vena cava (IVC) [yellow arrow] and extraluminal compression (green arrows) by enlarged lymph nodes (red arrows). (b, c) Coronal CECT images of the abdomen of a 53-year-old patient show a complex cystic lesion in the pelvis and left adnexa (stars), with bland thrombi (black arrows) in the infrahepatic IVC (white arrows) and the right renal vein (red arrows).

Table 3. Differentiating imaging features between tumour thrombus and bland thrombus.^{8,13-15}

Tumour thrombus	Bland thrombus
Shows contrast enhancement on CECT and MRI	Does not enhance with contrast
May expand the vascular lumen	Does not expand the vascular lumen
Contiguous with the primary malignant lesion	Not contiguous with the primary malignant lesion
May invade the vessel wall	Does not invade the vessel wall
Shows relatively lower ADC values on MRI	May show higher ADC values on MRI
Hypermetabolic on FDG-PET/CT	Does not show FDG uptake on PET/CT

Abbreviations: ADC = apparent diffusion coefficient; CECT = contrast-enhanced computed tomography; FDG-PET/CT = fluorodeoxyglucose positron emission tomography/computed tomography; MRI = magnetic resonance imaging.

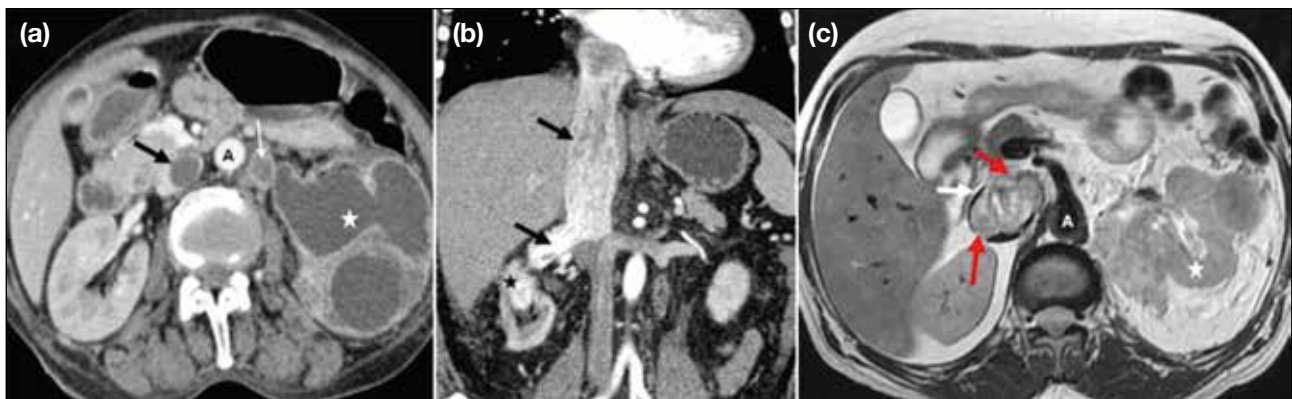


Figure 16. Renal cell carcinoma (RCC) involving the inferior vena cava (IVC) in three patients. (a) Patient 1. Axial contrast-enhanced computed tomography (CECT) image shows left RCC (star) with an enhancing tumour thrombus in the dilated left renal vein (white arrow) and a bland thrombus in the IVC (black arrow). (b) Patient 2. Coronal CECT image shows intense heterogeneous enhancement of right upper-pole RCC (star), with an enhancing tumour thrombus in the right renal vein and IVC (black arrows), extending up to the right atrium. (c) Patient 3. Axial T2-weighted magnetic resonance image shows left RCC (star) with tumour thrombus in the IVC (white arrow) focally invading the IVC wall (red arrows).

Abbreviation: A = aorta.

INFERIOR VENA CAVA IN PAEDIATRIC MALIGNANCIES

Anatomical variants in the hepatic vasculature and the IVC should be identified before segmental resection in hepatoblastoma (Figure 17). Retroperitoneal malignancies in children may involve the abdominal vasculature, including the IVC (Figure 18). Thrombosis and vascular displacement are more common in Wilms tumours than vessel encasement, whereas vascular invasion occurs more frequently in neuroblastomas⁴ (Figure 19).

POSTSURGICAL COMPLICATIONS

Compression and narrowing of the IVC may occur as immediate or delayed complications in patients undergoing extensive retroperitoneal surgeries and abdominal lymph node dissections (Figure 20).

CONCLUSION

Comprehensive evaluation of the IVC and its tributaries is a critical component of pre-surgical imaging. Cancer-associated thrombosis of the IVC and abdominal veins remains underrecognised and requires a high index of clinical suspicion due to non-specific symptoms. Identifying abnormal drainage patterns and congenital variations, along with recognising intrinsic or extrinsic involvement of the IVC by abdominopelvic malignancies, is vital before undertaking major oncological surgery.

REFERENCES

1. Eitler K, Bibok A, Telkes G. Situs inversus totalis: a clinical review. *Int J Gen Med.* 2022;15:2437-49.
2. Bass JE, Redwine MD, Kramer LA, Huynh PT, Harris JH Jr. Spectrum of congenital anomalies of the inferior vena cava: cross-sectional imaging findings. *Radiographics.* 2000;20:639-52.
3. Malaki M, Willis AP, Jones RG. Congenital anomalies of the



Figure 17. A 3-year-old child with biopsy-proven hepatoblastoma. (a) Greyscale and (b) colour Doppler ultrasound images show a mixed echogenic lesion (star in [a]) in the liver with narrowing of the intrahepatic inferior vena cava (IVC) [white arrows in (b)]. (c) Coronal contrast-enhanced computed tomography image of the abdomen shows a heterogeneously enhancing hypoattenuating lesion (star) in the right lobe of the liver with pronounced luminal narrowing of the intrahepatic IVC (white arrow). Hepatomegaly with patchy heterogeneous parenchymal enhancement and architectural distortion is also noted.

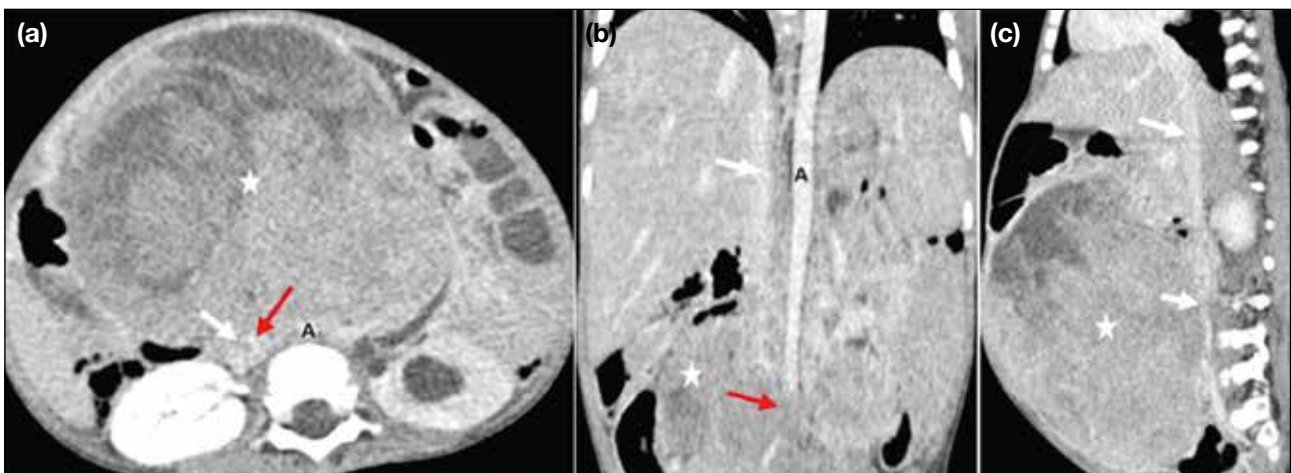


Figure 18. Retroperitoneal rhabdomyosarcoma in a 4-year-old child. (a) Axial, (b) coronal, and (c) sagittal contrast-enhanced computed tomography images show a large heterogeneously enhancing soft tissue-attenuation mass (stars) partially encasing, compressing, and narrowing the inferior vena cava (white arrows), with infiltration of the vessel wall (red arrows in [a] and [b]). Abbreviation: A = aorta.

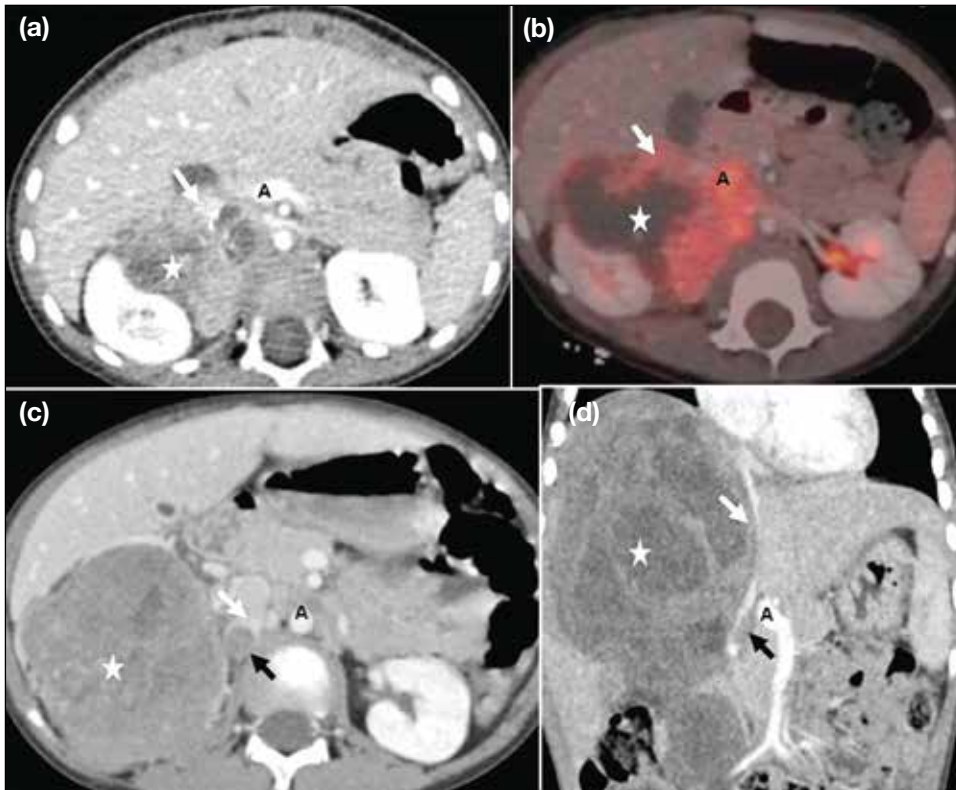


Figure 19. (a) Axial contrast-enhanced computed tomography (CECT) and corresponding (b) positron emission tomography/computed tomography fusion images of a 5-year-old child with neuroblastoma of the right adrenal gland show a hypermetabolic enhancing lesion with non-enhancing necrotic areas in the right suprarenal region (stars), encasing and infiltrating the inferior vena cava (IVC) [white arrows]. (c) Axial and (d) coronal CECT images of the abdomen of a 7-year-old child with Wilms tumour of the right kidney show a large heterogeneously enhancing tumour in the right kidney (stars), with tumour thrombus in the right renal vein (black arrows). The lesion also compresses the right lobe of the liver and causes extraluminal compression of the IVC (white arrows). Abbreviation: A = aorta.

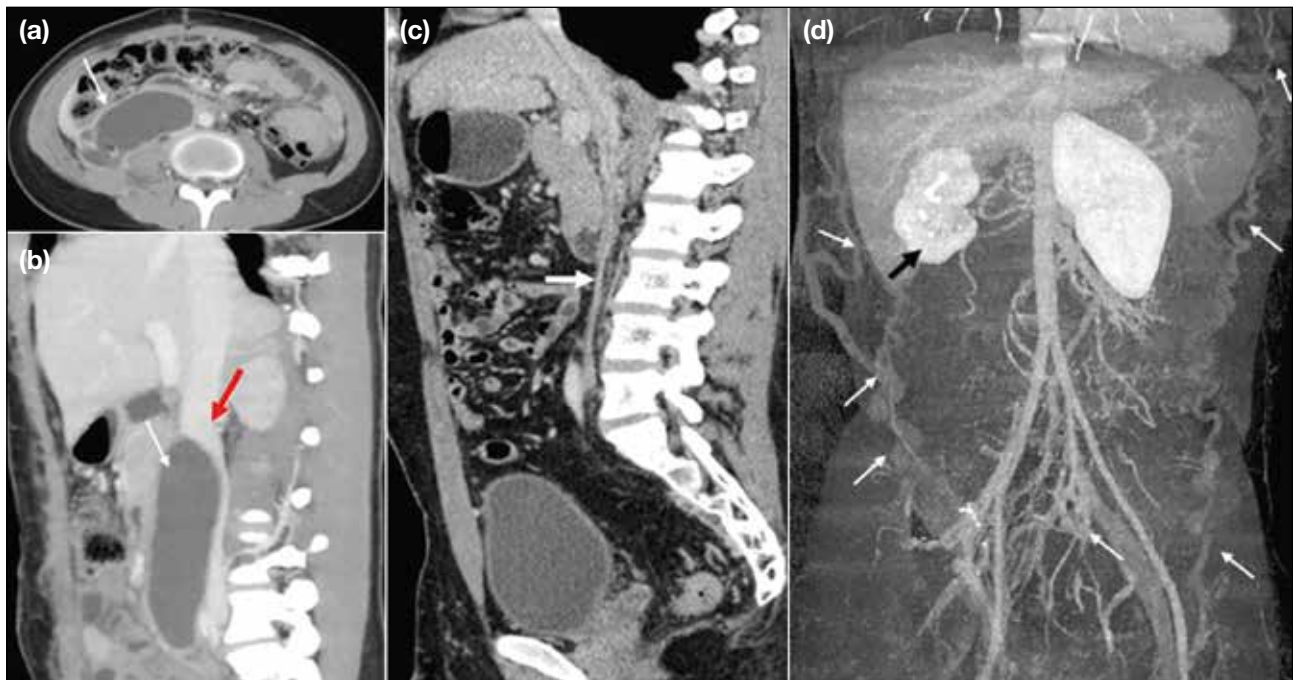


Figure 20. Immediate postsurgical complications on day 8 after para-aortic nodal dissection. (a) Axial and (b) sagittal contrast-enhanced computed tomography (CECT) images of the abdomen show a large hypodense collection (white arrows) causing extraluminal compression of the infrarenal inferior vena cava (IVC) [red arrow in (b)]. Delayed postsurgical complications in a case of carcinoma of the testis, status post-orchidectomy, and para-aortic lymphadenectomy demonstrate chronic IVC thrombosis with collateral formation. (c) Sagittal CECT image of the abdomen shows significant luminal narrowing of the IVC (white arrow). (d) Coronal maximum intensity projection image shows multiple dilated, tortuous collateral vessels in the pelvis and abdomen extending into the thoracic walls (white arrows), along with a contracted right kidney (black arrow).


- inferior vena cava. Clin Radiol. 2012;67:165-71.
- Smillie RP, Shetty M, Boyer AC, Madrazo B, Jafri SZ. Imaging evaluation of the inferior vena cava. Radiographics. 2015;35:578-92.
 - Onbaş O, Kantarci M, Koplay M, Olgun H, Alper F, Aydinli B, et al. Congenital anomalies of the aorta and vena cava: 16-detector-row CT imaging findings. Diagn Interv Radiol. 2008;14:163-71.
 - Alkhouli M, Morad M, Narins CR, Raza F, Bashir R. Inferior vena cava thrombosis. JACC Cardiovasc Interv. 2016;9:629-43.
 - Jacob T, Modgil V, Rana KK, Das S. Multiple vascular anomalies in the abdomen—a gross anatomical study. Int J Morphol. 2008;26:563-6.
 - Li SJ, Lee J, Hall J, Sutherland TR. The inferior vena cava: anatomical variants and acquired pathologies. Insights Imaging. 2021;12:123.
 - Mahajan A, Brunson A, Adesina O, Keegan TH, Wun T. The incidence of cancer-associated thrombosis is increasing over time. Blood Adv. 2022;6:307-20.
 - Abdol Razak NB, Jones G, Bhandari M, Berndt MC, Metharom P. Cancer-associated thrombosis: an overview of mechanisms, risk factors, and treatment. Cancers (Basel). 2018;10:380.
 - Agnelli G, Bolis G, Capussotti L, Scarpa RM, Tonelli F, Bonizzoni E, et al. A clinical outcome-based prospective study on venous thromboembolism after cancer surgery: the @RISTOS project. Ann Surg 2006;243:89-95.
 - Teter K, Schrem E, Ranganath N, Adelman M, Berger J, Sussman R, et al. Presentation and management of inferior vena cava thrombosis. Ann Vasc Surg. 2019;56:17-23.
 - Engelbrecht MR, Akin O, Dixit D, Schwartz L. Bland and tumor thrombi in abdominal malignancies: magnetic resonance imaging assessment in a large oncologic patient population. Abdom Imaging. 2011;36:62-8.
 - Catalano OA, Choy G, Zhu A, Hahn PF, Sahani DV. Differentiation of malignant thrombus from bland thrombus of the portal vein in patients with hepatocellular carcinoma: application of diffusion-weighted MR imaging. Radiology. 2010;254:154-62.
 - Adams LC, Ralla B, Bender YY, Bressemer K, Hamm B, Busch J, et al. Renal cell carcinoma with venous extension: prediction of inferior vena cava wall invasion by MRI. Cancer Imaging. 2018;18:17.

Private Healthcare Facilities Ordinance (Cap. 633)
Application for Clinic Licence and Letter of Exemption launched
- Reminder -


**Deadline of application for provisional clinic licence
on or before**


13 APRIL 2026

Apply now



 衛生署
Department of Health


Join our briefing


Simple guide to
Cap. 633

Enquiry
3107 8451 (medical)
2631 1782 (dental)

CATEGORIES OF PAPERS

Hong Kong Journal of Radiology publishes various categories of articles. Each category serves a distinct purpose and is judged by different criteria.

EDITORIAL

Commissioned article presenting the author's opinion on a topical subject or an article published in the current issue. Unsolicited Editorials are not accepted.

Format: An abstract is not required. The text is limited to 1000 words, with a maximum of 1 table or figure, and up to 10 references.

REVIEW ARTICLE

Systematic reviews or meta-analyses of recent developments in a specific topic. Scoping reviews of the literature that identify area(s) for future research will also be considered. No new information is described, and no subjective opinion or personal experiences are expressed.

Format: A structured abstract of ≤ 250 words; headings should include: Introduction, Methods, Results, Conclusion. The text is limited to 5000 words, with a maximum of 20 tables and figures (total), and up to 60 references.

ORIGINAL ARTICLE

Provides new information based on original research. Includes prospective studies with in-depth statistical analysis, unique retrospective observations of a disease or disorder, and studies of novel applications of an interventional procedure or treatment method.

Format: A structured abstract of ≤ 250 words; headings should include: Introduction, Methods, Results, Conclusion. The text is limited to 3500 words, with a maximum of 20 tables and figures (total), and up to 50 references.

PERSPECTIVE

Narrative review articles discussing recent developments in a specific topic. No new information is described; may include subjective opinion or personal experiences.

Format: An unstructured abstract of ≤ 250 words. The text is limited to 2500 words, with a maximum of 20 tables and figures (total), and up to 60 references.

PICTORIAL ESSAY

Teaching exercise with message in the figures and legends. Emphasis is on quality of the illustrations and clinical relevance of the message.

Format: An abstract is not required. The text is limited to 2500 words, with a maximum of 20 tables and figures (total), and up to 15 references.

CASE REPORT

Brief discussion of a case with unique features not previously described. Additional cases (case series) may be added to augment the discussion. The discussion should be succinct and focus on a specific message.

Format: An abstract is not required. The text is limited to 1500 words, with a maximum of 8 tables and figures (total), and up to 15 references.

BRIEF COMMUNICATION

This includes post-meeting commentary, update on new imaging or therapeutic advances, brief description of a specific technique or procedure or new equipment. Teaching exercise aimed at describing a certain radiological or radiotherapeutic technique for trainees and practising radiologists is also welcome.

Format: An abstract is not required. The text is limited to 1500 words, with a maximum of 8 tables and figures (total), and up to 15 references.

LETTER TO THE EDITOR

Short letter on any matter of interest to journal readers, including comments on an article that has previously appeared in the journal. The authors of the article commented on would be invited to reply.

Format: An abstract is not required. The text is limited to 500 words, with up to 5 references. Figures and tables are permitted only exceptionally.

INFORMATION FOR AUTHORS

Aims and Scope

Hong Kong Journal of Radiology is the official peer-reviewed academic journal of the Hong Kong College of Radiologists. It is a multidisciplinary journal covering research work pertaining to the science and practice of the component specialties of the College. The journal publishes various categories of papers, including Reviews, Original Articles, Perspectives, Pictorial Essays, Case Reports, Brief Communications, and Letters to the Editor. Manuscripts will be subject to rigorous peer review. *HKJR* adheres to the Recommendations for the Conduct, Reporting, Editing, and Publication of Scholarly Work in Medical Journals of the International Committee of Medical Journal Editors (ICMJE; www.icmje.org), and the Core Practices of the Committee on Publication Ethics (COPE; publicationethics.org/).

Journal Policies

Reporting Guidelines: *HKJR* recommends the use of reporting guidelines in the preparation of manuscripts, such as those advocated by the EQUATOR Network (eg, CONSORT for randomised trials).

Funding: Any sponsor(s) of the research involved, along with grant number(s) should be provided.

Conflicts of interest: All authors must provide a statement reporting any conflicts of interest. Where none exist, please state 'The authors have no conflicts of interest to declare.'

Ethics: All studies must be conducted in accordance with the Declaration of Helsinki. For studies involving humans, a statement must be included in the manuscript that provides the name of the review board and approval number (or waiver). A statement on patient/guardian consent must also be included. For studies involving animals, appropriate ethics approval is required, and this should be stated in the manuscript.

Submission: Manuscripts should be submitted online via HKAMedTrack (www.hkamedtrack.org/hkjr). Manuscripts must be unpublished works that are not under consideration by another publication.

Copyright: On acceptance of an article by the journal, the corresponding author will be asked to transfer copyright of the article to the College.

Editing: Accepted manuscripts will be copyedited according to journal style. Authors are responsible for all statements made in their work, including changes made by the copy editor.

Proofs and Reprints: The corresponding author will receive page proofs, which should be proofread and returned promptly. Corrections are limited to printer's errors — no substantial author's changes will be made without charge. Quotes for extra copies of reprints are available at the Editorial Office.

Manuscript Preparation

In general, manuscripts should be prepared following the 'IMRaD' structure as recommended by the ICMJE. Please provide a **blinded** manuscript and separate title page in Word format (.doc or .docx). Manuscripts must be written in English. For accepted manuscripts, an abstract in Traditional Chinese will also be required.

Authors: Provide the full name, qualifications (maximum of two), and affiliation (where the study was conducted) for all authors. The authors' names in Chinese characters, if available, should also be provided. **The corresponding author**, on behalf of the authors, is responsible for all contact with the journal. Provide the full name, postal address, telephone and fax numbers, and email address of the corresponding author.

Title: Concisely convey the main topic of the study. Avoid obvious terms such as "a study of" or "novel". If appropriate, please include the study design in the title (eg, 'randomised controlled trial', 'systematic review', 'case report'). An abbreviated title of <45 characters is also required.

Abstract: For article types requiring an abstract, this should provide a complete summary of the article, including the aims/purpose, main methods, key results, and conclusions. Abbreviations and clinical or technical jargon should be avoided. Please refer to the Categories of Papers for details.

Key Words: A maximum of five relevant index terms should be provided, selected from the Medical Subject Headings (MeSH; www.ncbi.nlm.nih.gov/mesh).

Tables: Submit tables on separate pages in as simple a format as possible. They should be numbered and concisely titled. Abbreviations should be defined in footnotes.

Figures: Restricted to the minimum necessary to support the textual material. Illustrations should be submitted as separate files (.jpg format, ≥350-dpi resolution). All figures should be numbered with a legend to indicate the anatomical area and pathological condition shown. All symbols and abbreviations should be defined in the legend. Please ensure that legends and illustrations correspond.

References: Should be numbered in the order in which they are first cited in the text. Each reference citation should be in superscript Arabic numerals after full-stops and commas. In the reference list, include the complete title, and names and initials of all authors.

Acknowledgement(s): Any individuals who contributed substantially to the study but does not qualify for inclusion as an author should be acknowledged. Written permission from acknowledged individuals is required.

Please refer to the *HKJR* website for further guidance: <http://www.hkjr.org/page/information-authors>



**2nd Annual
Global AI
Conference
2026**

**Save on your
registration.**

**Book by 8 June 2026
(11.59 pm BST)**

Human + machine: clinician-led AI for tomorrow's healthcare

29-30 June 2026 QElI Centre, London and Online

Programme is live!

Shape your learning:

with our clinician-led programme of five streams and 30 live sessions

Learn from global speakers:

hear from 100+ world-class experts sharing approaches to AI implementation

Connect with a global community:

join 1,000+ peers from 50+ countries

Discover real-world innovation:

in our abstract gallery, showcasing 100+ innovative AI projects. Submit a late-breaking abstract by 26 March 2026

Earn CPD:

through live attendance and on-demand access

Take part:

in our silent symposiums, escape room, drinks reception and more!

 The Royal
College of
Radiologists

NHS

Explore the programme
rcraiconference.com



The Hong Kong Society of Diagnostic Radiologists Trust Fund



Hong Kong Society of Diagnostic Radiologists Research Grant

The Hong Kong Society of Diagnostic Radiologists (HKSDR) was founded in 1977 to promote interflow of professional knowledge in diagnostic radiology and to foster close contact among doctors working in the field of diagnostic radiology. The HKSDR Trust Fund was established in 1985.

Taking into account the rapid progress in imaging technology and thus the need to promote research to advance our knowledge and to serve our patients better, the Trust Fund offers three awards of up to HK\$17,000 each and is open to application.

The application should be made by the principal investigator of the research project related to the scientific or clinical aspects of diagnostic radiology to be conducted in Hong Kong. The principal investigator should be a trainee/specialist in the field of diagnostic radiology. He/she has to be a registered medical practitioner in Hong Kong.

Application and enquiry can be directed to:

Dr. Lam Chiu Ying Flora, Hon Secretary of Trust Fund Working Group
c/o Ms. HY Ng, Department of Diagnostic & Interventional Radiology

Kwong Wah Hospital

25 Waterloo Road, Yaumatei, Kowloon, Hong Kong.

Tel: (852) 3517 5189